UNIVERSITY OF OKLAHOMA

GRADUATE COLLEGE

# EVALUATION OF TRANSFEMORAL PROSTHESIS PERFORMANCE CONTROL USING ARTIFICIAL NEURAL NETWORK CONTROLLERS

A DISSERTATION

SUBMITTED TO THE GRADUATE FACULTY

in partial fulfillment of the requirements for the

Degree of

DOCTOR OF PHILOSOPHY

By

FAUZIA AHMED
Norman, Oklahoma
2021

EVALUATION OF TRANSFEMORAL PROSTHESIS PERFORMANCE CONTROL USING ARTIFICIAL NEURAL NETWORK CONTROLLERS

A DISSERTATION APPROVED FOR THE
SCHOOL OF ELECTRICAL AND COMPUTER ENGINEERING

BY THE COMMITTEE CONSISTING OF

Dr. Yan Zhang, Chair

Dr. Sesh Commuri

Dr. Joebob Havlicek

Dr. Choon Yik Tang

Dr. Zahed Siddique

*To my Aunt, Jinat Ara, and my children, Fardis and Nimaat*

# Acknowledgements

Thanks to the Almighty for giving me the opportunity to successfully complete my doctoral research. I would like to express my appreciation to my advisor Dr. Yan (Rockee) Zhang. He has been a great support for me from last summer, he guided me thoroughly during my dissertation writing and in different academic issues. Without his co-operation and continuous direction, it would not be possible. My deepest respect and gratitude go to my late advisor Dr. Thordur Runolfsson. He is the one who not only helped me succeed in my research but also boosted my confidence in pursuing my career goals. I feel fortunate to have him as my mentor, my guardian, and my idol in navigating the amazing maze of my PhD, especially during the frustrations, struggles, and uncertain times. I was so shocked to hear about his sudden death. My appreciation goes to Dr. Sesh Commuri for sharing his knowledge and experience during this long period. He helped me a lot with different dynamic ideas anytime I was stuck with any problems along my way. I also appreciate the continued support from the rest of the committee members; Dr. Choon Yik Tang, Dr. Joe Havlicek and Dr. Zahed Siddique for serving on my doctoral committee and advising me at all stages of my doctoral study. I had gone through different academic protocols during this journey, and they always considered my situation and managed time to help me with the issues. My appreciation also goes to Dr. Tang, and Dr. Hjalti Sigmarsson not only for the knowledge I gained in their classes and as their teaching assistant, but also for their enthusiasm in guiding and mentoring me. My special thanks to Dr. Rodney Clint Keele, Mrs. Stephanie Gill and Graduate college for helping me a lot. My heartiest gratitude to Dr. Musharraf Zaman, Dr. Mohammed Atiquzzaman and their families for their encouraging words and valuable suggestions.

The medical personnel and graduate students from the University of Oklahoma Health Sciences Center deserve acknowledgement for their assistance and guidance in carrying out the clinical works reported in this dissertation. I would especially like to mention the help and support from Dr. Carol Dionne and her team. My special appreciation extends to the subjects who participated in the gait studies. I would like to thank my friends and lab mates in the School of Electrical and Computer Engineering for all their support. I should mention Dr. Syed Asif Imran, Dr. Ridwan Alam, Dr. Anh Mai and Harish Gadigota specially for their help during my graduate studies and data collection.

I would like to thank my family members, my dad Mr. Bahar Ahmed, my mom Dr. Arzumand Ara, my sister Dr. Naziba Tashriq and her family, my cousins and my aunts who are the source of my inspiration. Their encouraging words and faith in me helped me stay focused and persistent during my doctoral study.

Last but not the least, my deepest appreciation goes to my husband Dr. Nazmul Arefin and my children, Fardis Abyan Arefin and Nimaat Amnaan Arefin, for always being by my side through the challenging moments. Their unconditional love and sacrifices are my greatest motivation in completing this dissertation.

Thankfully

Fauzia Ahmed

# Contents

# List of figures

# Abstract

Transfemoral (Above-knee) amputation of the leg of an individual as a result of traumatic injury or due to complications arising out of diabetes or vascular disorders is a common occurrence worldwide. Following the surgical amputation procedure, the subject is fitted with prosthetic leg to help regain mobility. Prosthetic sockets are designed to transfer the body weight to the leg during locomotion. During normal human gait, the lower limbs perform four major functions: balance, positioning, support, and power. Prosthetic legs currently available in the market are mostly passive devices that provide limited support and functionality during walking. These devices also have limited adaptability during walking or to enable a more active lifestyle. The common problems of the existing above-knee prosthesis for the unilateral amputees include asymmetry between motion of the prosthetic leg with the intact leg, reduced speed along with increased energy expenditure. Not only that, but there are also different types of forces, counter forces and errors associated with gait which was ignored in some active prosthesis designs. If these technical problems are left un-addressed, they may end up with secondary medical issues requiring further surgery. While it is desirable for the prosthetic limb to have similar or close efficiency or tracking to the intact limb, it is more important for the prosthetic leg to be able to replicate the movement of a normal human leg as much as possible. Most of the studies earlier were limited to pathological gait tests in laboratory environments using inertial sensor/motion trackers which restricted the mobility of the individuals. Recently, smarter data acquisition systems are designed to capture the human locomotion in an easier and effective way. Combination of these factors result in greater advancement of prosthetic research.

Prior research in lower-limb amputee gait has focused mostly trans-tibial (below knee) amputees as they are the highest in number. In general, available prostheses for people with lower

limb amputation are primarily passive devices whose performance cannot be adjusted or optimized to meet the requirements of different users. The adverse complications of wearing poorly functioning prosthetic devices include asymmetric gait, increased metabolic energy consumption, limited blood flow, instability, sores, and joint pain. The amputees might have to undergo further joint (knee/hip) replacement procedure and that increases the chance of the increased number of trans femoral amputee in the long run. There exists a high and increasing demand for an advanced prosthetic foot that is comfortable and able to replicate the function of the biological foot. Trans-femoral amputees are the second highest and the research is more challenging as the amputees lost two of their vital joints (ankle and knee). So, to design an efficient prosthetic ankle-knee system, (including all the challenges for transtibial amputees) it is very important to consider the coupling effects of the two joints and different associated errors, or force associated with the gait like ground reaction force.

Currently available prosthetic knees are either simple mechanical hinges or sophisticated computer controlled. Development of active powered prosthetic knees (focused on the control with little emphasis) results in uncomfortable, low efficient, low energy consuming device. The inherent nonlinearities of the actuators make it difficult to control. Again, interaction forces between residual limb and the socket are dynamic in nature and are a result of gait pattern of individuals, interaction of the feet with the terrain, and the transfer of rest of the body weight during gait. These factors made the prosthetic device control and design advancement challenging for researchers.

Earlier literatures address assessing gait symmetry, movement of the healthy joints, activities of the residual muscles and the metabolic energy consumption in individuals who had undergone traditional amputation. There were research studies done showing considerable residual muscle activity in the transtibial and transfemoral amputees and minimal or random muscle activity based

on the co-relation between residuum socket interface (RSI) force and EMG to the type of gait. These forces are a source of interest for researchers to investigate for better controlling. Adaptive controllers like PD, PID and combinations are used in the development of active prosthetic devices. But PID and other traditional adaptive controllers cannot handle these nonlinearities and challenges of human locomotion properly. Moreover, most of the designs do not have consistent performance over the total gait cycle or consecutive steps.

All prostheses require some sort of stability mechanism, either manual or a weight-activated locking system. The main joints made of mechanical hinges should control the flexion and extension motion to mimic human gait. For unilateral amputee, the development of Artificial optimized neural network controller is important in this regard as it can train the neurons with the input data from the intact leg and mimic similar trajectory for the residual limb to follow.

This dissertation addresses the limitations of traditional controllers in an orderly fashion by building a strong platform to develop intelligent knee-ankle prosthesis system. The following are the key steps adopted in this dissertation.

- First, a mathematical model will be developed for a leg movement during normal gait. Algorithms for gait analysis will be developed to study the gait of people with above-knee amputation in real time during work-related activities. Simulations will be done to observe the performance of the controller.
- A more reliable and realistic learning-based control strategy will be developed to adaptively compensate for the unknown, changing ankle-knee dynamics and drive the prosthetic ankle-knee joint along the desired trajectories. Different combinations of control parameters will be changed to see the performance

improvement and error reduction. Comparative results will be shown for different controllers.

- Finally, a framework for experimental transfemoral amputee gait study will be proposed to collect data using force sensors and EMG sensors attached to the residual limbs and muscles during work related activities and normal gait.

It is anticipated that the learning capabilities of the control strategies will enable the prosthetic ankle-knee joints to not only replicate the movement of the healthy knee-ankle system, but also improve the stability of the gait and optimize the performance to a great extent. Learning-based control of the prosthetic ankle-knee joint algorithms used here consider the ankle-knee dynamics, foot-ground interaction, and the movement of the rest of the body to make it appropriate to be used for transfemoral unilateral amputee. The first strategy uses an artificial neural network-based controller to learn the unknown and changing dynamics of the ankle-knee joint and to track a desired ankle knee displacement profile. In the subsequent strategies, the neural dynamic programming-based controller is improvised by increasing the number of neurons and other parameters, comparative performance was shown for two joints also. Later a centralized controller is used to control both the joints. Additional PID is used and comparative analysis between controller schemes are presented to have a balanced and better control. Actual gait data (obtained from the healthy human subjects) of this dissertation is used to study the effectiveness of the controller. It will be interesting to see the performance of the adaptive neural network controller for unilateral transfemoral amputee with changes in terrain and in user requirements. It is anticipated that the strategy developed in this dissertation will help build an intelligent prosthetic system that can significantly improve the mobility and long-term health of people with lower limb amputation followed by proper rehabilitation.

# Chapter 1 Introduction

## 1.1 Background

Functionality and rehabilitation of a transfemoral (above knee) amputee is affected by the design of the prosthesis which is designed to transfer the body weight during locomotion. Developing and studying mathematical model to represent human gait is necessary to evaluate different changing forces, joint moments and effects that should be taken into consideration and develop an efficient controller for transfemoral amputees [1]. Previously, different controllers and their performances are analyzed to mimic the natural locomotion in active prosthesis. However, most of the traditional controllers have failed to show similar performance for different terrains. Vision-based as well as qualitative measurements, were used to evaluate the gait of the amputee [2]. These measurements are not adequate to address the challenges in the design of the artificial prosthetic limbs. Thus, learning-based Neural Network controllers are introduced to overcome the existing problems.

The word ‘amputee’ refers to an individual who has undergone removal of a limb or part of a limb as the result of trauma, a tumor, diabetes, vascular diseases, or congenital complexities. Amputation of the lower extremity is often the treatment of choice for a functionally unsatisfactory or irreproducible limb [3]. Lower-limb amputees (Below-Knee and Above-Knee) form the largest group of amputees in the nation. Amputation of the lower limb is a life-altering event as the human leg plays a very important role in balance and locomotion. The major joints of the lower extremity are the hip, knee, ankle, and the foot joints. Transfemoral amputees suffer from lack of control of the joints (knee, ankle, and foot joints) and co-ordination among major joints for locomotion. Knee is a hinge joint which joint plays an important biomechanical role in allowing human gait by

flexing and rotating and at the same time, provides required stability during the activities of daily life. It provides support when people stand, allows smooth motion when people walk, and it shortens or extends lower limb for comfortably sitting, bending, or kneeling [4-6]. The ankle joint is also hinge type which basically allows gliding, dorsiflexion, and plantar flexion. The foot joints mainly provide stability to the other joints. The muscles of the lower segment of human body have three main purposes to serve for locomotion: to stabilize, to accelerate and to decelerate [7]. A prosthetic limb is a traditional rehabilitation treatment to replace function ability loss because of lower-limb amputation. Thus, prosthesis comes into play as an extended device to replace the missing body part for lower limb amputee for their daily activities.

During the amputation, physicians try to preserve as much length of muscle, limb, and bones as is medically feasible because longer stumps provide better control over the prosthesis [8]. Doctors, along with rehabilitation specialists, consider an amputee's age, health, activity level, and lifestyle while taking decisions about the types of prosthetic knees and their available options for stability and motion. Generally, it is advised to fit the prosthesis as earlier as possible for the betterment of the amputee following the surgery. Proper fitting of the prosthetic device is crucial as improperly fitted devices can lead to secondary medical problems due to permanent sores, diabetes, and other vascular diseases. This may result in, below-knee amputees requiring, additional amputations above their knees, or even unilateral amputees lose their intact limb. Prosthetic legs available in the market are of different forms and design based on the amputees' need and comfort. Designing a prosthetic leg is a challenge as the fit, comfort and functionality should be satisfied at the same time. There are issues like smoothing out the performance of the prosthetic leg close to the intact leg. Although the trans-femoral amputation is lower in number compared to the trans-tibial amputations, the design of prosthetic legs for trans-femoral amputees

is more complex than the other one as it involves mutual torque due to the loss of knee and ankle joint. This complexity requires advanced design resulting in a more user-friendly and adaptive prosthetic leg for the lower extremity amputees. New technologies included gait analysis systems that could measure both the spatial and temporal aspects of the gait. Researchers studied biomechanics, interfacial force, and metabolic energy consumption to evaluate the effect of prosthesis on gait [9, 10]. Different devices are developed to measure the interaction forces of an amputee to improve the design of a prosthetic socket, but they are not capable of reliably measuring these forces in areas of high curvature evenly. Reliable measurement of the interfacial forces plays a significant role in the performance evaluation of the controller [11]. Improvements in the controller design will result in improved quality of life of an amputee and enable him/her to join the active workforce. The effect of the prosthetic socket on the gait of the amputee is required for these improvements, which can be studied through the interaction forces between the residual limb and the socket. These forces are dynamic in nature and depend on several factors: including the type of amputation (unilateral or bilateral), level of amputation (transfemoral or transtibial), age and health condition of the individual [12]. The muscle activity required for the amputee locomotion can be observed through the recording of Electromyography (EMG) signals. Therefore, the design of a reliable, cost effective data acquisition device is required to measure the residual muscle force in the prosthetic socket.

In this dissertation, the design and testing of a portable Prosthetic Activity Monitor (PAM) that can measure the interfacial forces between the residual limb and the socket will be proposed as a data acquisition tool. This type of data collection and measurements have subjective and objective importance to the researchers [13, 14]. The PAM will simultaneously record the muscle activity using electromyography (EMG) electrodes as the interfacial forces are a good indicator of

the gait of the amputee. A similar type of PAM was developed and used for transtibial amputee and led to different successful research outcomes [15, 16].

## 1.2 Problem Statement

Most of the prosthetic legs available in the market are passive elements. They are uncomfortable to use again needs additional energy consumption. Active micro-controlled prosthetic legs are a better solution, they are in the market, but most of them are expensive, and the control is not up to the mark. Modelling of the human gait provides a clear picture of different kinetic and kinematic parameters. Simulation of the gait gives an idea of how different force and torques influence the locomotion. Based on the gait data from healthy individuals, a trajectory can be developed and by training the artificial neural network with this data; an intelligent ankle-knee system can be controlled more efficiently. For unilateral amputees, it could be a better solution as the neural network can be trained with the real-time gait data from the intact leg, and the prosthetic leg can follow the trajectory accordingly.

Commercially available powered automatic prosthesis controllers are rare and improving the functionality of amputees is challenging. The current trend of replacing the lower limb amputee's missing limb is the development of bio-mimic prostheses, both for the ankle and knee joints. These prostheses are designed not only to reproduce healthy joint mechanical motion but also its characteristic torque-angle relationship. Controlling of prosthetic devices can be complicated due to numerous challenges such as actuator redundancy, mixed actuator dynamics, electromechanical delay, and muscle fatigue. Above knee amputees commonly develop asymmetrical gait patterns and comorbidities in the residual and intact legs. Prosthetic control must be developed to minimize these asymmetries by utilizing elastic energy storage and return to help

provide important walking subtasks including body support, forward propulsion, and leg swing initiation, which are normally provided by the ankle and knee in healthy walking.

The human motor-control system uses muscle synergies to achieve fluid and coordinated gait despite a high degree of freedom and multiple muscles. Human gait is a dynamic control problem where the key performance requirement is to guarantee tracking of reference joint trajectories to accomplish a locomotion task. The lower limb extremity can be modelled as a multiple input multiple output (MIMO) system. A central challenge in control of such a system comes from the interdependence between the control channels. Hence, when designing the control system these cross connections must be considered or in other cases the performance will be limited. The goal of every control system is to minimize the effect of system uncertainties upon the controlled variables. In the case of human gait such disturbances are ground reaction force, center of mass location, terrain geometry, friction parameters, etc. Since most of these disturbances cannot be precisely measured; a closed loop control approach is almost inevitable despite some open loop (feedforward) components can be beneficial too.

Classical control strategies for lower limb prosthetics are developed based on the recording of the kinematics of the sound limb motion with sensors. Another family of controllers for lower-limb prostheses rely on finite-state machines decomposing the gait cycle into successive phases associated with distinct control laws. In general, bioinspired controllers do not necessarily rely on a finite-state machine, but are based on principles identified in healthy humans, such as reflexes, motor primitives and balance control. However, the main requirement for the new generation of prosthetic controllers is higher level of adaptation to environmental perturbations, which is typical of healthy subjects. Therefore, a more adaptive bio-inspired approach to mimic natural neuro-muscular dynamics could be beneficial.

Artificial neural networks are widely used in robotics, but there are some existing constraints that make it difficult to attain a certain level of accuracy in lower limb prosthesis. So, comparative results with traditional controllers should be presented, and parameter adjustments are required to improve the performance and error reduction [17]. Lower limb amputees often express their dissatisfaction about the existing prosthesis for being uncomfortable, which results in reduced usage of the prosthesis [18, 19]. It is quite common for amputees to develop serious skin problems on the residual limb such as blisters, sores, cysts, edema, skin irritation, and dermatitis [20-22]. These problems are severe when the amputees are aged, diabetic patient or having some chronic diseases. Due to this discomfort experienced at the interface to the prosthetic socket, lower limb amputees avoid prosthetic devices unless it is extremely emergency.

## 1.3 Motivation

Almost one in every 190 Americans is currently living with limb loss now [23]. It is projected that the number of people living with the loss of a limb will be more than double by the year 2050. Each year more than 150000 people undergo amputations in the lower limbs in the United States [24]. Approximately 86% of the total number of amputees are amputees of lower extremities' loss (lower part of the body), of which 61.6% are trans-tibial (below-knee) amputees and 38.4% are trans-femoral (above-knee) amputees. In 1996, it is reported that 52% of the amputees were younger than 65 years old, (this age group is considered as the working age in the United States). Approximately 199,000 persons in the United States were using an artificial limb in 1994 [25]. Diabetic patients have an astounding 30 times greater lifetime risk of undergoing an amputation when compared to nondiabetic patients, which translates to an economic strain in healthcare systems of over $4.3 billion in annual costs in the USA alone [26]. Road accidents and other trauma can lead to amputation in over 20% of patients when associated with severe wound

contamination and significant soft tissue loss [27]. Not only that but battle also-related events and combat causalities can significantly increase the number of lower limb amputations. Explosives in wars cause 93% of cases and combat causalities cause 2% of cases lead to limb amputation [28]. Although a limb is removed, the amputees still feel the same sort of urge to return to healthy locomotion, and this has resulted in a gradually increasing market for improved prosthetic legs [29]. Studies have shown that the long-term health of people with limb loss is greatly influenced by the quality and functionality of the prosthetic device. The desire for increased mobility as well as the pressures of lowering the cost of long-term health care has motivated the control and design of improved artificial prosthetic devices.

The statistical data mentioned above explains the significance of developing suitable protocols to improve the rehabilitation outcomes for transfemoral amputees by studying their kinetic and kinematic parameters carefully. During the movement of a lower limb amputee, dynamic interaction forces are created against the residual limb, and when these forces are optimized, they convert the power of the body into mobility. If these forces are not properly balanced, they increase the risk of asymmetry in gait, unwanted falling off, leading to reduced gait activity over time. Significant research has been done investigating the changes in muscle activity during the amputee walking using EMG data, and a significant number of differences have been identified in the muscle activity of several residual leg muscles, compared to the intact leg and non-amputees [30]. Though, EMG is widely used in the field of management and rehabilitation of motor disability of the amputees, EMG signal acquires noise while travelling through different tissues; thus, it is not so easy to monitor or record accurately. This fact gives another scope of research which can impact the improvement of prosthetic devices.

Understanding of the biomechanics of locomotion and the interaction forces between the residual limb and the prosthetic socket is necessary for the proper design of prosthetic ankle-knee. The controller design is not an easy task here, especially as it is real time motion and terrain related. It is important to study the muscles that are active and stabilizing or transferring the weight of the rest of the body during locomotion. Not only that, it is very important to understand how the residual limb tissues respond to the external loads and other physical phenomena at the socket interface [31]. New amputation techniques and available prosthetic device performance can be compared with the traditional ones by studying the strength of the residual limb muscle activity level. Based on these studies, amputees can choose and evaluate the best possible solution (prosthetic device) for their daily use.

## 1.4 Objectives of Dissertation

The research proposes an extension of the classical direct torque control with a dynamic optimization loop based on artificial neural networks for development of gait restoration devices. This makes the prosthesis control adaptive to the subject's behavior by continuous learning to minimize a dynamic optimization criterion. The reference torque and angle patterns will adapt to the walking speed and to the locomotion tasks being performed (e.g., stair ascending or descending). Proposed adaptive neural network is a system that can improve its performance over time through interactions with the environment and through past experiences. The problem at hand is to consider a learning control process consisting of interactions between the learning system and the external environment. At each time step, the learning system determines a control action correction and receives a reinforcement signal indicating success or a failure because of that control action. The goal of the learning system is to choose controls such that the overall reward over the long run is maximized. This research concentrates on the improved control strategies for

Transfemoral prosthesis. To avoid the complexities of calculation, the leg will be considered as a link segment diagram ignoring the musculoskeletal effects. Trans-tibial prosthesis focuses on lost major joints like- ankle and foot but they receive natural control over the lower extremity from the intact knee joint. In Transfemoral prosthesis, the knee-joint is also absent, thus requires a very "human-like" active knee prosthesis also to perform the gait. Based on the current situation, stable control over the full gait cycle is necessary as the transition from one phase to another requires same degree of control performance. This study develops a learning-based control strategy to optimize the gait performance of a trans-femoral prosthesis. There are two active joints controlling the gait of a TF prosthetic leg: the knee joint and the ankle joint. Synchronization of these two joints is an essential step to accomplish while ensuring quality gait performance. A neural network control system will be implemented termed as centralized neural network. In this process, the output of the system will be continuously compared with the input, and simultaneously the performance index of the system will also be optimized by the designed neural network.

Controlling human interface system like unilateral transfemoral amputee gait in real time is challenging as the rest of the body and the residual limb are biological and producing corresponding momentum and forces, reacting against ground reaction force and other obstacles with human intelligence. So, an appropriate practical controller is needed to balance the prosthetic joints (prosthetic knee and ankle) coordinating the rest of the system. Optimization-based models can take care of large number of degrees of freedom optimizing any human related performance measure simultaneously. While simulating human walking, the method produces optimal motions and joint force profiles subjected to all the necessary constraints. The optimal control method drives the model from the initial state to the final state and on the way minimizes a cost function. The second objective of the research is to optimize the controller by minimization of error norm

when tracking the healthy human gait or the reference trajectory, tracking performance improvement, better stability of the controller, less computation time, reliability enhancement, better learning convergence. We developed a centralized neural network which can better handle the existing challenges. Comparative results are presented to have a better decision for the improvement of the prosthetic device performance.

The following chapters of the dissertation are organized as below:

The research background on lower limb anatomy, human gait, amputee gait, different available prosthesis, and recent control approaches are discussed in Chapter 2. The mathematical modelling, algorithm and simulation of the human gait will be covered in Chapter 3. Neural network controller design improvement and performance evaluation will be presented in Chapter 4. The results of the dissertation are presented and discussed in Chapter 3 and 4. Initial measurement design and requirements for data acquisition and data collection protocol for transfemoral amputee subjects will be discussed in Chapter 5. The limitations of the research, scopes for future research work and conclusion will be presented in Chapter 6 accordingly.

# Chapter 2 Research review

The two primary concerns of lower extremity amputees are comfort and mobility [32]. Despite continuous research, 55% of amputees expressed their dissatisfaction with their current prosthesis [33]. Most trans-femoral prostheses are passive devices that include friction and controlled hydraulic swing phases. These non-computerized prosthetic legs are subject to constant knee swing because of the knee extension controlling the constant resistant setting. Thus, due to limited swing over a very limited walking speed, non-optimal kinematics is observed during amputee gait. In addition, non-computerized prostheses do not offer adaptive stance control and cause the individual to lock the knee mechanism in full extension during stance to avoid buckling. These prostheses cause asymmetry in gait resulting in increased prosthetic swing phase knee flexion and decreased prosthetic stance phase knee flexion [34, 35]. This results in increased metabolic cost and secondary disability.

Different control approaches have been pursued to find a solution to optimize the prosthesis gait. These approaches differ mostly in control strategies, and it appears that there are different responses for trans-tibial and trans-femoral amputees. In addition, use of artificial neural networks as gait adaptation scheme provides stronger stability to the system than regular feedback control techniques. This chapter focuses on studies involving trans-tibial and trans-femoral gait, followed by discussion on the control strategies using ANNs for optimizing the gait.

## 2.1 Anatomy of Lower Extremity

Human body can be divided into two extremities: (a) upper (above the hip) and (b) lower (below the hip). Lower extremity amputations are of two types: (i) Trans-femoral (TF) or above-knee (AK) amputation and (i) Trans-tibial (TT) or below-knee (BK) amputation. The process that helps a human to stand upright and move about on two limbs (legs) is termed as bipedalism. This

requires the lower limbs to address three unique functions, namely, (a) bear weight, (b) aid in locomotion, and (c) maintain equilibrium. In the case of a lower extremity amputee, these three functions are severely limited in comparison to able-bodied individuals. Lower extremity amputation can be of two types: (i) unilateral (one leg) and bilateral (two legs). Figure 2.1 represents the muscles of the lower extremity of a human body. In the next subsection, the activities of different muscles will be analyzed as a part of the human gait.

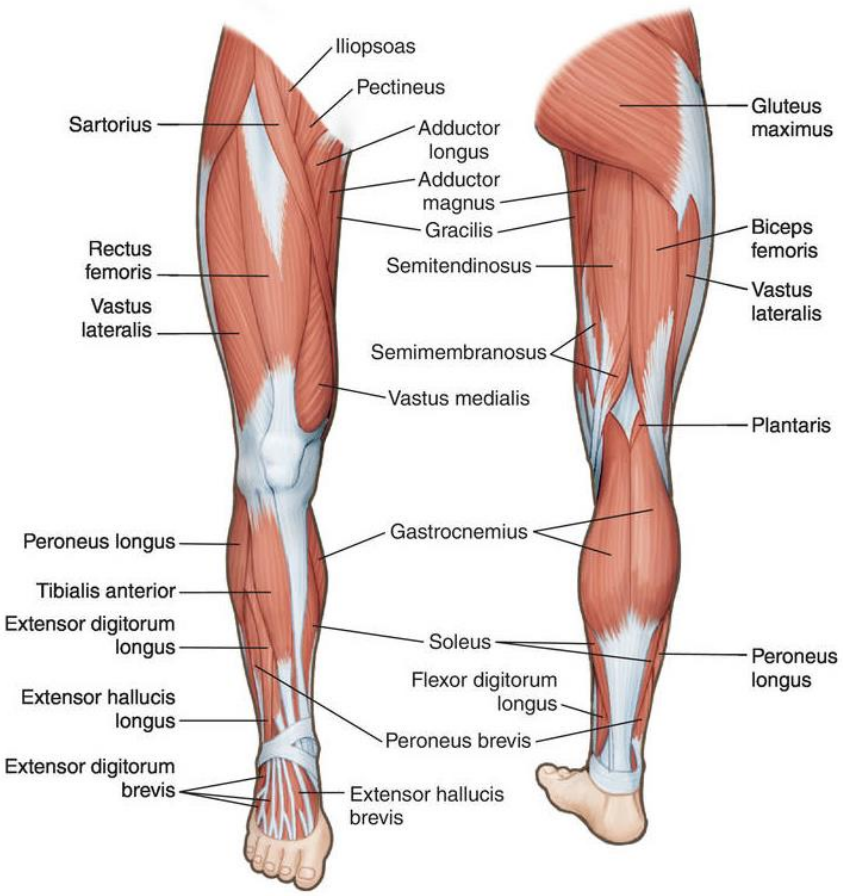


Figure 2.1 Muscles and bones of a human leg [36].

## 2.1.1 Healthy Subject Gait

Human gait can be studied as the movement of human limbs in initiating and continuing locomotion. Figure 2.2 presents the human gait cycle showing the step-by-step progression of a

single stride. As can be seen, there are two main phases in a gait cycle: (i) the stance phase (62% of a gait cycle) and (ii) the swing phase (38% of a gait cycle) [1]. In the stance phase, the reference foot is on the ground, but in the following swing phase, that same foot is no longer on the ground rather the leg (reference) swings to reach the ground to make a new strike on the ground (initiation of next stance phase). In addition, authors have subdivided the stance phase in three separate phases:

(a) First double support: the initial stage of the stance phase having both the feet in contact with the ground.

(b) Single limb stance: when the reference foot is on the ground allowing the other leg to swing through locomotion.

(c) Second double support: when both feet are again in ground contact.

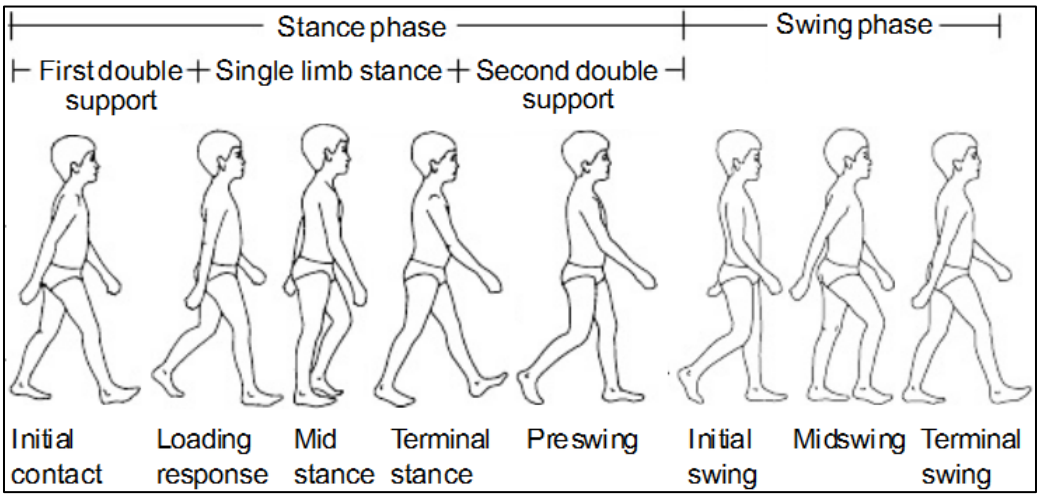


Figure 2.2 The normal human gait cycle [1].

The total gait cycle is comprised of eight events as described by [37]. Table 2.1 presents the cycle percentage of the events, as they are noted in Figure 2.2 as well. However, the gait of a TF or AK amputee is significantly different than the natural human gait shown in Figure 2.2, as the bipedal synchronization is tough to achieve with the prosthetic legs.

Table 2.1 Event of a healthy human gait cycle [37]

| **Event** | **Corresponding Gait Phase** | **Percentage of Gait Cycle** |
|---|---|---|
| Initial contact | Stance | 0% |
| Loading response | Stance | 0 – 10% |
| Mid-stance | Stance | 10 – 30% |
| Terminal Stance | Stance | 30 – 50% |
| Pre-swing | Stance | 50 – 60% |
| Initial swing | Swing | 60 – 70% |
| Mid-swing | Swing | 70 – 85% |
| Terminal swing | Swing | 85 – 100% |

The knowledge of the biomechanics is important to improve the functionality of the prosthetic devices and for the long-term health of the amputee [38]. Hence, the gait analysis is useful to develop and improve the rehabilitation strategies of an amputee. Human gait analysis can be used to detect any deviations in the gait, determine the factors for these deviations also [39]. Gait analysis required a large amount of time and effort earlier. Both the testing protocol and to process and analyze the data made gait analysis less practical for clinical purposes. The recent advances in technology have improved the measurement techniques and have provided a better

Table 2.2 Lower extremity muscle activity during gait [40].

| **Interval** | **Joint** | **Position** | **Muscle Activity** |
|---|---|---|---|
| Acceleration to Heel Strike (before initial contact) | Hip | Flexed | Gluteus Maximus, Hamstrings, Gluteus medius & minimus |
| | Knee | Flexed | Quadriceps femoris |
| | Ankle | Neutral | Anterior crural muscles |
| Heel Strike to Mid-stance (After loading response) | Hip | Neutral | Gluteus medius & minimus |
| | Knee | Extended | Quadriceps femoris |
| | Ankle | Dorsiflexed | Gastrocnemius; soleus |
| | Tarsal | Inverted | Tibialis anterior, Tibialis posterior |
| Mid-stance to Toe Off (mid-stance to pre-swing) | Hip | Extended | - |
| | Knee | Flexed | Gastrocnemius |
| | Ankle | Plantar Flexed | Gastrocnemius; soleus |
| | Tarsal | Everted | Fibularis longus, Fibularis brevis |
| Toe Off to Acceleration (Pre-swing to terminal swing) | Hip | Flexed | Iliopsoas, Adductors longus, brevis, magnus |
| | Knee | Flexed | Gastrocnemius |
| | Ankle | Neutral | Anterior crural muscles |
| | Tarsal | Neutral | - |

understanding of the biomechanical functions of the amputee. Gait analysis can be done using qualitative or quantitative measurements or a combination of both. In general practices, qualitative measurements are often used to determine the type of quantitative measurements to be performed [41].

### 2.1.2 Amputee Gait

Human locomotion is a complex functional task that requires interaction and co-ordination among major body parts especially lower limbs. Gait has always been a center of interest and studied in experiments to tease out the neural, muscular, and mechanical mechanism that are employed to walk. After amputation, the patients prefer to use prosthetic legs to promote recovery time and get habituated with daily activities. Thus, it becomes important to study the gait symmetry of amputees compared to similar control subjects, to study the gait pattern from kinetic and kinematic point of view to comment on the variability of gait parameters. Different studies have been reported on the trans-femoral and trans-tibial amputee gait. The following discussion provides a glimpse of the studies reported so far.

#### 2.1.2.1 Trans-Femoral (TF) Amputee Gait

Although it appears that gait cycle of an amputee is different from a healthy subject, statistical analysis of the electromyography (EMG) data shows that the level walking, stair ascending, and descending tasks show almost no significant difference (shown in Table 2.3). Bae et. al [42] collected EMG data from major muscles of both transfemoral amputees and healthy subjects. During level walking, all parameters of the healthy group were statistically different (in terms of mean and standard deviation of kinetic data, $p < 0.05$) from the transfemoral amputees. To be specific, pelvic obliquity of the amputees was lower than that of the healthy group as one of

the gait characteristics of the transfemoral amputees. In addition, the stance phase of a gait cycle during stair climbing is statistically similar ($p > 0.05$) for both kinds of subjects.

Table 2.3 Mean (SD) time – distance parameters for level walking and stair climbing [42].

| | Level Walking | | Stair Ascent | | Stair Descent | |
|---|---|---|---|---|---|---|
| | Healthy (n = 20) | Amputee (n = 8) | Healthy (n = 20) | Amputee (n = 8) | Healthy (n = 20) | Amputee (n = 8) |
| Gait Speed (m/s) | 1.36 | 0.82 | 0.49 | 0.35 | 0.87 | 0.65 |
| Cadence (steps/s) | 1.87 | 1.47 | 1.57 | 1.45 | 1.82 | 1.61 |
| Cycle Duration (s) | 1.01 | 1.62 | 1.28 | 1.27 | 1.10 | 1.15 |
| Stride Length (m) | 1.39 | 1.29 | 0.63 | 0.47 | 0.96 | 0.75 |
| Stance Phase (%) | 61.14 | 58.91 | 62.71 | 65.31 | 62.59 | 61.53 |

For gait event detection and TF prosthesis control scheme, Ledoux et. al [43] used a single inertial measurement unit (IMU) mounted on the shank. After collecting data from healthy and TF amputee subjects, Heel strike (HS) and toe off (TO) gait events, after collecting from healthy and TF amputee subjects, were compared as experimental data with three different control algorithms performance for the same gaits: Thresholding (THR), linear discriminant analysis, and quadratic discriminant analysis. As seen, THR was the most accurate model with 100% gait detection with an average of 2% stride for both the healthy and the amputee subjects. Ledoux's work demonstrated a robust, simple, and cost-effective method for gait detection which does not rely on a load cell and thus established it as a potential method for lower limb prosthesis gait detection.

The biomechanics of trans-femoral amputations is an important issue to be addressed. Normally, the adductor magnus has a major mechanical advantage of holding the femur in its normal anatomical axis as it has the bulk and consequent capacity of force development [41]. The biomechanics of the adductor muscles of the thigh can explain the importance of a muscle preserving surgical technique to hold the femur in its normal mechanical alignment. In case of transfemoral amputations, loss of function of adductor magnus leads to abduction of the residual femur. Experiments show that the loss of the distal third of results in a 70% loss of the effective

moment arm of the muscle. If the muscle is intact, it prevents abduction of the residual femur and may allow for easier walking. The activity of adductor magnus during the gait cycle can be explained by its dual function as a hip adductor and extensor. By changing socket shape and alignment, the residual femur of a trans-femoral amputation could be better controlled within the socket to ensure the patient's gait. A biomechanical model of the adductors was developed where the femur and thigh were divided into thirds to correspond to the attachments of the three major adductor muscles to project lines of action of the muscles and the vertical and horizontal resultant acting forces. The adductor muscle is preserved intact with its blood and nerve supply and reattached to the distal lateral of the residual femur by a traditional surgery process. The directions of the components of force normal to the lines joining the points of attachment of these muscles and the center of rotation of the hip joint are the components producing adduction. The forces of the muscles are acting on the middle of the attachment to the femur of each muscle. Medial portion of adductor magnus makes the greatest contributions to the rotational moment which is 4 to 5 times greater than that of adductor longus and adductor brevis as calculated from the resultant forces. If the distal third of the femur is amputated, then almost 70% of the adduction moment is lost and the intact adductor longus and brevis would provide the only mechanism for holding the femur in adduction. The ultimate surgical technique is to preserve the adductor magnus and re-anchor it adequately to the residual femur by suturing to the lateral distal femur to maintain the normal femoral anatomical alignment. The femur is preserved in the middle of the muscle envelope of the thigh. The abnormal gait in trans-femoral amputees is the mechanical disadvantage of an abducted position of the residual femur. Standard trans-femoral amputation had decreased muscle strength because of reduced muscle mass, inadequate fixation, and atrophy of the thigh muscles. To preserve a large amount of the adductor power; the muscle bulk and attachment of the distal end

of the muscle to the distal end of the residual femur can be done with the stump held in an over corrected position. This correction can maintain the length and tension of the muscle and keeps enough muscle power to overcome the shorter horizontal moment arm. The femur is no longer in an abducted position and this helps the abductor mechanism to function properly. The hip abductor mechanism (Gluteus medius, minimus and parts of maximus) is intact at the time of a trans-femoral amputation. However, tensor fasciae latae plays the most important role in hip abduction during the stance phase of gait. The most distal attachment of tensor fasciae latae is sacrificed in a trans-femoral amputation, the muscle can still function as a thigh abductor because of its indirect attachment from the fascia latae to the linear aspera via the lateral intermuscular septum. Keeping adductor magnus intact and adequately re-anchoring it to the residual femur will maintain the balance between the hip abductors and adductors. It is impossible to hold the residual femur adducted with a prosthetic socket irrespective of its shape or design. Due to the dual innervation of adductor magnus and its dual function of hip extensor and thigh adductor, different experiments show disagreements about which phases of gait cycle is the muscle active. In a standard trans-femoral amputation, the position of the femur may vary from 6" of adduction to 14" of abduction irrespective of the type of prosthetic socket whereas the normal anatomical position of the femur is 7-10" of adduction. The mechanical axis of the lower limb is a line from the center of the hip through the middle of the knee and ankle has been well established in orthopedic surgery, especially when total knee replacement is done. Trans-femoral amputation maintaining the anatomical alignment of the residual femur will have a mechanical alignment when a prosthesis is fitted as close as a normal intact limb. Combination of a normal mechanical alignment and maintenance of the muscle moment arm improve the patient's walking ability.

2.1.2.2 Trans-Tibial (TT) Amputee Gait

Like Bae et al, Isakov et al [44] demonstrated the comparative gait analysis of trans-tibial amputees and healthy subjects. They reported that step length, step time, and swing time for TT amputees were longer, while stance time and single support time were significantly shorter on the amputee side. Powers et al [45] conducted a similar analysis during level walking and reported slower walking speed and similar cadence. Vanicek et al [46] compared the statistics of trans-tibial amputees with a focus on which subjects tend to fall during gait. The summary of data reported in [44-46] is presented in Table 2.4.

Table 2.4 Mean (SD) time – distance parameters for level walking [44].

| | Isakov et al [44] | Powers et al [45] | | Vanicek et al [46] |
|---|---|---|---|---|
| | Amputed Leg (n = 14) | Healthy (n = 10) | Amputee (n = 10) | Amputee (n = 5) |
| Gait Speed (m/s) | 1.25 | 1.30 | 1.06 | 1.07 |
| Cadence (steps/s) | | 1.82 | 1.75 | 1.73 |
| Cycle Duration (s) | 0.582 | 64.4 (% of GC) | 63.3(% of GC) | 63 (%of GC) |
| Stride Length (m) | 0.7379 | 1.42 | 1.21 | 0.63 |

## 2.1.3 Comparative Gait Analysis of TF and TT Amputees

Gait summary measures have been developed as a convenient method to communicate overall clinical gait pathology. For gait symmetry measures, Gillette Gait Index (GGI) is the first utilized one [47, 48], which uses the instantaneous values from the gait cycle in its calculation. But it has a couple of issues to be pointed, as it uses instantaneous data: (1) GGI neglects a significant portion of the gait cycle, and it neglects the pattern of the waveform [49]. However, [50] reports the GGI with a modified version that counts the total gait waveform response. The second one is Gait Deviation Index (GDI) [51] that assigns a score out of 100 for a gait pattern. The third index is Gait Profile Score (GPS) is expressed in degrees and is based on the root mean square difference

between the subject and ideal model data. GPS is used in conjunction with the Movement Analysis Profile (MAP), calculated from the kinematic variables of the amputee gait performance.

Modified (m) versions of three published gait summary measures mentioned above, were investigated by Kark et. al [50] – the Gillette Gait Index (mGGI), the Gait Deviation Index (mGDI) and the Gait Profile Score (mGPS) in conjunction with the Movement Analysis Profile (MAP). Twenty unilateral lower limb amputees underwent gait analysis in [50]. All measures reported significant differences between levels of amputation on the prosthetic limb. The mGGI and mGPS detected significant differences between the levels of amputation on the intact side, but the mGDI did not. Table 2.5 shows the gait summary indices from [50].

Table 2.5 Summary of gait cycle measures ($n_{TF}$=8, $n_{TT}$=11) [50].

| | | | Mean | S.D. |
|---|---|---|---|---|
| mGGI (-) | Int | TF | 68.1 | 45.9 |
| | | TT | 17.6 | 9.4 |
| | Pro | TF | 66.3 | 43.9 |
| | | TT | 17.5 | 9.4 |
| | Ave | TF | 67.2 | 44.4 |
| | | TT | 17.6 | 8.9 |
| mGDI (-) | Int | TF | 73.1 | 11.0 |
| | | TT | 86.2 | 11.6 |
| | Pro | TF | 64.5 | 7.9 |
| | | TT | 82.1 | 9.0 |
| | Ave | TF | 68.8 | 8.8 |
| | | TT | 84.2 | 9.4 |
| mGPS ($^o$) | Int | TF | 8.8 | 1.9 |
| | | TT | 6.3 | 1.4 |
| | Pro | TF | 10.5 | 1.5 |
| | | TT | 7.1 | 1.8 |
| | Ave | TF | 9.7 | 1.5 |
| | | TT | 6.7 | 1.4 |

As shown in Table 2.5, higher mGGI and mGPS correspond to worse kinematic patterns yielding worse gait performance, while higher mGDI corresponds to better gait profile. As shown, the mGGI and mGPS detected significant variation between the TF and TT amputee group on the

intact side, while the mGDI showed no difference. There are significant differences between the levels of amputation for the average score for all the measures ($p_{mGGI, ave} < 0.001$, $p_{mGDI,ave} < 0.001$, $p_{mGPS,ave} < 0.001$).

Thus, it is revealed that with the prosthetic leg the amputee is not as feasible as the healthy persons in terms of walking speed and muscle activity. A controlled prosthetic leg can help them walk with balance, while synchronization between legs is critical. In addition, the residual limb is affected adversely if there is a lack of interaction between the prosthetic leg and the rest of the body. Synchronization between legs during walking in different terrains and asymmetrical body weight on the prosthetic socket makes the control design of the prosthetic leg more challenging. The main target of the research in prosthesis is to provide comfort, which needs advanced control.

### 2.1.4 Different types of available lower limb prosthesis

Prosthetics help amputees with missing body parts to attain a normal life. A transtibial prosthesis is an artificial limb that replaces the function of missing anatomical segments from below the knee whereas a trans-femoral prosthesis is designed to replace any amputated limb above the knee. The basic components that make up the trans-femoral prosthesis: solid ankle cushion heel, hexagonal-head bolt and lock washer, convex ankle, concave cylinder, and pin, set of washers with a nut and bolt, convex disc, conical cup, trans-femoral cup and knee shell [52]. The prosthesis is basically made from a high-quality raw material polypropylene. In recent designs, after involving hydraulics; carbon fiber, mechanical linkages, motors, computer microprocessors, and combinations of these technologies give more control to the users and are showing considerable potential.

The process to getting a prosthesis start few days/weeks after the amputation. The patient can be fit with a shrinker which is a compressive garment wrap used to help shape the limb for

prosthetic process and reduce edema in the residual limb. After surgery, the shrinker helps to stabilize the limb size. The liner is a soft interface to wear over the skin. It absorbs the forces created when ambulating in your prosthesis.

Once the liner is ready to be fit, casting methods will be used based upon the suspension style. A plastic diagnostic socket is used to start with as parts of the main socket to appropriately contour the residual limb. A second diagnostic socket adjusts the first diagnostic socket to give the patient a better appropriate fitting socket. The better the fit of the final socket of prosthesis, the higher the rate of success. The laminated socket is fabricated using durable carbon fiber to ensure a higher tensile strength with lighter weight. The part of the prosthetic that attaches to the remains of the limb is prosthetic socket. It is one of the most important aspects of prosthetics. A primary goal in transfemoral socket design is to maintain the residual hip joint in adduction, which maintains the hip abductors' length and to produce force for locomotion. Sockets have evolved from quadrilateral designs toward shapes that prosthetists refer to using acronyms like IC (ischial containment), narrow ML (alluding to their distinctive shape), and NSNA (normal shape-normal alignment) and CAT-CAM (Contoured Adducted Trochanteric-Controlled Alignment Method).

There are many different types of knees available for transfemoral patients offering different features to different activities from having stance stability to a Microprocessor Otto Bock C-leg 4 that can swing and flex the knee during the gait cycle. Previously prosthetics would attach with just a square type of ‘bucket’ regardless of the individual. In 1990s, Sabolich Prosthetics made sockets with a patient contact model that was specifically designed for the patient. Now the socket was made to fit the individual’s bony prominences and muscle tissue to attach like a glove and ‘lock’ into place while distributing the weight evenly across the residual limb. Later, Sabolich

continued subsequent developments to the legs – bio elastic sockets, suction sockets and more that allowed patients to run and walk with one or both legs missing for the first time ever [53].

The different types of knees available are- single axis, manual locking, stance control, poly-centric, fluid-controlled and microprocessor based. A single axis is a simple hinge with adjustable friction for swing phase damping. Manual locking is the most stable knee used during gait and the patient releases the lock mechanism to sit down. Patients having very short residual limbs and/or poor hip strength use this type of knee. Stance control knee is very stable and does not bend until the weight placed on it; is displaced totally. During leg swing, it works as system functions as a constant-friction knee but is held in extension by a braking mechanism as weight is applied during stance phase. This is widely used for older or less active amputees. Polycentric knees have multiple centers of rotation to provide different unique functional capabilities. These knees offer enhanced knee stability in early stance phase, combined with the ability to flex under-weight bearing before swing phase. This is advantageous for longer residual limbs and knee disarticulations. Fluid controlled knees have chambers filled with gases, air or silicone. These knees allow a variable speed swing phase. Computerized knees consist of a microprocessor, software, sensors, a hydraulic or pneumatic resistance system and a battery. Sensors monitor and detect changes in the environment, based on that feedback, the microprocessor adjusts the resistance to knee flexion and extension to accommodate walking speed and terrain. The technology continues to evolve, offering smarter and cheaper knees with improved sensors and longer battery life. There are MCP systems that connect the knee to the foot to communicate throughout the gait cycle. The foot sends a corresponding signal to the knee to increase knee flexion resistance to make it safer to walk down the ramp. One of the examples of the MCP knee is the C-leg 4 by Otto Bock [25].


Figure 2.3 Transfemoral Prosthesis [25].

Robotic limbs and direct bone attachment are the newest technological advancement that have made tremendous success. Among all the innovations, C-Leg 4 is an advanced microprocessor prosthetic for transfemoral amputees that offers precise adjustments at every step, providing support and balance to help reduce the risk of trips and falls regardless of speed or terrain.

The use of 'intelligent prosthesis' which used microchips to control a prosthetic knee was released by Chas. A. Blatchford & Sons, Ltd. In 1998, the Adaptive Prosthesis added hydraulic and pneumatic controls along with the microprocessor design to provide the amputee with a gait that was adaptive to different walking speeds. However, the Adaptive Prosthesis is incredibly expensive for patients.

Otto Bock Orthopedic Industry made a revolution to create the C-Leg which was released in the States in 1999. This is an affordable and adaptable prosthesis to mimic the movements of

the knee and create a dynamic gait for the amputee on a variety of gradients and calculates necessary angles and force in order to adapt to the situation. But it has the limitation that it cannot be used for running and can only be used for around 3 miles daily due to the lithium-ion battery. The 'Flex-Foot' is used by Oscar Pistorius and was designed by Van Phillips. The company 'Flex-Foot Incorporated' developed limbs using carbon graphite 'blades' that could bend and store kinetic energy like a spring. Later, the Flex-Foot was merged to Ossur to manufacture and develop the foot.

Figure 2.4 Transfemoral Prosthesis, C-Leg [25].

POWER KNEE helps the user to move from a seated to a standing position, support the user while ascending inclined surfaces. POWER KNEE restores natural walking dynamics during each step and enables pelvic rotation for a more natural gait [54].

From the knowledge gained from experience with thousands of C-Leg® wearers and decades of development, the unique Genium bionic prosthetic knee system is evolved. This is a sophisticated new technology platform built to gather exponentially greater microprocessor inputs that result in very precise responses. For the wearer, obstacles become an unconscious part of life instead of an interruption. Genium helps to cross obstacles smoothly without risking stability. At this point, Genium knees are the best available one in terms of addressing the many challenges of

real movement and speed or surface variation. But the price (120,000$) is too high to be used by the patients.


Figure 2.5 Transfemoral Prosthesis, Genium Bionic [54].

In this sub-section, different advancements and available prosthesis are described briefly. In general, due to the higher price, lesser flexibility, and shorter power life; the microprocessor based artificial prosthesis are not used widely. In next section, current research focus on prosthetic gait control will be discussed.

## 2.2 Current Research on Prosthetic Gait Control

Walking with a Transfemoral prosthesis requires up to 65% more energy than able-bodied walking [29], which mostly arises from the loss of knee function during the stance phase of gait. The increased energy cost suggests excessive compensatory muscle actions, which may be responsible for adverse health conditions in amputees, such as osteoarthritis. Conventional prosthetic knees are controlled dampers that cannot generate positive work at any time, and therefore do not replicate able-bodied muscle activity. Optimization, as well as control-based method, demonstrates the more accurate replication of healthy human gait, even

though the implementation requires complex mathematical modeling as well as experimental data collection (in case of control-based method). Back in 1991, Popovic et al [55] proposed an above-knee prosthesis using a rule-based approach. Here the predictive control method is applied which relates the input (trajectory) and output (joint torque) of the system. But, as appeared in the citing articles [55-57] the performance of rule-based control method improves if at the lower level of the system, information on the dynamic control of the system is embedded. Then, a PID controller was introduced to overcome the problems.

A PID based control method for transfemoral amputee prosthesis is demonstrated by Scandaroli et al [58]. For the knee angle, a non-linear model along with a parameter estimation procedure, were presented. Results showed that the designed model could be approximated by a reduced first-order model with limited transitory losses.

Two PID controllers were tested based on a transformed linear form of the reduced model. The first attempt is a root-locus based PID controller, and the result is problematic to achieve a null steady-state error. An experimental tune of the PID gains results in a larger proportion and integral gains. The experimentally tuned controller has a small overshoot response, but as a result, the system is oscillating when working at the vertical angle region. So, the system becomes unstable. So, the system becomes unstable.

An adaptive MRAC (model reference adaptive controller) strategy is evaluated experimentally, presenting satisfactory reference following, and in most cases, null steady error. The MRAC adapts well to higher opening angles but was not able to adapt well when working at the vertical angle region, leading to small oscillations. On the other hand, as it was expected, MRAC presented more robust results than classical PID design.

MRAC adaption capability allows small errors in modeling and identification once the controller adapts according to the instantaneous error between reference model and real system response which is an important characteristic for a controller [58]. Simulation based real-time control is required to check the performance of this type of adaptation process.

Popovic et al [55] demonstrated a Lyapunov tracking method for above-knee prosthesis, where a real-time control system equipped with artificial reflex control (for coordination between different parts) is designed. Their simulations showed that limiting the maximal knee torque to 60 N-m offers good tracking of the knee-joint motion and small perturbations of the thigh motion from the already defined (pre-defined from experiment) trajectory. Lawson et al [59] concentrated on the standing controller for the TF amputees (with powered knee and ankle prosthesis) using the ground-adaptive control mechanism formulated using finite state controller mechanism comprised of a ground searching phase, a slope estimation phase, and a joint impedance modulation phase, all together enabling the prosthesis to quickly conform to the ground and provide stabilizing assistance to the user.

Shultz et al [60] presented a control architecture for powered knee and ankle prosthesis that enables a Transfemoral amputee to run and quickly adopt the transition between walking and running, mimicking the same for a healthy individual. With a series of trials (running) the efficacy of the system was verified, and motion-captured data were recorded as the gait characteristics were defined using the double float phase and CoM (center of mass) motion where the vertical excursion of the CoM reaches a minimum near mid-stance.

Tirtashi et al [61] demonstrated the optimal design and control of an electromechanical TF prosthesis that is enabled through energy regeneration. Studies show that recent computer-controlled dampers have only reduced the energy cost by 3%-5%, compared

to a passive mechanical knee. Active prostheses overcome this limitation. A powered ankle prosthesis was presented that can reduce the metabolic energy, cost of walking, as well as improve the quality of gait [1]. Another powered knee-ankle prosthesis has recently been described and has the potential to fully replicate able-bodied muscle function in TF amputees. Regenerative electromechanical above-knee prosthesis for both knee and ankle was designed that is capable of modelling the system with a combination of DC motor, spring, gear and a controllable power converter for each knee and ankle, and an ultracapacitor to store and release the energy within the system.

Azimi et al [62] discussed a model-based adaptive control of TF prosthesis which has been developed through translation of the bipedal robotic walking gait to that of a TF prosthesis. Three model-based controllers are applied to powered TF prostheses to address the limitations of model-free control approaches (i.e., VI-variable impedance and PI-proportional-derivative controllers) and they claimed better performance with model-based controllers after comparing the stability of the controllers as per each was converged to the desired gait using Lyapunov stability theorem.

Prosthetic impedance controller combining a control Lyapunov function with model independent quadratic programs was recently developed in [37] and [42]. Three different model-based controllers, ADC, RSAC, and AIC were presented to control the prosthetic knee joint while the other joints are controlled by a feedback linearization human-inspired controller [62]. Usually, all joints are controlled by the amputee other than the active prosthetic knee. This framework results in the convergence of the outputs of the human/prosthesis system $y_a$ to the desired $y_d$ exponentially and provides stable and healthy human walking. Predictive forward dynamic simulation of human gait is extremely useful to calculate the muscle load profiles for a given walking pattern as well as estimating metabolic energy consumption.

Millard et al presented simulation-based foot contact model to predict human gait. From control point of view; as the foot forms kinematic and kinetic boundary condition between the model and the ground; metabolic cost will be adversely affected by a poorly performing foot contact model. Precomputed joint trajectories were used to define the gait of the model and each joint is controlled by PD controller (used for modification and regulation of predefined joint trajectories). The experiments were done based on data collected from a healthy individual's gait's swing phase.

Most of the prosthetic feet currently available utilize classical control techniques. The main drawback associated with the controller is if it is tuned, the parameters are usually fixed irrespective of the changing gait. To design the controller of a prosthetic leg for a unilateral above-knee amputee, firstly, the prosthetic leg should be trained with the usual gait pattern, and then, with time, it will be accustomed to following it. An artificial neural network-based adaptive controller can be employed to have better control of the nonlinear system. The approximation capabilities of artificial neural networks are used to learn and to compensate for the unknown dynamics of the system and to generate feedback control signals. In the next section, an artificial neural network approach will be discussed in brief for its acceptance to overcome the problems associated with the classical control techniques.

## 2.3 Artificial Neural Network (ANN)

Artificial Neural networks are artificially designed adopting the functional behavior of human brain. ANNs offer the advantages of system's self-adaptation in response to prompt environmental changes. It is expected that ANN based control design ensures better stability of the system. It is capable in figuring out the responses to the unseen input parameters.

### 2.3.1 Structure of an Artificial Neural Network

An artificial neural network works in two stages: (i) learning or training and (ii) operation or execution [63]. The internal parameters of the network, which act as the synapses describing relationship between two adjacent/interconnected nodes, are updated in the training stage. The training is assumed to be concluded when some cost such as prediction error and/or mean square error (MSE), fall below a preset threshold value. The training can be done in three ways: supervised, unsupervised and reinforced training [64]. After the NN is trained, it is ready to accept new input parameters and produces new outputs of them simply performing function evaluation. Figure 2.5 shows the structure of a multiple layer feed-forward artificial neural network model. It shows the transformation of I inputs ($x_1$, $x_2$, ……, $x_i$, ……, $x_I$) into K outputs ($y_1$, $y_2$, ……, $y_i$, ……, $y_K$) through J hidden neurons ($z_1$, $z_2$, ……, $z_i$, ……, $z_J$). Let $b_j$ be the bias for neuron $z_j$; $c_k$ be the bias for neuron $y_k$; $w_{ji}$ be the weight connecting neuron $x_i$ to neuron $z_j$, and $w_{kj}$ be the weight connecting neuron $z_j$ to neuron $y_k$, thus, the output of the neural network,

$f : R^I \rightarrow R^K$, is defined as (based on the Stone-Weierstrass Theorem [65]):

$$y_k = f_y\left(\sum_{j=1}^{J} w_{kj}\, z_j + c_k\right) \tag{2.1}$$

With

$$z_j = f_z\left(\sum_{i=1}^{I} w_{ji}\, x_i + b_j\right) \tag{2.2}$$

Where $f_y$ and $f_z$ are nonlinear activation functions.

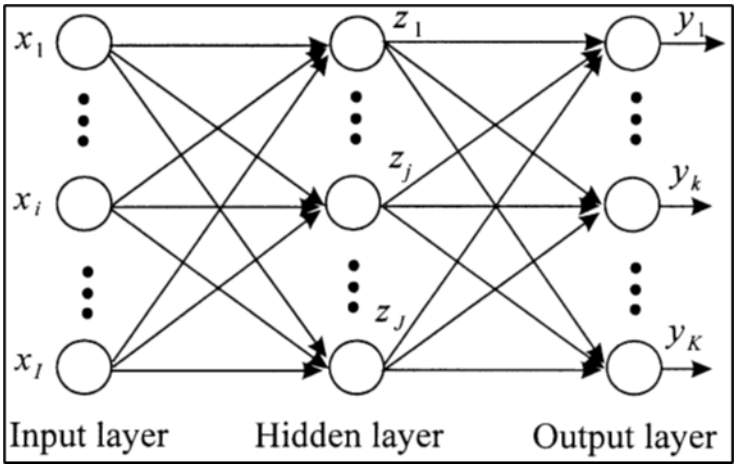

Figure 2.6 Multilayer feed-forward artificial neural network model [66].

Lafuente et al [67] used a standard feed-forward ANN with cadence, velocity and parameterization of five kinetic magnitudes as input data. They were able to distinguish between four gait categories with 80% accuracy. Apparently, their success lies in establishing the potential for multicategory classification of complicated pathological gait using standard feed forward ANNs. ANN mapping being highly non-linear, investigators became very interested in modeling the relationships between EMG, kinetic, and kinematic parameters. However, initially, standard feed-forward networks have been used widely. Heller et al [56] assembled a ANN with one hidden layer and attempted to reconstruct the EMG of the semitendinosus and vastus medialis muscles from the kinematic data, having the hip and knee angles, angular velocities, angular accelerations, and integrated foot contacts as ANN inputs during both normal and fast walking speed. Their success lies in reproducing EMG of different muscles from kinematic data using only one layered ANN. However, as they used a very generic mathematical model, the human biomechanics was not easy to reproduce accurately using this method.

Au et al [68] developed a single layer feed-forward finite-state machine-based ANN which helped to detect terrain during locomotion using the myoelectric signals from the amputee's residual limb. Later a myoelectric processing unit was designed to detect the amputee's choice on

a finite state controller, having raw myoelectric signals from the residual muscles. They described the level walking and stair descending locomotion using myoelectric signals collected from residual limbs from amputated region. But stair ascending prosthesis control was not demonstrated.

Amali et al [30] used ANN to determine the load between the residual limb and the prosthetic socket for below-knee amputees. They used simulated load data to train and validate the ANN and then used clinical load data to predict the residual limb socket's internal loads. In addition, delta-bar-delta algorithm is used as a more efficient momentum factor, which results in faster convergence of the network allowing each network weight to have its own learning rate. According to this process, the learning rate varies with time as training progresses. It was observed that with increased number of loops in the training session and the operation stage, the MSE reduces.

Anh Mai et al [69] focused on transtibial amputees, emphasis has been given on the gait pattern recognition from measurement of ground reaction force (GRF). First, a healthy human gait pattern and identification of different phases of the gait was studied. GRF data was collected from an amputee's transtibial prosthesis socket, through piezo-resistive sensors' responses. The normalized gait data is sampled and matched with different defined gait phases for the amputee prosthesis gait. A rule-based gait phase detection algorithm was used following some conditional rules. It successfully demonstrated identification of different phases starting from initial contact.

Anh Mai et al [69] designed the control system with the following goals to recognize the type of gait and detect the gait events in real time using actual gait data measured from amputees. An ankle joint displacement profile was shown corresponding to the selected gait of amputees. A control algorithm was used to learn the dynamical interactions and generate a control torque that

provides guaranteed tracking performance. They presented a comparative gait performance between conventional PD controlled system and ANN engaged PD control system. Using simulation, it has been shown that in tracking the reference gait cycle, the ANN engaged PD control architecture performs better compared to the conventional PD control system alone.

Later, Anh Mai et al studied the details of the need of human ankle dynamics and its interaction with the ground reaction force (GRF) and with the healthy human knee and hip joint has been demonstrated on how the prosthetic ankle performance can be influenced by these effects. An artificial neural network (ANN) based control algorithm is proposed based on hierarchical adaptive learning strategy. The control system performs multitasking as learning the ankle dynamics, recognizes the carrying gait intent of the user, and thus generate an appropriate torque to drive the ankle joint along a desired angle displacement profile. The closed-loop stability of the proposed approach is rigorously analyzed using Lyapunov stability theory, and the robustness of the controller is studied using actual gait data collected from human subjects.

So far, simple feed-forward artificial neural network-based control systems have performed better compared to the traditional PID controllers for prosthetic legs. But, as seen above, no model is capable to handle all the required gait functions alone, and a need for a ‘stand-alone’ control system remains. In the next chapter, an artificial neural network system will be presented demonstrating better control over the gait input parameter fluctuations, ensuring better prosthesis control for TF amputees.

# Chapter 3 Problem statement and DNDP algorithm

## 3.1 Introduction

In previous chapters, the need for a constructive problem statement for two degree of freedom gait tracking and its control methodology has become important for better gait control, which is a significant part of prosthetic device development. This chapter will focus on the problem statement of the dissertation describing the modelling of the human gait (from a 2-DOF approach) and followed by the direct neural dynamic programming (DNDP) algorithm introduction along with its components. DNDP will be employed as the 2-DOF system improvement control strategy.

### 3.1.1 Prosthetic Gait: Modeling and Control Mechanism

There are different approaches in gait analysis that help to model the natural locomotion of a subject. With proper approximation, these models can be applied to prosthetic gait analysis. Some of these models are simple in design and can investigate the basic principles of human walking. However, simplicity offers only a few degrees of freedom which ultimately make the task difficult to replicate the gait pattern of a human subject. Thus, it requires designing a better-optimized model with a higher capability to replicate human gait with prosthetic leg. Optimization-based model can take care of large number of degrees of freedom optimizing any human related performance measure simultaneously [70]. While simulating human walking, the method produces optimal motions and joint force profiles subjected to all the necessary constraints. Three basic categories are involved [70, 71] in optimization-based methods: (i) forward dynamics, (ii) inverse dynamics, and (iii) predictive dynamics. In forward dynamics optimization process, forces are the design variables for optimization and during optimization iteration; motion is calculated by integrating the motion equations with initial conditions. In inverse optimization, joint angle profile

acts as the process design variable, and during optimization iteration, forces are directly calculated from equation of motion, avoiding the necessity of numerical integration. This one is more computationally efficient than forward dynamics optimization. Finally, predictive optimization process comprises of the two objectives of the previous two methods, performing simultaneous optimization of force and motion and this process is computationally more efficient than the other two.

Control-based walking methods are extensively used in robotics and biomechanics as it approximates the actual human control systems in a better way so that both normal and pathological walking motions can be accurately tracked, simulated, and analyzed. Control methods are used to generate online walking synthesis for humanoid robots. Therefore, a robot can interact with its environment, react to external disturbances, and execute a task in real-time. Control methods have been used to track human motions, analyze pathological gait, and calculate muscle excitations and forces in biomechanics. Like the optimization-based method, the control-based method has three different categories [71]: (i) tracking control, (ii) optimal control, and (iii) predictive control. Tracking control uses a proper input variable (either torque or force) allowing the desired motion, and this process utilizes the tracking control after it verifies the desired walking trajectory using collected experimental data and producing a desired human trajectory of the data. Thus, in the case of experimental data usage, a database is maintained for the gait analysis. The optimal control method drives the model from the initial state to the final state and on the way minimizes a cost function [72]. The standard optimal control problem is stated minimizing the performance measures in the time difference $[t_0, t_f]$:

$$f = \emptyset(t_f, q_f) + \int_{t_0}^{t_f} L(t, q, \tau)dt \tag{3.1}$$

Subject to the system dynamics equations:

$$\dot{q} = l(t, q, \tau) \tag{3.2}$$

And the prescribed initial and final conditions:

$t_0 = t_{0s}$, $q_0 = q_{0s}$, $\emptyset(t_f, q_f) = 0$

where q is the vector of state variables, t is the time parameter, l is a vector function, and ∅ and L are scalar functions of the indicated arguments. In addition, $t_{0s}$ and $t_f$ are the initial and final time points, $q_{0s}$ is the prescribed initial state vector, and ∅ is a vector function for state variables at final time.

Figure 3.1 demonstrates the human central nervous system (CNS) adopting the optimization-based and control-based methods (individually). In a summary, the optimization-based method holds the potential of predicting motions and conducting cause-and-effect studies, while the control-based method better approximates human control systems which is helpful in describing neurological motion study of human. Thus, depending on the requirement and nature of objective, prosthesis design is influenced by either of the two methods.

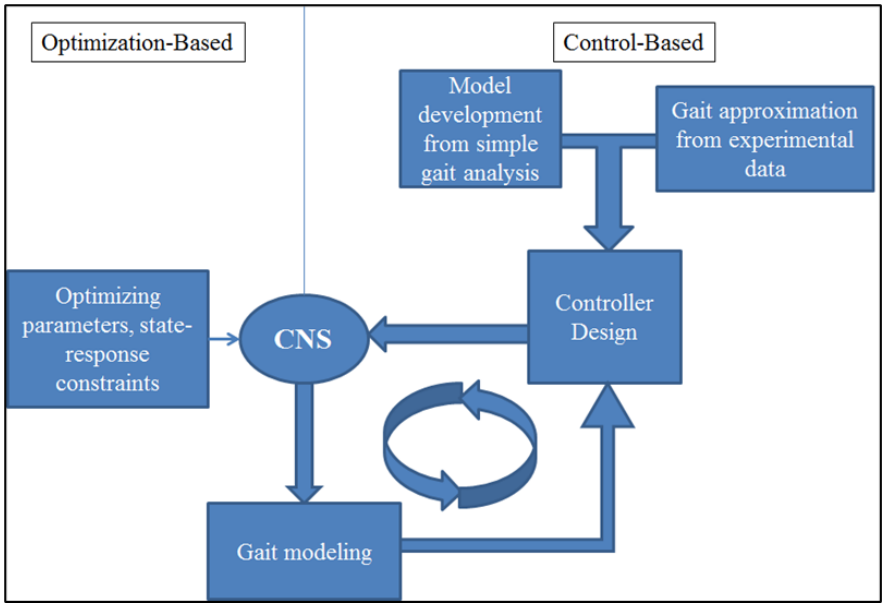


Figure 3.1 Optimization-based and control-based gait approximation.

### 3.1.2 Control Formulation

By nature, all engineering systems are non-linear in behavior. Though, all non-linearity cannot be optimized due to periodic oscillatory behavior. Thus, it impacts the stability of the system. Human leg has two major joints (ankle and knee). Hip joint is another major one playing a significant role in locomotion. Below-knee (trans-tibial) amputees are deprived of the benefit of ankle whereas above-knee (trans-femoral) amputees lack of both knee and ankle joints. Joints accelerate torque so modeling of human leg is vital to design a smooth walking of amputees with the help of prosthetic leg. Hence modeling of human like locomotion for lower extremity amputees needs special consideration. We can formulate human locomotion as a first order non-linear system, as stated below:

$$\dot{x} = f\big(t, x(t), u(t)\big); \tag{3.3}$$

$$x(t_0) = x_0 = \text{initial state at initial time } t_0.$$

$$y = g\big(x(t), u(t)\big) \tag{3.4}$$

here, $t \in \mathbb{R}, x(t) \in \mathbb{R}^n, u(t) \in \mathbb{R}^m$

$$f \text{ and } g \text{ are continuosly differentiable}$$

$$u = \text{controller}, x = \text{input}, y = \text{output}$$

For the system stated above, the cost function is defined as following:

$$J(u) = \int_{t_0}^{t_f} L\big(t, x(t), u(t)\big)dt + K(t_f, x_f) \tag{3.5}$$

$L(t, x, u)$ = running cost.

Here, $t_f$= final time, $x_f$= $x(t_f)$ = final state and $K(t_f, x_f)$ is called the final/terminal cost.

$$\text{So, } J(u) = J(t_0, x_0, t_f, u) \tag{3.6}$$

$J(u)$ is a variable commonly used in reinforcement learning.

For example, if r(t) is a binary reinforcement signal provided from the external environment with

r = 1 (meaning success) and r = 0 (meaning failure),

Function of system state, X = joint angles and velocity and applied control signal.

Then a discounted total reward-to-go R(t) at time t is R(t) = r(t +1) + a r(t +2)+ a^2 r(t +3)+ ...

where 0<a<1 is a discount factor.

R(t) requires future values of the success signal r(t) to calculate it, but these parameters are obviously unavailable. So, an approximation is needed from J(t) to the R(t). The control signal u(t) is selected to minimize (or maximize) the R(t) depending how the reward function r(t) is chosen. The aim of the critic subsystem is to find the best approximation J(t) of the R(t), which is judged by the critic error,

Ec = R(t) - J(t), which is approximated by [{r(t) +a J(t)} - J(t -1)].

The intended control system in our research is model-free. Model-based techniques for controlling prostheses can come up against limitations when an accurate model is unavailable, due to parameter uncertainty [73]. In case of a model-based approach, to formulate a control-based robotic system, conventionally, a mathematical model describes the dynamics of the system [74]. Generally, such a mathematical model consists of non-linear partial differential equations, most of which are based on approximations and simplifications. Due to the presence of these approximations, the inverse dynamics model is not very accurate when derived from the developed mathematical model which leads us to a model-free learning system.

## 3.2 Gait Modelling

The multi-body mechanical model of human walking is a non-linear, time-varying, MIMO (Multiple Input Multiple Output) system. The model consists of three rigid segments: thigh, shank and foot connected by revolute joints. This type of physical model is widely and effectively used to study the prosthesis design on kinematic, kinetic, and other characteristics of amputee

locomotion. The expectation from an ideal control system for human walking simulation is to reproduce the behavior of a human gait as closely as possible. However, number of simplifications in the controller/model prevent achieving of this goal. To develop the mathematical model of the human leg, a similar human gait modeling approach is presented in Figure 3.2 is expanded to include the detail kinematics from the knee amputation related variations. The basic model of the human leg is shown in Figure 3.2 shows all the variables needed for derivation of the equations of motion. The state of the system is given by position of the hip denoted by $x$ and $y$ and the angles at the hip $\theta_1$, knee $\theta_2$ and ankle $\theta_3$. The angles are calculated from vertical axis toward the corresponding line segment (line hip-knee for the hip angle, line knee-ankle for the knee angle and line ankle – fifth metatarsal for the ankle angle) in counterclockwise direction. We will consider a sagittal model of human leg for avoiding complicacy of calculation. The human structure is constituted by a skeleton and muscles, which are collectively called the human musculoskeletal system. The leg can be represented topologically using a kinematic chain structure in which links represent main three segments. Here the proposed model is kinematically redundant, as it possesses more degrees of freedom than those required to place the effector in a specified goal.

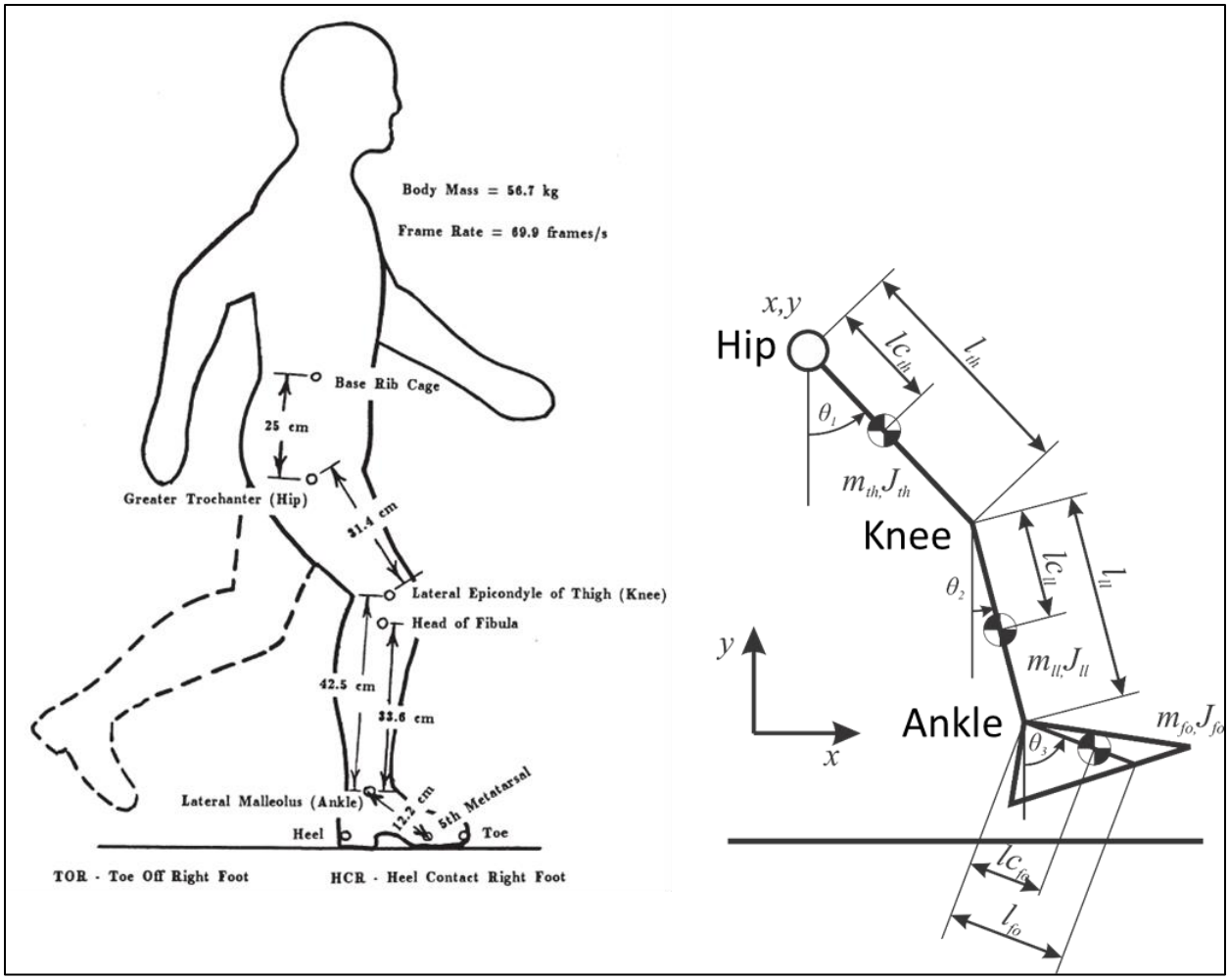


Figure 3.2 Human leg model with major physical joints, and corresponding mathematical parameters [75].

## 3.2.1 Kinematic and dynamic data

In kinematic gait analysis, the position, velocity, and acceleration of the subject are measured, without considering the forces that create the body movement. Video and optoelectronic systems consisting of integrated hardware and software components are used to obtain the kinematic measurements and thus, graphical curves representing the complete human gait cycle is produced [76]. Previous studies using kinematic data to determine the effect of different prosthetic components on the gait of the amputee [77-79] did not show significant differences among the different widely used prosthesis. Thus, kinematic data is not particularly proved to be useful to

compare the performance between different prosthesis [80]. But kinematic data can be used to create a predefined trajectory and train the artificial neural network designed in the artificial active prosthesis to work more efficiently.

On the other hand, in kinetic gait analysis, the actual forces that create the movement of the body are measured. Kinetic gait analysis is useful as it helps to identify the abnormal gait pattern and investigates the primary cause for this abnormality. The total amount of energy expended by the amputee during locomotion is directly related to the overall walking efficiency. Several researchers used energy expenditure to investigate the differences between different types of prosthesis and significant inconsistencies were observed as energy expenditure is the level of easiness during walking with the prosthesis, it depends on the personal physical health features also to some extent [78, 81-83]. Kinematic data correspond to the lengths of the segments, while dynamic data corresponds to the masses, positions of the centers of masses moments of inertia of each segment. Kinematic data has been taken from the appendix A.1 from [75]. So, the lengths of the thigh, lower leg and foot are:

Thigh length, $$l_{th} = 0.314m \tag{3.7}$$

Leg length, $$l_{ll} = 0.425m \tag{3.8}$$

Foot length, $$l_{fo} = 0.112m \tag{3.9}$$

Mass of the human subject, $$m = 56.7kg \tag{3.10}$$

Again from [75] obtained the anthropometric data. Based on that table, masses of the segments, location of the center of the mass:

Thigh (Greater trochanter/femoral condyles), $$m_{th} = 0.1 \times m \tag{3.11}$$

Leg (Femoral condyles/medial malleolus), $m_{ll} = 0.0465 \times m$ (3.12)

Foot (Lateral malleolus/head metatarsal II), $m_{fo} = 0.0145 \times m$ (3.13)

Thigh (Proximal center of mass), $lc_{th} = 0.433 \times l_{th}$ (3.14)

Leg (Proximal center of mass), $lc_{ll} = 0.433 \times l_{ll}$ (3.15)

Foot (Proximal center of mass), $lc_{fo} = 0.5 \times lc_{fo}$ (3.16)

For our model, we will use moment of inertia for the center of mass in each segment ($J_{th}: Thigh, J_{ll}: leg, and\ J_{fo}: foot$):

$$J_{th} = m_{th}{\rho_{th}}^2 = 0.1 \times m \times 0.323^2 l_{th} \quad (3.17)$$

$$J_{ll} = m_{ll}{\rho_{ll}}^2 = 0.0465 \times m \times 0.302^2 l_{ll} \quad (3.18)$$

$$J_{fo} = m_{fo}{\rho_{fo}}^2 = 0.0145 \times m \times 0.475^2 l_{fo} \quad (3.19)$$

### 3.2.2 Equations of motion

To derive equations of motion, total kinetic and potential energy of the system needs to be derived. Thus, positions and velocities of center of mass of each segment of the system needs to be derived. Using simple mathematical formula, positions of the centers of mass of the thigh, lower leg and foot are:

$$r_{th} = [x + lc_{th}\ sin\ sin\ \theta_1\ \ y - lc_{th}\ cos\ cos\ \theta_1\ ] \quad (3.20)$$

$$r_{ll} = [x + l_{th}\ sin\ sin\ \theta_1\ + lc_{ll}\ sin\ sin\ \theta_2\ \ y - l_{th}\ cos\ cos\ \theta_1\ - lc_{ll}\ cos\ cos\ \theta_2\ ] \quad (3.21)$$

$$r_{fo} = [x + l_{th}\ sin\ sin\ \theta_1\ + l_{ll}\ sin\ sin\ \theta_2\ + lc_{fo}\ sin\ sin\ \theta_3\ \ y - l_{th}\ cos\ cos\ \theta_1\ - l_{ll}\ cos\ cos\ \theta_2\ - lc_{fo}\ cos\ cos\ \theta_3\ ] \quad (3.22)$$

Using simple kinematic definition of the velocities of the centers of mass are the first derivative of the positions of the center of mass with respect to time:

$$v_{th} = \frac{dr_{th}}{dt} = \left[\dot{x} + lc_{th}\,\dot{\theta}_1\, cos\, cos\, \theta_1 \;\; \dot{y} + lc_{th}\dot{\theta}_1\, sin\, sin\, \theta_1 \;\; \right] \quad (3.23)$$

$$v_{ll} = \frac{dr_{ll}}{dt} = \left[\dot{x} + l_{th}\dot{\theta}_1\, cos\, cos\, \theta_1 \; + lc_{ll}\dot{\theta}_2\, cos\, cos\, \theta_2 \;\; \dot{y} + l_{th}\,\dot{\theta}_1\, sin\, sin\, \theta_1 \; + lc_{ll}\dot{\theta}_2 \right.$$

$$\left. sin\, sin\, \theta_2 \;\right] \quad (3.24)$$

$$v_{fo} = \frac{dr_{fo}}{dt} = \left[\dot{x} + l_{th}\dot{\theta}_1\, cos\, cos\, \theta_1 \; + l_{ll}\dot{\theta}_2\, cos\, cos\, \theta_2 \; + lc_{fo}\dot{\theta}_3\, cos\, cos\, \theta_3 \;\; \dot{y} + l_{th}\,\dot{\theta}_1 \right.$$

$$\left. sin\, sin\, \theta_1 \; + l_{ll}\dot{\theta}_2\, sin\, sin\, \theta_2 \; + lc_{fo}\dot{\theta}_3\, sin\, sin\, \theta_3 \;\right] \quad (3.25)$$

3.2.2.1 Energy of the system

To derive equations of motion using Lagrangian equations, the energy of the system needs to be calculated, as well as Lagrangian which is the difference between the kinetic and potential energy. Kinetic energies of each of the segment are:

$$E_{th} = \frac{1}{2}m_{th}\left({v_{xth}}^2 + {v_{yth}}^2\right) + \frac{1}{2}J_{th}{\dot{\theta}_1}^2 = m\Big(0.05\,\dot{x}^2 + 0.05\,\dot{y}^2 + l_{th}(0.0433$$

$$cos\, cos\, \theta_1\,\dot{x} + 0.0433\, sin\, sin\, \theta_1\,\dot{y}\,)\dot{\theta}_1 + 0.0146 l_{th}^2{\dot{\theta}_1}^2\Big) \quad (3.26)$$

$$E_{ll} = \frac{1}{2}m_{ll}\left({v_{xll}}^2 + {v_{yll}}^2\right) + \frac{1}{2}J_{ll}{\dot{\theta}_2}^2 = m(0.02325\,(\dot{x}^2 + \dot{y}^2) + 0.0465 l_{th}\dot{\theta}_1(cos\, cos\, \theta_1\dot{x} +$$

$$sin\, sin\, \theta_1\,\dot{y}) + 0.02325 l_{th}^2{\dot{\theta}_1}^2 + 0.0201 l_{ll}(cos\, cos\, \theta_2\,\dot{x} + sin\, sin\, \theta_2\,\dot{y} \; + cos\, cos\, (\theta_1 -$$

$$\theta_2)\; l_{th}\dot{\theta}_1)\dot{\theta}_2 + 0.00648 l_{ll}^2{\dot{\theta}_2}^2) \quad (3.27)$$

$$E_{fo} = \frac{1}{2} m_{fo} \left( {v_{xfo}}^2 + {v_{yfo}}^2 \right) + \frac{1}{2} J_{fo} {\dot{\theta}_3}^2 = m \Big( 0.00725 \Big( \dot{x}^2 + \dot{y}^2 + l_{th}^2 {\dot{\theta}_1}^2 + l_{ll}^2 {\dot{\theta}_2}^2 + l_{fo} \dot{\theta}_3 \big( sin\ sin\ \theta_3\ \dot{y} + cos\ cos\ (\theta_2 - \theta_3)\ l_{ll} \dot{\theta}_2 \big) \Big) + l_{th} \dot{\theta}_1 \big( 0.145 \big( sin\ sin\ \theta_1\ \dot{y} + cos\ cos\ (\theta_1 - \theta_2)\ l_{ll} \dot{\theta}_2 \big) + 0.00725\ cos\ cos\ (\theta_1 - \theta_3)\ l_{fo} \dot{\theta}_3 \big) + \dot{x} \big( 0.0145 \big( cos\ cos\ \theta_1\ l_{th} \dot{\theta}_1 + cos\ cos\ \theta_2\ l_{ll} \dot{\theta}_2 \big) + 0.00725\ cos\ cos\ \theta_3\ l_{fo} \dot{\theta}_3 \big) + 0.0145 l_{ll}\ sin\ sin\ \theta_2\ \dot{y} \dot{\theta}_2 + 0.003448 l_{fo}^2 {\dot{\theta}_3}^2 \Big) \tag{3.28}$$

Potential energies of the three segments are:

$$\Pi_{th} = m_{th} g\ r_{yth} = 0.1 gm (y - 0.433 l_{th}\ cos\ cos\ \theta_1\ ) \tag{3.29}$$

$$\Pi_{ll} = m_{ll} g\ r_{yll} = 0.0465 gm (y - l_{th}\ cos\ cos\ \theta_1\ - 0.433 l_{ll}\ cos\ cos\ \theta_2\ ) \tag{3.30}$$

$$\Pi_{fo} = m_{fo} g\ r_{yfo} = 0.0145 gm \big( y - l_{th}\ cos\ cos\ \theta_1\ - l_{ll}\ cos\ cos\ \theta_2\ - 0.5\ l_{fo}\ cos\ cos\ \theta_3\ \big) \tag{3.31}$$

The total kinetic energy of the system is the sum of the kinetic energies of each of the segments. The same holds for potential energies. Lagrangian designated by *L* is difference between total kinetic and total potential energy so it can be written:

$$L = E_{th} + E_{ll} + E_{fo} - \Pi_{th} - \Pi_{ll} - \Pi_{fo} \tag{3.32}$$

After Lagrangian is calculated, the equations of the motion can be derived:

$$\frac{d}{dt} \frac{\partial L}{\partial \dot{\theta}_1} - \frac{\partial L}{\partial \theta_1} = \tau_1 - \tau_2 \tag{3.33}$$

After calculating proper derivatives, the following can be obtained:

$$ml_{th}\Big(0.1043\big(cos\,cos\,\theta_1\,\ddot{x}+sin\,sin\,\theta_1\,(\ddot{y}+g)\big)+0.0901818l_{th}\ddot{\theta_1}+$$

$$0.0346345l_{ll}\Big(sin\,sin\,(\theta_1-\theta_2)\,\dot{\theta_2}^{\,2}+cos\,cos\,(\theta_1-\theta_2)\,\ddot{\theta_2}\Big)+0.00725l_{fo}\Big(sin\,sin\,(\theta_1-$$

$$\theta_3)\,\dot{\theta_3}^{\,2}+cos\,cos\,(\theta_1-\theta_3)\,\ddot{\theta_3}\Big)\Big)=\tau_1-\tau_2 \quad (3.34)$$

Using the same method, the other two equations can be obtained as well:

$$ml_{ll}\Big(0.0346345\big(cos\,cos\,\theta_2\,\ddot{x}+sin\,sin\,\theta_2\,(\ddot{y}+g)\big)\;+0.0346345l_{th}\Big(-sin\,sin\,(\theta_1-$$

$$\theta_2)\,\dot{\theta_1}^{\,2}+cos\,cos\,(\theta_1-\theta_2)\,\ddot{\theta_1}\Big)+0.02746l_{ll}\ddot{\theta_2}+0.00725l_{fo}\Big(sin\,sin\,(\theta_2-\theta_3)\,\dot{\theta_3}^{\,2}+$$

$$cos\,cos\,(\theta_2-\theta_3)\,\ddot{\theta_3}\Big)\Big)=\tau_2-\tau_3 \quad (3.35)$$

$$ml_{fo}\Big(0.00725\big(cos\,cos\,\theta_3\,\ddot{x}+sin\,sin\,\theta_3\,(\ddot{y}+g)\big)\;+0.00725l_{th}\Big((\theta_1-\theta_3)\,\dot{\theta_1}^{\,2}+$$

$$cos\,cos\,(\theta_1-\theta_3)\,\ddot{\theta_1}\Big)+0.00725\,l_{ll}\Big(-sin\,sin\,(\theta_2-\theta_3)\,\dot{\theta_2}^{\,2}+cos\,cos\,(\theta_2-\theta_3)\,\ddot{\theta_2}\Big)+$$

$$0.006897l_{fo}\ddot{\theta_3}\Big)=\tau_3 \quad (3.36)$$

The above three equations can be written in the matrix form:

$$M\big[\ddot{\theta_1}\;\ddot{\theta_2}\;\ddot{\theta_3}\;\big]+V\big[\dot{\theta_1}\;\dot{\theta_2}\;\dot{\theta_3}\;\big]+G+F[\ddot{x}\;\ddot{y}\;]=B[\tau_1\;\tau_2\;\tau_3\;] \quad (3.37)$$

From the equations of motion, we can deduce the values matrices $M$(‘inertia matrix’), $C$ (coriolis and centrifugal forces), $G$ (gravitational loads), $F$ (influence of hip acceleration) and $B$ (input matrix):

$$M=m\big[0.0901818l_{th}^2\;\;0.0346345l_{ll}l_{th}\,cos\,cos\,(\theta_1-\theta_2)\;\;0.00725l_{fo}l_{th}\,cos\,cos\,(\theta_1-$$

$$\theta_3)\;\;0.0346345l_{ll}l_{th}\,cos\,cos\,(\theta_1-\theta_2)\;\;0.02746l_{ll}^2\;\;0.00725l_{ll}l_{fo}\,cos\,cos\,(\theta_2-$$

$$\theta_3)\;\;0.00725l_{fo}l_{th}\,cos\,cos\,(\theta_1-\theta_3)\;\;0.00725l_{ll}l_{fo}\,cos\,cos\,(\theta_2-\theta_3)\;\;0.006897l_{fo}\;\big] \quad (3.38)$$

$$V = m\big[0\ 0.03463 l_{th} l_{ll}\ sin\ sin\ (\theta_1 - \theta_2)\ \dot{\theta}_2\ 0.00725 l_{fo} l_{th}\ sin\ sin\ (\theta_1 - \theta_3)\ \dot{\theta}_1\ -$$
$$0.03463 l_{th} l_{ll}\ sin\ sin\ (\theta_1 - \theta_2)\ \dot{\theta}_1\ 0\ 0.00725 l_{fo}\ l_{ll}\ sin\ sin\ (\theta_2 - \theta_3)\dot{\theta}_2\ -0.00725 l_{th} l_{fo}$$
$$sin\ sin\ (\theta_1 - \theta_3)\dot{\theta}_1\ -0.00725 l_{ll} l_{fo}\ sin\ sin\ (\theta_2 - \theta_3)\dot{\theta}_2\ 0\ \big] \quad (3.39)$$

$$G = mg\big[0.1043 l_{th}\ sin\ sin\ \theta_1\ \ 0.0346345 l_{ll}\ sin\ sin\ \theta_2\ \ 0.00725 l_{fo}\ sin\ sin\ \theta_3\ \big] \quad (3.40)$$

$$F = m\big[0.1043 l_{th}\ cos\ cos\ \theta_1\ \ 0.1043 l_{th}\ sin\ sin\ \theta_1\ \ 0.0346345 l_{ll}\ cos\ cos\ \theta_2\ \ 0.0346345 l_{ll}$$
$$sin\ sin\ \theta_2\ \ 0.00725 l_{fo}\ cos\ cos\ \theta_3\ \ 0.00725 l_{fo}\ sin\ sin\ \theta_3\ \big] \quad (3.41)$$

$$B = [1\ -1\ 0\ 0\ 1\ -1\ 0\ 0\ 1\ ] \quad (3.42)$$

This mathematical formulation is used for the simplification of the calculation. Here the vector of torques is not pre-multiplied by matrix $B$ .

3.2.2.2 Contact forces

Contact force needs to be included in the model. It is assumed that force acts at the 5th metatarsal of the foot, so to calculate the influence of the force to the movement of the joints, transpose Jacobian (matrix $D$) needs to be calculated. To do so, firstly, the position of the metatarsal bone needs to be calculated:

$$r_{meta} = \big[x + l_{th}\ \ sin\ sin\ \theta_1\ + l_{ll}\ \ sin\ sin\ \theta_2\ + l_{fo}\ \ sin\ sin\ \theta_3\ \ y - l_{th}\ cos\ cos\ \theta_1\ - l_{ll}$$
$$cos\ cos\ \theta_2\ - l_{fo}\ cos\ cos\ \theta_3\ \big] \quad (3.43)$$

Jacobian is the matrix of partial derivatives of the Cartesian coordinates of the point with respect to joint angles. So, transpose matrix is calculated as:

$$D = \left[\frac{\partial r_{xmeta}}{\partial \theta_1}\ \frac{\partial r_{xmeta}}{\partial \theta_2}\ \frac{\partial r_{xmeta}}{\partial \theta_3}\ \frac{\partial r_{ymeta}}{\partial \theta_1}\ \frac{\partial r_{ymeta}}{\partial \theta_2}\ \frac{\partial r_{ymeta}}{\partial \theta_3}\right]^T = \big[\ l_{th}\ cos\ \cos\theta_1\ \ l_{th}\ sin\ \sin\theta_1\ \ \ l_{ll}$$
$$cos\ cos\ \theta_2\ \ l_{ll}\ \ sin\ sin\ \theta_2\ \ l_{fo}\ cos\ cos\ \theta_3\ \ l_{fo}\ \ sin\ sin\ \theta_3\ \big] \quad (3.44)$$

Also, the contact force is calculated from the model from the [84]. For the calculation of the contact force, the velocity of the contact point is needed:

$$v_{meta} = \frac{dr_{meta}}{dt} = \left[\dot{x} + l_{th}\dot{\theta}_1 \, cos\, cos\, \theta_1 \; + l_{ll}\dot{\theta}_2 \, cos\, cos\, \theta_2 \; + l_{fo}\dot{\theta}_3 \, cos\, cos\, \theta_3 \quad \dot{y} + l_{th}\, \dot{\theta}_1 \right.$$

$$\left. sin\, sin\, \theta_1 \; + l_{ll}\dot{\theta}_2 \, sin\, sin\, \theta_2 \; + l_{fo}\dot{\theta}_3 \, sin\, sin\, \theta_3 \; \right] \tag{3.45}$$

Now we can calculate vertical force using:

$$F_y = kr_{ymeta}^{e} + step(r_{ymeta}, 0{,}0, d_{max}, c_{max})v_{ymeta} \tag{3.46}$$

In the first term, the contact parameters $k$ and $e$ are the spring coefficient and spring exponent, respectively. The second term is a damping force that is proportional to the penetration rate. The damping coefficient is a function that varies linearly between 0 and $c_{max}$ (maximum damping coefficient) as $r_{ymeta}$ varies between 0 and $d_{max}$ as overlap required for maximum damping. The damping coefficient is 0 for $r_{ymeta} = 0$, and $c_{max}$ for $r_{ymeta} = d_{max}$. This step function smoothly ramps up the damping force as contact penetration increases.

The horizontal force at the contact point is modeled using a Coulomb friction force given by the expression:

$$F_x = -\mu F_y v_{xmeta} \tag{3.47}$$

where $\mu$ is the coefficient of friction; the $v_{xmeta}$ term ensures that $F_x$ acts in a direction opposing the relative motion. Two coefficients of friction were used, $\mu_{static}$ static when $v_{xmeta}$ is sufficiently small (below 0.05 m/ s) and $\mu_{dynamic}$ otherwise. The values of these parameters are taken from [84], as shown in the table below:

Table 3-1 Contact model parameter [84].

| Parameter | Symbol | Value |
|---|---|---|

| | | |
|---|---|---|
| Spring coefficient | $k$ | 2 x $10^6$ $Nm^{-1}$ |
| Spring exponent | $e$ | 2.2 |
| Max damping coefficient | $c_{max}$ | 1500 $Nm^{-1}s^{-1}$ |
| Max damping penetration | $d_{max}$ | 1 mm |
| Static friction coefficient | $\mu_{static}$ | 0.8 |
| Dynamic friction coefficient | $\mu_{dynamic}$ | 0.2 |

After the force has been calculated, the complete equation of motion of the system can be written:

$$B^{-1}M\left[\ddot{\theta}_1\ \ddot{\theta}_2\ \ddot{\theta}_3\ \right] + B^{-1}V\left[\dot{\theta}_1\ \dot{\theta}_2\ \dot{\theta}_3\ \right] + B^{-1}G + B^{-1}F[\ddot{x}\ \ddot{y}\ ] = [\tau_1\ \tau_2\ \tau_3\ ] + B^{-1}D\left[F_x\ F_y\ \right] \quad (3.48)$$

## 3.3 Dynamic walking gait simulation

For analyzing the kinematics, dynamics and energy consumption of human gait, mechanical simulations are often used to model human walking. The two methods widely used in this aspect are- inverse dynamic calculations and forward dynamics (direct dynamic simulation). For inverse dynamics, the kinetics and ground reaction forces are measured experimentally and fed to a dynamic model of the system and based on that, the instantaneous forces and torques at each joint can be calculated. But the inverse dynamics requires repeated experimental data measurements for accuracy of results. Again, the results are limited by the precision of the match between the model parameters and experimental measurement. On the other hand, forward dynamics is used for the dynamic model to integrate the equations of motion in advance for successive steps, starting from initial conditions and driven by force and torques. The predicted kinetic motion is the output of the simulation. This simulation will be used here as it allows for comparative analysis by varying model parameters as needed for a better performance. In this method, a forward dynamic simulation with a specified set of joint angle trajectories for several steps is used, and it measures the change in energy cost as the kinematic or model parameters are changed. The inherent problem is instability as small errors are propagated each time. So, the

increased error between the actual and desired gait no longer results in an unstable configuration of specified joint kinematics, and the model fails. To increase the stability of the system for many steps, a feedback loop is required. Most of the researchers have investigated swing phase of amputee locomotion. Some other investigated the effects of knee controller performance during the swing phase only. Researchers developed A dynamic model for above knee prosthesis during complete gait cycle (swing and stance) considering a 2-dimensional multi-body mechanical system. This specific study developed a prosthetic leg model having three joint controllers with all geometrical and functional details. An optimization method was followed to obtain the optimal values, unlike other studies that investigated experimental tests or numerical trials and errors. This one was an energy-efficient model mimicking the natural walk with most efficient stride length and speed.

Gait is represented by kinematic patterns of angular positions velocities and accelerations of each of the joints. The quantities are obtained from the gait lab database [75] from the real human subjects and are widely used in simulations of human gait. From the gait lab database, the analytical forms of desired joint trajectories in time domain are generated to allow arbitrary step simulation model. The joint trajectories of the hip $\theta_1$, knee $\theta_2$ and ankle $\theta_3$ joint and vertical position of the hip $y$ are approximated by five term Fourier series. The horizontal movement of the hip $x$ includes the linear term to encompass forward speed of the walk. As a result, we can write:

$$x = a_0 + a_1 t + \sum_{k=1}^{5} (b_k \, sin \, sin \, k\omega t \; + c_k \, cos \, cos \, k\omega t \,) \tag{3.49}$$

$$y = a_0 + \sum_{k=1}^{5} (b_k \, sin \, sin \, k\omega t \; + c_k \, cos \, cos \, k\omega t \,) \tag{3.50}$$

$$\theta_1 = a_0 + \sum_{k=1}^{5} (b_k \, sin \, sin \, k\omega t \; + c_k \, cos \, cos \, k\omega t \,) \tag{3.51}$$

$$\theta_2 = a_0 + \sum_{k=1}^{5}(b_k \; sin \; sin \; k\omega t \; + c_k \; cos \; cos \; k\omega t \;) \tag{3.52}$$

$$\theta_3 = a_0 + \sum_{k=1}^{5}(b_k \; sin \; sin \; k\omega t \; + c_k \; cos \; cos \; k\omega t \;) \tag{3.53}$$

Where each of the coordinate has its own set of weight parameters $a_0, a_1, b_k, c_k$, and $\omega$ is the angular frequency of the walk which is calculated as $\omega = \frac{2\pi}{T}$, where $T$ is the duration of full walking cycles (time between the two consecutive touchdowns of the one leg). Now procedure for calculating the weight parameters is needed to be derived. It is important to note that these functions are linear in parameters. To calculate the parameters timestamps ( $t_1, \; t_2, \ldots, t_n$) $a$nd values of the coordinates at those timestamps needs to be provided. Those values are taken from the table A.3 from [75]. Once the data has been obtained following matrices are constructed:

$$M_x = [1 \; t_1 \; 1 \; t_2 \; \vdots \; 1 \; \vdots \; t_n \quad sin \; sin \; \omega t_1 \quad cos \; cos \; \omega t_1 \quad sin \; sin \; \omega t_2 \quad cos \; cos \; \omega t_2 \quad \vdots$$
$$sin \; sin \; \omega t_n \quad \vdots cos \; cos \; \omega t_n \quad \cdots \cdots \ddots \cdots \quad sin \; sin \; 5\omega t_1 \quad cos \; cos \; 5\omega t_1 \quad sin \; sin \; 5\omega t_2$$
$$cos \; cos \; 5\omega t_2 \quad \vdots sin \; sin \; 5\omega t_n \quad \vdots cos \; cos \; 5\omega t_n \quad ] \tag{3.54}$$

$$M_y = [1 \; 1 \; 1 \; 1 \quad sin \; sin \; \omega t_1 \quad cos \; cos \; \omega t_1 \quad sin \; sin \; \omega t_2 \quad cos \; cos \; \omega t_2 \quad \vdots sin \; sin \; \omega t_n \quad \vdots$$
$$cos \; cos \; \omega t_n \quad \cdots \cdots \ddots \cdots \quad sin \; sn \; 5\omega t_1 \quad cos \; cos \; 5\omega t_1 \quad sin \; sin \; 5\omega t_2 \quad cos \; cos \; 5\omega t_2 \quad \vdots$$
$$sin \; sin \; 5\omega t_n \quad \vdots cos \; cos \; 5\omega t_n \quad ] \tag{3.55}$$

Now using the pseudoinverse of matrices $M_x$ and $M_y$ weighting coefficients can be calculated:

$$[a_0 \; a_1 \; b_1 \; c_1 \; \vdots \; b_5 \; c_5 \;] = M_x^{\dagger}[x_1 \; x_2 \; \vdots \; x_n \;] \tag{3.56}$$

$$[a_0 \; b_1 \; c_1 \; \vdots \; b_5 \; c_5 \;] = M_y^{\dagger}[y_1 \; y_2 \; \vdots \; y_n \;] \tag{3.57}$$

The first equation is used only to calculate weighting coefficients for $x$, while the second equation is used to calculate weighting coefficients for angle at hip $\theta_1$, knee $\theta_2$ and ankle $\theta_3$ joint and vertical position of the hip $y$.

### 3.3.1 Calculating the position, velocity, and acceleration

Once the data is recorded and parameters of the Fourier series ($a_0, a_1, b_k, c_k$) are estimated it is important to know how to calculate the position, velocity, and acceleration at some arbitrary time $T$. To calculate the position, the new time is just plugged into equations (3.49-3.53). As an example, $x$, position of the pelvis, at the time instant, $T$, would be calculated using:

$$x(T) = a_0 + a_1 T + \sum_{k=1}^{5}(b_k \, sin \, sin \, k\omega T \; + c_k \, cos \, cos \, k\omega T \;) \tag{3.58}$$

For the velocities, firstly, the equations (3.49-3.53) need to be differentiated with respect to time. After that, the time is plugged into the equation. As an example, velocity in $x-$direction of the pelvis at the time instant $T$ is calculated using:

$$\dot{x}(T) = a_1 + \sum_{k=1}^{5} k\omega(b_k \, cos \, cos \, k\omega T \; - c_k \, sin \, sin \, k\omega T \;) \tag{3.59}$$

To calculate accelerations, the equations (3.49-3.53) need to be differentiated with respect to time, and then the equation is evaluated at the given time instance. Example for acceleration in x-direction at the time instant $T$ is calculated using:

$$\ddot{x}(T) = \sum_{k=1}^{5} k^2\omega^2(-b_k \, sin \, sin \, k\omega T \; - c_k \, cos \, cos \, k\omega T \;) \tag{3.60}$$

For the other degrees of freedom ($y$, $\theta_1$, $\theta_2$, $\theta_3$) the procedure for calculating positions, angles and velocities is the same as given by equations (3.58-3.60). The only difference is that each of the degrees of freedom has its own set of coefficients ($a_0, a_1, b_k, c_k$) and that for these four parameters ($y$, $\theta_1$, $\theta_2$, $\theta_3$), linear term does not exist so than the $a_1$ should be considered as 0.

### 3.3.2 Control torque calculation

This section shows how the control torque at each of the joints are calculated. As stated in paper [69] control torques for first two joints are calculated using computed torque control approach. In such an approach, desired joint accelerations are calculated based on the reference joint acceleration and positioning and velocity errors. That can be written in matrix form as:

$$\ddot{\theta}_{des} = \ddot{\theta}_{ref} + K_D \cdot \dot{e} + K_P \cdot e \tag{3.61}$$

where $\ddot{\theta}_{des}$ represents the desired joint accelerations in all of the joints ( $\ddot{\theta}_{des} = [\ddot{\theta}_{1des}, \ddot{\theta}_{2des}, \ddot{\theta}_{3des}]^T$). Reference values $\ddot{\theta}_{ref} = [\ddot{\theta}_{1ref}, \ddot{\theta}_{2ref}, \ddot{\theta}_{3ref}]^T$ of the accelerations are calculated from the fitted data and equation (3.60). Error $e = \theta_{ref} - \theta$ is the difference between the reference angles $\theta_{ref} = [\theta_{1ref}, \theta_{2ref}, \theta_{3ref}]^T$ and angle obtained by simulation $\theta = [\theta_1, \theta_2, \theta_3]^T$. Reference angles are obtained using equation (3.58). Similarly velocity error $\dot{e} = \dot{\theta}_{ref} - \dot{\theta}$ is the difference between the reference joint velocities $\dot{\theta}_{ref} = [\dot{\theta}_{1ref}, \dot{\theta}_{2ref}, \dot{\theta}_{3ref}]^T$ and angle obtained by simulation $\dot{\theta} = [\dot{\theta}_1, \dot{\theta}_2, \dot{\theta}_3]^T$. Reference velocities are obtained using equation (3.59). Proportional gain is $K_P$ , while derivative gain is $K_D$. Once the desired accelerations are calculated, they can be introduced into equation (3.48) and the formula for calculating torque using computed torque approach is calculated:

$$[\tau_1\ \tau_2\ \tau_3] = B^{-1}M\ddot{\theta}_{des} + B^{-1}V\dot{\theta} + B^{-1}G + B^{-1}F[\ddot{x}\ \ddot{y}] - B^{-1}D\begin{bmatrix}F_x\ F_y\end{bmatrix} \tag{3.62}$$

Matrices $M, V, G, F$ and $D$ are dependent on joint angles and joint velocities, and they are calculated using the values obtained by simulation. In this way, the control torque for all three joints is calculated.

3.3.2.1 Control torque for ankle

In the paper [69] the foot is controlled separately, not using computed torque method, so the $\tau_3$ needs to be recomputed. As stated in the same paper, the torque at the ankle would be computed as:

$$\tau_3 = \widehat{f_3} + K_{V3} r_3 \tag{3.63}$$

where $\widehat{f_3}$ is estimate of the control-torque input, $K_{V3} r_3$ is Proportional-Derivative control term and the $r_3 = e_3 + \lambda \dot{e}_3$ is the damped error term. To calculate $\widehat{f_3}$, the DNDP neural network has been employed.

## 3.4 DNDP network

Adaptive dynamic programming (ADP) is used to handle complex non-linear systems using the trial-error based learning process while Direct-Neural-Dynamic-Programming (DNDP) control algorithm which steps up from traditional trial-error algorithm is used as optimization of the feedback signal within the neural network by internal interactions to achieve the most optimized output. The DNDP-based control structure comprises of two neural networks: critic network and action network. The critic network is responsible for generating the approximate of the long-term cost function. The action network is responsible for generating control signal (in this case, $\widehat{f_3}$) which leads to optimization of long-term cost. Details about DNDP are given below [81]. Here we will show how outputs of the network are calculated and how the networks are trained.

### 3.4.1 Critic network

Figure 3.3 shows the schematic of a DNDP control applied to a 2-DOF system to control human gait optimizing the applied torques to ankle and leg (knee). Inputs to a critic network, are:

$$x_C = [e_3, \dot{e}_3, e_2, \dot{e}_2, \theta_3, \dot{\theta}_3, \theta_2, \dot{\theta}_2, \widehat{f_3}, \widehat{f_2}]^T \tag{3.64}$$

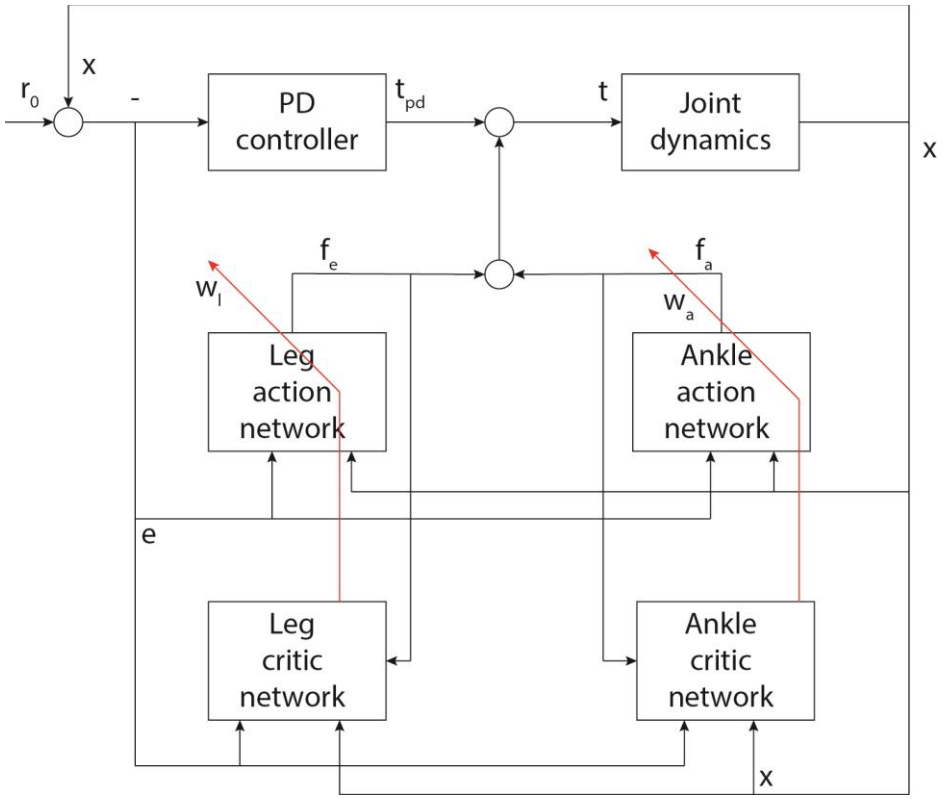

Figure 3.3 Schematic of DNDP control algorithm.

where $\widehat{f_3}$ would be calculated as an output from the action network. The output of the critic network is designated by $J$, and it is calculated using:

$$J = {W_C}^T({V_C}^T x_C) \tag{3.65}$$

where $W_C$ represents the weights of the output layer of the critic network and the $V_C$ represents the weights of the hidden layer of the critic network. Sigmoidal function which is calculated using:

$$(x) = \frac{1-e^{-x}}{1+e^{-x}} \tag{3.66}$$

To train the network, the error function must be defined. In this case the error function of the critic network is:

$$e_c(t) = \big(J(t-1) - S(t)\big) - \alpha J(t) \tag{3.67}$$

where $S(t)$ represents the current value of short-term goal, $J(t-1)$ is the output of the critic network at previous time step, $J(t)$ is the output of the critic network at current time step, and $\alpha$ is the discount factor. The short-term goal is calculated as:

$$S(t) = -\left(\frac{e_3}{\theta_{3max}}\right)^2 - \left(\frac{\dot{e}_3}{\dot{\theta}_{3max}}\right)^2 \tag{3.68}$$

Where $\theta_{3max}$ and $\dot{\theta}_{3max}$ represent maximal angle and angular velocity at the ankle joint respectively. Once the error function has been defined (3.60), it is possible to calculate the updates of the network parameters:

$$\Delta W_C = \alpha F_c e_c (V_C{}^T x_C) - k_c F_c \|e_c\|_2 W_C \tag{3.69}$$

$$\Delta V_C = \alpha G_c e_c x_C W_C{}^T (V_C{}^T x_C) - k_c G_c \|e_c\|_2 V_C \tag{3.70}$$

where $F_c$, $G_c$ and $k_c$ are design parameters, $\|e_c\|_2$ represents Euclidean norm of $e_c$ and $(\cdot)$ is the first derivative of sigmoidal function which can be calculated by:

$$'(x) = \frac{1}{2}(1 - gsig(x)^2) \tag{3.71}$$

Once the weight updates are calculated new weights can be calculated using:

$$W_C := W_C + l_r \Delta W_C \tag{3.72}$$

$$V_C := V_C + l_r \Delta V_C \tag{3.73}$$

Where $l_r$ is the learning rate of the critic network is a vital design parameter.

### 3.4.2 Action network

Inputs to an action network, are:

$$x_A = [e_3, \dot{e}_3, e_2, \dot{e}_2, \theta_3, \dot{\theta}_3, \theta_2, \dot{\theta}_2]^T \tag{3.74}$$

The output of the action network is designated by $\widehat{f_3}$ which represents estimate of the required torque at an angle, and it is used to calculate control torque. It is calculated using:

$$\widehat{f_3} = {W_A}^T({V_A}^T x_A) \tag{3.75}$$

where $W_A$ represents the weights of the output layer of the action network and the $V_A$ represents the weights of the hidden layer of the action network. The error function of the action network is:

$$e_A(t) = U(t) - J(t) = -J(t) \tag{3.76}$$

where $U(t)$ is the ultimate position. Since the ankle is expected to perfectly follow the recorded motion, the ultimate position equals zero as stated in [69]. The updates of the weighting parameters according to [69]:

$$\Delta W_A = F_A e_A({V_A}^T x_A)V_{CA}\ ({V_C}^T x_C)W_C\ - F_A({V_A}^T x_A){V_A}^T x_A r_3 - k_A F_A\ \|e_A\|_2 W_A \tag{3.77}$$

$$\Delta V_A = G_A e_A x_A V_{CA}({V_C}^T x_C)W_C{W_A}^T({V_A}^T x_A)\ \ - k_A G_A \|e_A\|_2 V_A \tag{3.78}$$

Where $F_A$, $G_A$ and $k_A$are design parameters. Matrix $V_{CA}$ maps outputs of the action network to the critic network and in our case, the only output of the action network maps to fifth input of the critic network so:

$$V_{CA} = [0, 0, 0, 0, 1] \tag{3.79}$$

Once the weight updates are calculated new weights can be calculated using:

$$W_C := W_C + l_r \Delta W_C \tag{3.80}$$

$$V_C := V_C + l_r \Delta V_C \tag{3.81}$$

As described above, the critic network feeds input to the action networks to optimize the output responses to the system. As shown in [69], similar critic-action network has been employed

for ankle motion control, while in this dissertation, the method will be expanded to employ the DNDP benefit to optimize the action network optimized signal for both knee/leg and ankle being modified by the weighed cost harnessed from the respective critic network.

## 3.5 Simulation of 2-DOF human gait using DNDP network

A standard model topology for gait studies uses a 2D, 7 segment, 9 degree of freedom anthropomorphic model. In our simulation, we use a general mechanical model which can be applied to any mechanical system composed of rigid bodies, hence, the model can be extended with additional segments. Foot contact forces are calculated using a 2-point foot contact model, with a point contact located at the heel and metatarsal. The contact model calculates normal force as a function of penetration depth, penetration rate, material stiffness, and material damping. A dry Coulomb model was used to calculate the force of friction between the points and the plane with stiction and dynamic friction values. Pre-computed joint trajectories are used to define the gait of the model at the position level. Each joint is actuated using a proportional-derivative (PD) controller that models and regulates the predefined joint trajectories. The initial joint trajectories were taken from an existing experimental data set of a healthy gait of an average-sized male. The computationally efficient, but low-fidelity foot contact model produced ground reaction forces and foot pad compressions that were drastically different than those observed in healthy human gait, and negatively affected the simulated joint kinetics. A high-fidelity foot contact model is especially important for a predictive gait simulation: contact forces at the foot will affect the loads at the joints of the legs, and thus the metabolic cost of the leg muscles. If the model does not have a realistic foot contact model, it will be impossible to produce metabolic cost estimates that correspond to what one would expect from a human.

Figure 3.4 presents the simulation response of 2-DOF human gait, resembling the knee and ankle motion. In parallel to actual angle of the joints, the derivatives of the respective angular motion, i.e., the angular velocity at that ankle is also presented. As seen for more than 50% of the duty cycle, the DNDP control system tracks the desired joint signal and respective angular velocity. However, the tracking error in the knee joint is more prone to error with significant deviation from the desired signal. This describes that, even though the DNDP algorithm is functioning properly with significant amount of tracking, it requires further improvement and tweaking to have better tracking of the transient positions, as well as improving the knee joint tracking.

Figure 3.5 presents the complete gait cycle and different gait phases derived from the simulation. The transfemoral gait cycle is affected by the quality of the surgery, the type and alignment of the prosthesis, the condition of the stump and the length of the remaining muscular structure and how well these are reattached. From the graph, we can see the LR (loading response) phase is shorter compared to the normal healthy gait.

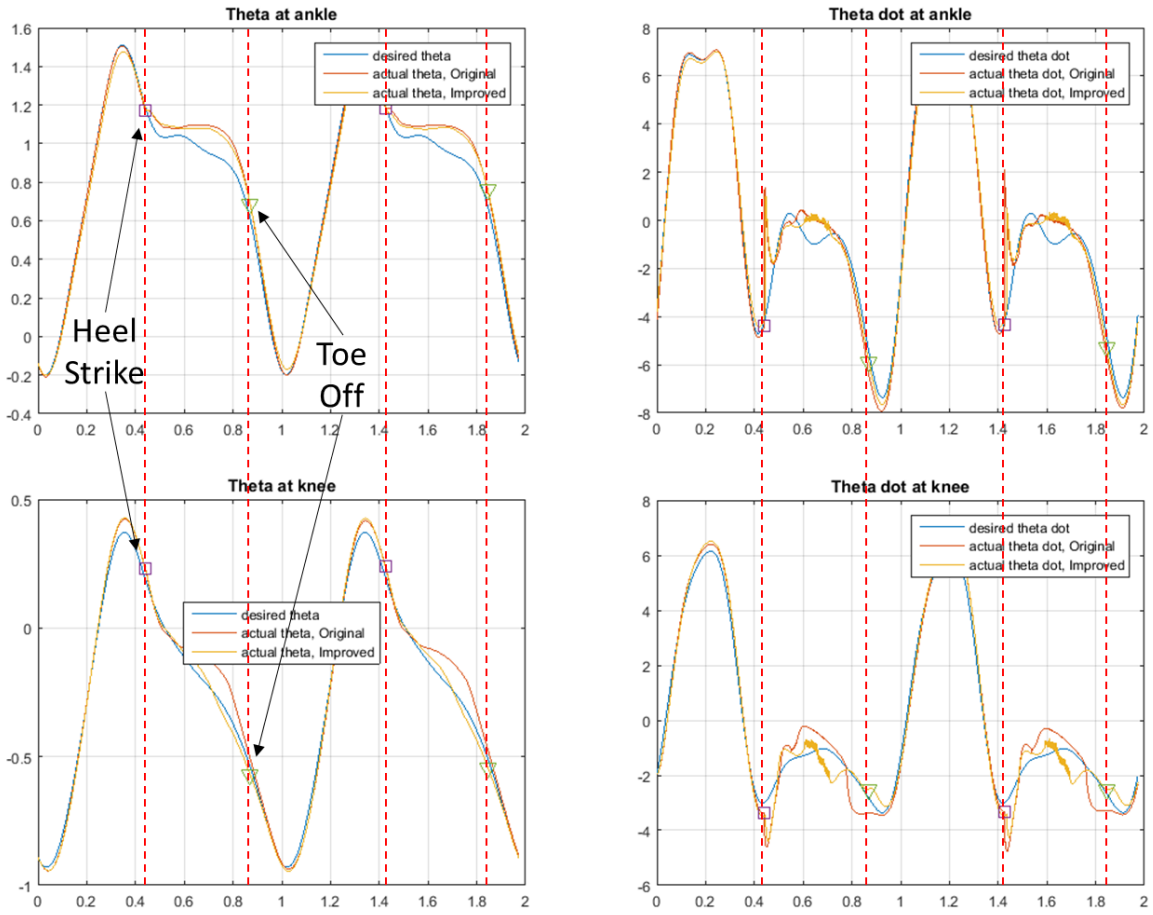


Figure 3.4 DNDP algorithm controlled 2-DOF human gait tracking: (a) ankle angle, (b) angular velocity at ankle, (c) knee angle, and (d) angular velocity at knee.

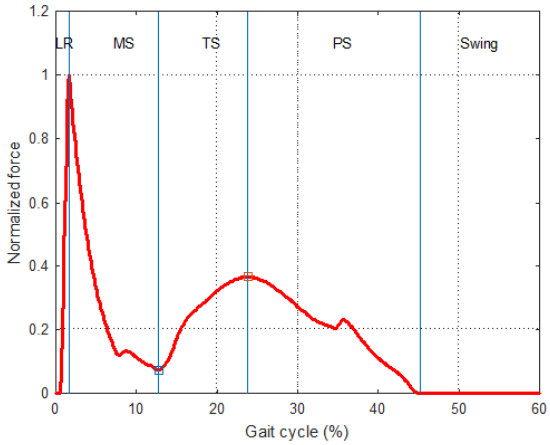


Figure 3.5 GRF (normalized) w.r.t gait phases.

In this chapter, the human gait modeling is described as used in this research work, with itemizing the key functional parameters required to develop a control algorithm that is expanded to simultaneously track both knee and ankle motion. However, from the first simulation cases, it appears the DNDP algorithm needs tweaking as the knee joint tracking lacks accuracy while compared to the performance of the ankle joint. The theoretical problem of optimal dynamic control can be solved only approximately and there are several different variants for that. We use a combination of action and critic neural networks. The critic network is trained toward optimizing the Bellman equation. The action network is trained such that the critic output approaches an ultimate objective of success. During the learning process, the action network is constrained by the critic to generate optimal control solutions. In on-line learning, the controller is not much efficient when it starts to control at time zero. This is because, initially, both the action and critic networks possess random weights/parameters. Once a system state is observed, an action will be subsequently produced based on the parameters in the action network. A better control under the specific system state should result in a reduced Bellman error. This set of system operations will be reinforced through memory or association between states and control output in the action network. Otherwise, the control will be adjusted through tuning the weights in the action network to minimize the Bellman error. In next chapter, different modifications will be applied to this 2-DOF DNDP control system to reflect better tracking.

# Chapter 4 Optimization of the network parameters

## 4.1 Introduction

Under investigation, the system is a 2DOF model of a human gait controller using DNDP algorithm composed of critic and action network trying to solve the optimal control problem in real-time. The structure of the control system is composed of a cascade of two neural networks – an action network and a critic network. The purpose of the action network is to implement a static nonlinear state feedback which minimizes the instantaneous cost function. In the case of the biped robot, the cost function, J(t), is joint angular error. The critic network minimizes the prediction error of the integral of the discounted error function.

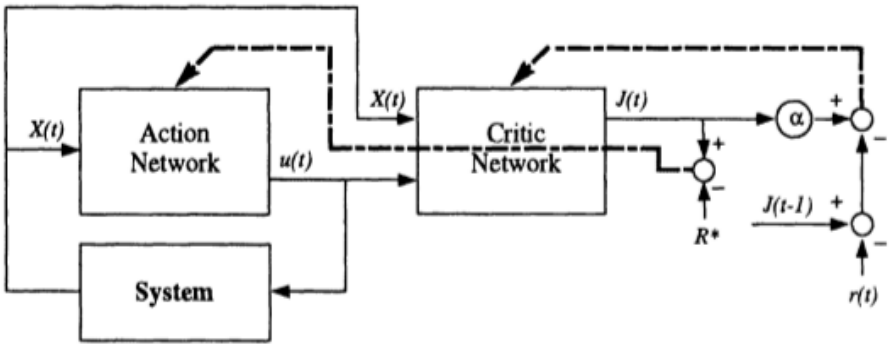


Figure 4.1 2DOF human gait controller using DNDP algorithm.

For the initial implementation, the critic and action network for both knee and ankle joints are sigmoid based feed-forward networks with a single hidden layer. The number of neurons in each of these four networks (action ankle, critic ankle, action knee, critic knee) can be varied to improve the performance. With the increment of the number of neurons in each network, the performance of the desired trajectory tracking will be improved. However, the problem with gradient-based NN learning is that only local extrema of the cost function are achieved, which may

differ a lot from the global extrema. This difference depends on several factors – initial values of the model parameters, the dimension of the hyperspace, learning rate, constraints, clipping options, regularization, cost function eights, etc. At first, the structural parameters of the action and critic network for knee and ankle joints will be varied to see the improvement compared to the existing structure. To compare the performance of the algorithms, 4 types of signal errors (error_ankle, error_ankle_dot, error_knee, error_knee_dot) and their 2-norms will be evaluated. This will allow comparing the performance of the system by 4 numbers representing the magnitude of these errors. The angular displacement of the ankle and knee joints will be examined first. The following two figures, Figure 4.2 and 4.3, compare the **desired** angular signal with the **original** (NAhA=8, NChA=10, NAhK=9, NChK=11) and with the **improved** (NAhA=11, NChA=2, NAhK=11, NChK=11) signal,

Where,

NAhA = Number of hidden nodes in the Action Network (for Ankle)

NChA = Number of hidden nodes in the Critic Network (for Ankle)

NAhK = Number of hidden nodes in the Action Network (for Knee)

NChK = Number of hidden nodes in the Critic Network (for Knee)

The error norm of the tracked signal subtracting the desired original from it is (3.0576,31.5038,2.3239,25.3380). The norm of the improved subtracted from the desired error is (2.9161,26.1761,1.2770,20.1386). As can be seen, the ankle angle error norm decreases from 3.06 to 2.92. The ankle angular velocity error norm decreases from 31 to 26. The knee angle error norm decreases from 2.32 to 1.27, and the knee angular velocity error norm decrease from 25.34 to 20.13. The iteration was done 12 times. The improvement is most evident in the ankle angle as in

Figure 4.2. It can be clearly noticed that the improved signal tracks closer to the desired reference for the ankle and knee angles and their derivatives (respective joint velocities). Also, it becomes evident that the mean value of the angular velocity error is less for Param2 compared to Param1.

Table 4.1 Comparison of error performance.

| **2-cases with hidden network param, Param1 and Param2, respectively** | | | | | **Norm of the error** | | | |
|---|---|---|---|---|---|---|---|---|
| Param | NAhA | NChA | NAhK | NChK | error_ankle | error_ankle_dot | error_knee | error_knee_dot |
| 1 | 8 | 10 | 9 | 11 | 3.0576 | 31.5038 | 2.3239 | 25.3380 |
| 2 | 11 | 2 | 11 | 11 | 2.9161 | 26.1761 | 1.2770 | 20.1386 |

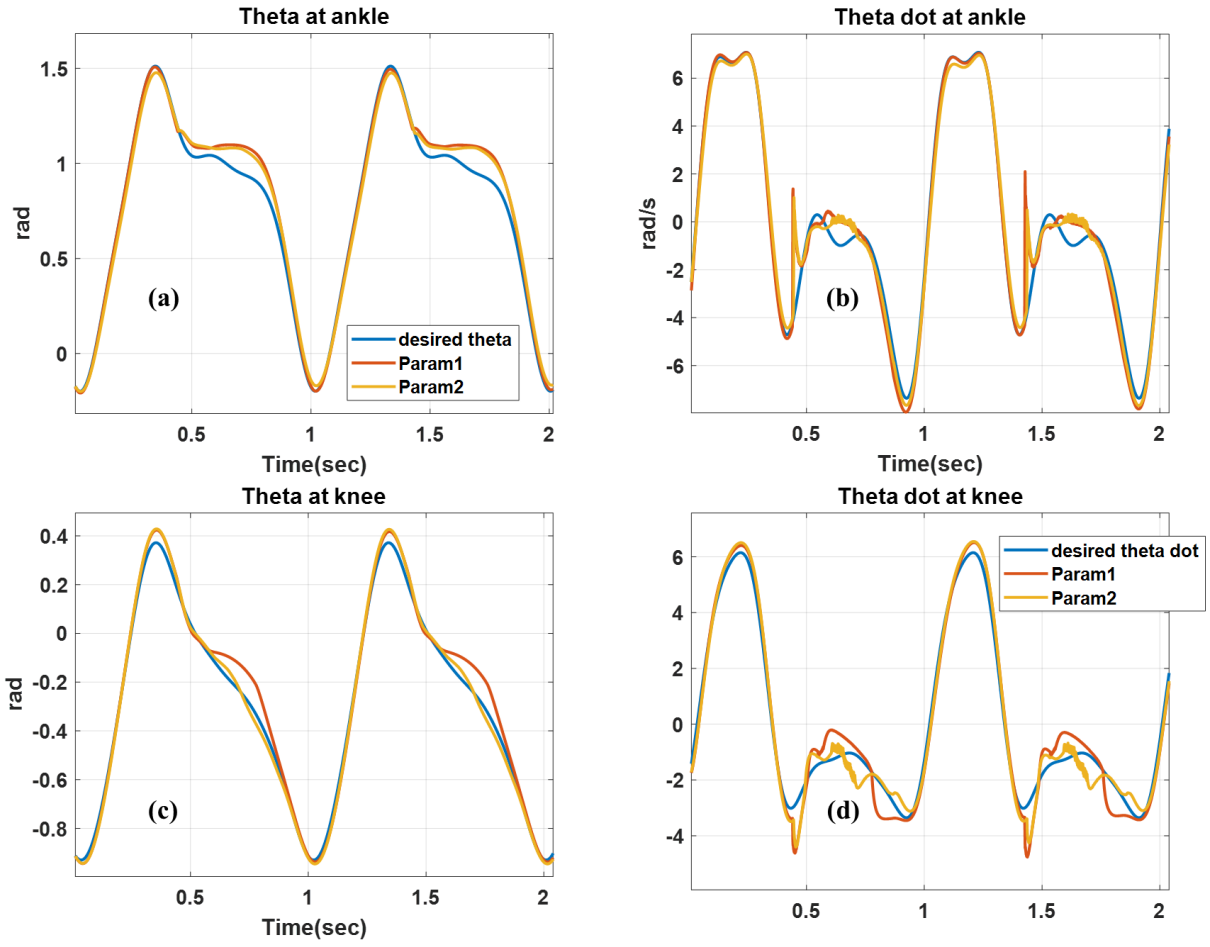


Figure 4.2 Improvement of tracking of angular positions in ankle and knee angles and their derivatives (joint velocity) as per observations from table 4.1.

The next figure, Fig 4.3, represents the Frobenius norm of the model parameters - input and hidden layer weights. The hyperparameters of the network are: *Wa, Va, Wc, Vc,* which represent

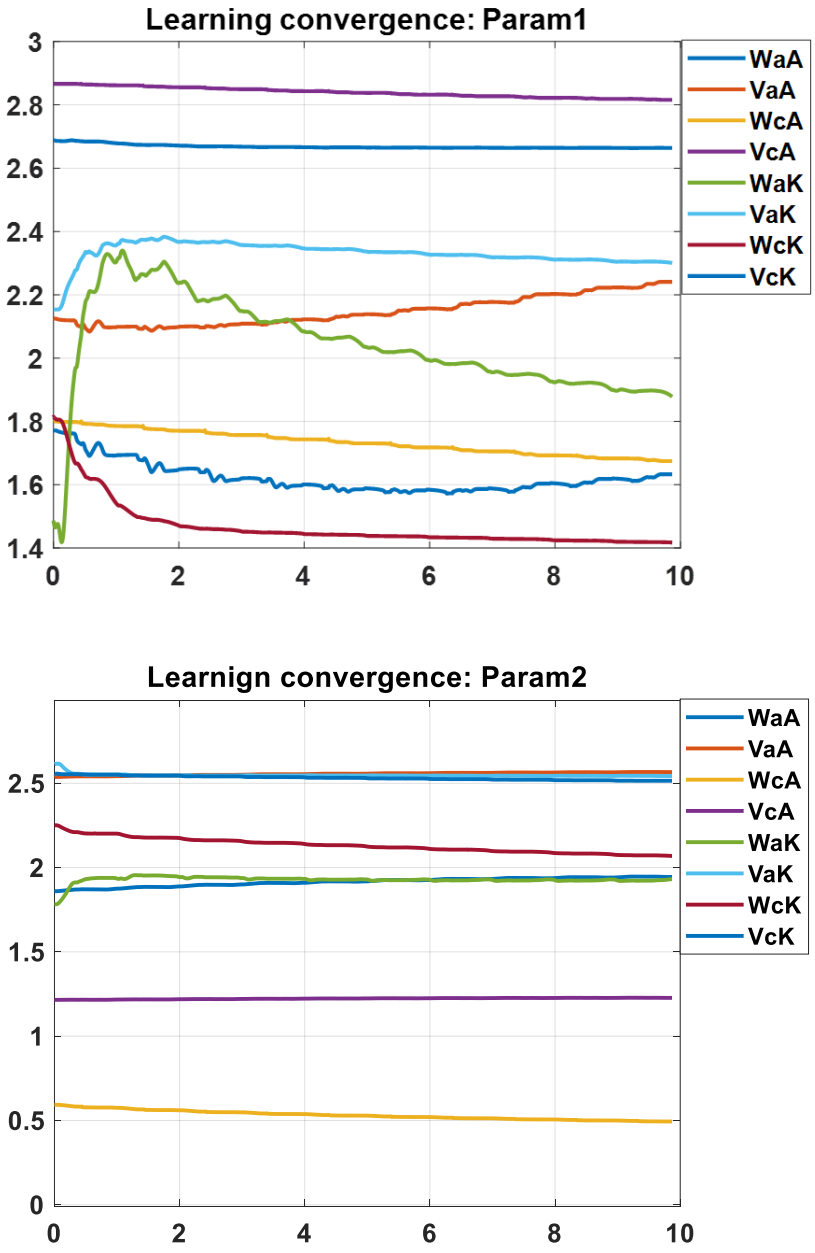


Figure 4.3 The Frobenius norm of the model parameters - input and hidden layer weights from the critic and action networks of the neural network of the controller.

the weights of fully connected input and hidden layers for action or critic network. Also, there are two of these networks, respectively, for the knee and for the ankle, totaling 8 weight matrices. To characterize the magnitude of each matrix, its norm is calculated on each iteration of the simulation. The expected behavior is to see these parameters settle at their steady state values. Since, the hyperparameters (weights) converge, this indicates that the learning algorithm reaches its final solutions where the gradient norm is close to zero preventing consequent changes in the model parameters.

In section 4.2, the capacity of the critic and/or action networks will be increased by adding additional hidden layers, as well as learning from the exploration of different parameters with a focus to reduce error. Depending on the result with changing the activation function of the networks, the performance of the controller will be evaluated. It is expected that using recurrent NN will be advantageous, but it will require more time to program and tune as the process will end up as time-consuming.

### 4.1.1 Controller linear analysis

The linearization in this section is used not directly for controller design but rather for controller analysis to get more insight into why one controller performs better than another. Therefore, a linear approximation of the closed loop is constructed as a feedback interconnection between the prosthetic leg and the controller. The performance of the system is demonstrated when the control algorithm is connected to the leg. Since both the leg dynamic model and DNDP controller are nonlinear, and also the controllers are nonlinear with different structures, a unique representation of the closed-loop dynamics is used, which will allow us to compare between these different controllers. We observed the particular transient parameters from the simulation and also compared the frequency responses and approximation accuracies between the linear models.

Having the nonlinear equations of the leg, we are able to extract the linear parameter varying model which will be an almost exact approximation.

Generally during the linearization of the nonlinear plant will of course have some unmodelled dynamics. The system identification technique we used does not lose any information from the nonlinear plant, and only decomposes the nonlinear behavior to linear approximation accompanied with noise model. So whatever information is not captured by the linear approximation is captured by a linear noise model driven by a white noise signal n(t). Ultimately, a particular variation of the n(t) will compensate for any differences between the linear model representation and the nonlinear one.

If we were able to find a perfect controller for the prosthetic leg, the closed-loop response will track exactly the desired joint angles without any error. No such perfect controller is practically available, so we get some non-unit frequency response. The linear model is estimated from a long sequence of simulated data with the addition of random excitation signal to the control input. The linear model is obtained between the desired and actual angle, and is not able to account for all the observed dynamics, which we describe with the level of fit and residual noise model. The smaller the noise model, the better the approximation.

To investigate the closed loop performance for various parameters, a linearized approximation of the closed loop system with inputs $r_{ankle}$ and $r_{knee}$ - the reference trajectories for the ankle and the knee is discussed. The respective outputs are $\theta_{ankle}$ and $\theta_{knee}$. The closed loop system (leg model plus DNDP controller) can be approximated with a linear model as evident from the performed system identification. To do such an approximation a small pseudorandom binary noise signals $n_{ankle}$ and $n_{knee}$ should be summed to $r_{ankle}$ and $r_{knee}$ to better excite the system dynamics. However, since the difference between reference trajectory and actual angular

parameter is large enough, we can identify without those noises. For the linear model, lets denote $u_1 = r_{knee}$ and $u_2 = r_{ankle}$. Also $y_1 = \theta_{knee}$ and $y_2 = \theta_{ankle}$. The linearized model is described in frequency domain with,

$$y_1(j\omega) = W_{11}(j\omega)u_1(j\omega) + W_{12}(j\omega)u_2(j\omega) \tag{4.1}$$

$$y_2(j\omega) = W_{21}(j\omega)u_1(j\omega) + W_{22}(j\omega)u_2(j\omega) \tag{4.2}$$

This linear representation will be valid equally for the angular and angular velocity signals, for example, considering knee joint,

$$r_{knee}(j\omega) = W_{11}(j\omega)\theta_{ankle}(j\omega) + W_{12}(j\omega)\theta_{knee}(j\omega) \tag{4.3}$$

$$j\omega r_{knee}(j\omega) = j\omega W_{11}(j\omega)\theta_{ankle}(j\omega) + W_{12}(j\omega)j\omega\theta_{knee}(j\omega) \tag{4.4}$$

$$d_t r_{knee}(j\omega) = W_{11}(j\omega)d_t\theta_{ankle}(j\omega) + W_{12}(j\omega)d_t\theta_{knee}(j\omega) \tag{4.5}$$

The resulting models are estimated as a state-space canonical representation in discrete Z domain with a sampling frequency of 0.001s and then converted to transfer functions. So, in a sense, these are average models which capture the essentials of closed-loop dynamical constraints.

Original: Param1 (NAhA=8, NChA=10, NAhK=9, NChK=11)

$$y_1(j\omega) = \frac{15(j\omega + 278)(j\omega + 69)}{(j\omega+65)((j\omega)^2+25(j\omega)+4592)}u_1(j\omega) + \frac{3(j\omega+342)(j\omega+14)}{(j\omega+65)((j\omega)^2+25(j\omega)+4592)}u_2(j\omega)\text{- 84 \% fit knee} \tag{4.6}$$

$$y_2(j\omega) = \frac{-77((j\omega)^2+43(j\omega)+1353)}{(j\omega+65)((j\omega)^2+25(j\omega)+4592)}u_1(j\omega) + \frac{70((j\omega)^2+28(j\omega)+5215)}{(j\omega+65)((j\omega)^2+25(j\omega)+4592)}u_2(j\omega)\text{- 69 \% fit ankle} \tag{4.7}$$

The original system is well fitted with a third order model. One of the poles is at -65 leading to 15 ms time constant. The remaining two poles are complex pair with natural frequency of the 68 rad/sec and damping of 0.2, which implies that the level of oscillation in the response will be large. In the numerator, all the zeros are in the left complex half plane. In $W_{21}$ transfer function, we have again two complex zeros which are closely located to the complex pole pair, but behind them as real values increasing the lag in the response. In $W_{22}$ transfer function, the second-order polynomial of the numerator matches the one in the denominator which causes their effect to be neglected and the oscillation in the ankle channel will be minimal.

For improved case: Param2 (NAhA=11, NChA=2, NAhK=11, NChK=11)

$$y_1(j\omega) = \frac{842((j\omega)^2+110(j\omega)+3379)}{(j\omega+804)\,((j\omega)^2+101(j\omega)+3052)}u_1(j\omega) + \frac{-39(j\omega-386)(j\omega-12)}{(j\omega+804)\,((j\omega)^2+101(j\omega)+3052)}u_2(j\omega) \quad \text{- 82\%fit knee} \tag{4.8}$$

$$y_2(j\omega) = \frac{-382((j\omega)^2+73(j\omega)+1498)}{(j\omega+804)\,((j\omega)^2+101(j\omega)+3052)}u_1(j\omega) + \frac{111(j\omega+43)(j\omega+591)}{(j\omega+804)\,((j\omega)^2+101(j\omega)+3052)}u_2(j\omega) \text{ - 79\%fit ankle} \tag{4.9}$$

In the improved controller (NAhA=11, NChA=2, NAhK=11, NChK=11), all hidden layer units are increased, as shown in the simulations earlier, which is equivalent to increasing the total feedback gain on both channels given the weights are randomly initialized. The poles at -804 make the dynamics on that channel far faster than the original controller (NAhA=8, NChA=10, NAhK=9, NChK=11), which could be expected in case of increased feedback gain. The complex pole pair is with natural frequency of 55 rad/sec, which is also decreased with respect to the original controller and damping of 0.9. This high value of damping makes the reaction of the improved controller without any oscillation or lower level of error compared to the original one where damping was 0.2.

This comparison between step response of both controllers can be observed in the next figure, Figure 4.4. In both cases, the correlation between both channels is minimized by the closed loop action. The most evident is the improvement in the ankle knee channel where the oscillatory response of the original controller is reduced.

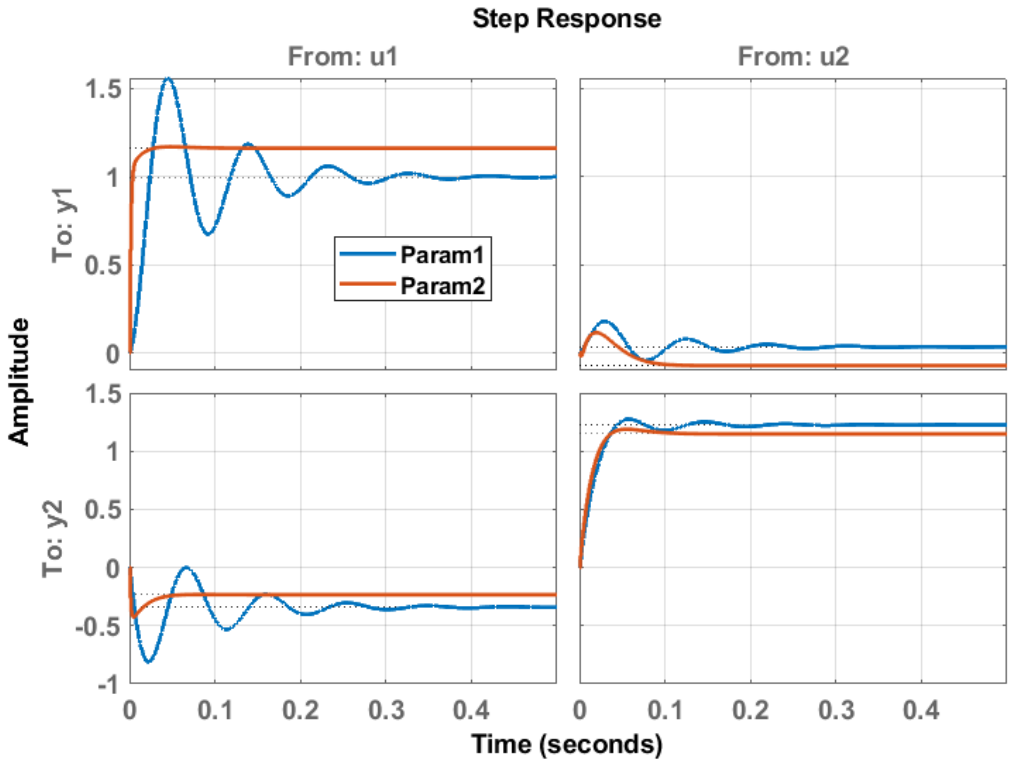


Figure 4.4 Step responses of the linear models of parameter sets from Table 4.1.

In section 4.2, the capacity of the critic and/or action networks will be increased by adding additional hidden layers, as well as learning from the exploration of different parameters with a focus to reduce error. Depending on the result with changing the activation function of the networks, the performance of the controller will be evaluated. It is expected that using recurrent NN will be advantageous, but it will require more time to program and tune as the process will end up as time-consuming.

## 4.2 Effect of NN hidden layer increment and relevant optimization

In this section, the critic and action network for both knee and ankle joints were extended from a single sigmoid-based feed-forward hidden layer to networks with two hidden sigmoidal layers. The number of neurons in each of the four networks (action ankle, critic ankle, action knee, critic knee) can be varied to improve the performance. However, we have 8 hyperparameters now – [NAhA_1, NAhA_2, NChA_1, NChA_2, NAhK_1, NAhK_2, NChK_1 and NChK_2], whereas in section 4.1 we worked with a single sigmoid consisting of 4 hyperparameters [NAhA, NChA, NAhK, NChK]. In order to accomplish that, the simulation code is modified to calculate the gradients and updates on the network cost function with respect to the first hidden layer.

As can be seen, the dimension of the parameter space is increased considerably with respect to the initial case, as presented in the previous section (having a single hidden layer on each network). So, by working in hyperspace with a higher dimension, a fine-tuning of the multivariate nonlinear function is defined with a particular network. Increasing the number of hidden layers or making the network deeper is a common approach to minimize loss and increase accuracy. However, finding the optimal parameter values to maximize the network performance is not achievable by simply expanding the network's capability and considering the different segments of the control system performing optimally. So many iterations are required, and hence 240 combinations among parameter values are examined. Again, the overall performance of the algorithm is evaluated with 4 signal errors (error_ankle, error_ankle_dot, error_knee, error_knee_dot) and their 2-norms. This allowed judging the performance of the system by four numbers representing the magnitude of these errors. All 240 iterations are recorded. The result is that with two hidden layers, there is around 15-20% improvement in the norms with respect to the

original case and around 3% compared with the improved case (from the previous result). However, we consider that 3% increment is too less for the large number of parameters introduced.

The angular displacement of the ankle and knee joints are evaluated. The following two figures compare the **desired** angular signal with the **original: Param1** (NAhA=8, NChA=10, NAhK=9, NChK=11) with the **improved: Param2** (NAhA=11, NChA=2, NAhK=11, NChK=11) and with the **Improved2: Param3** (NAhA_1=18, NAhA_2=21, NChA_1=8, NChA_2=20, NAhK_1=16, NAhK_2=15, NChK_1=22, NChK_2=27) signal; considering network with two hidden layers. The norm of the original: Param1 subtracted from the desired error is (3.0576, 31.5038, 2.3239,25.3380). The norm of the improvement: Param3 subtracted from the desired error is (2.9161, 26.1761, 1.2770,20.1386). The norm of the improved: Param2: subtracted from the desired error is (1.9918,22.9543,1.5950,20.5281). All these are shown in Figure 4.5. As can be seen, the ankle error norm decreases from 2.94 in the original to 2.91 in the single hidden layer network to 1.99 in the two hidden layers network. The improvement is most evident in the ankle angle, Fig 4.5(a), where the improved signal is closer to the reference.

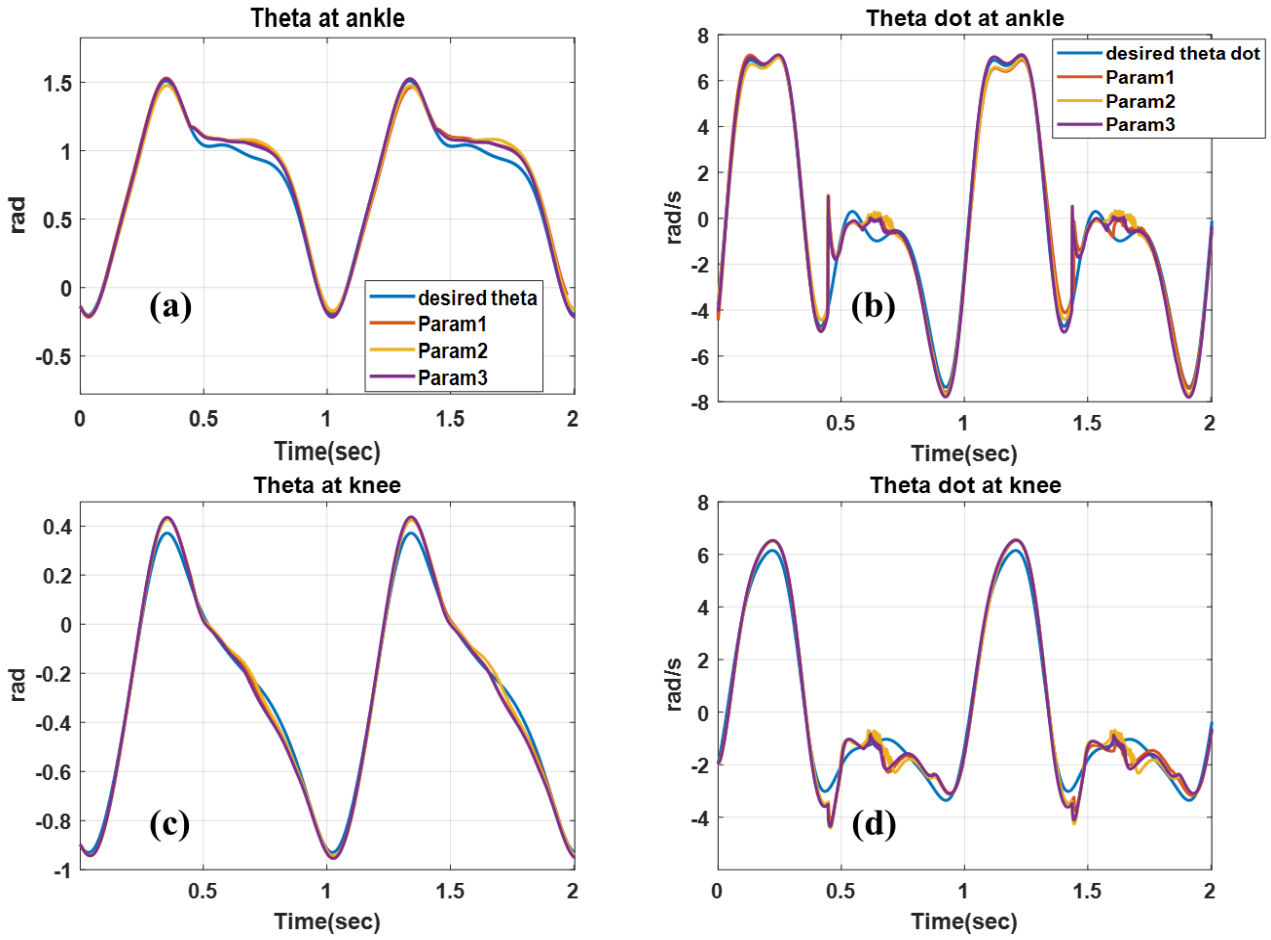


Figure 4.5 Improvement of angular velocity in ankle and knee as per observations from Table 4.2.

Table 4-2 Single sigmoid hidden layers cases with the best case of two sigmoid of hidden layers in action and critic networks, individually.

| **Run** | **NAhA** | **NChA** | **NAhK** | **NChK** | | | | |
|---|---|---|---|---|---|---|---|---|
| **Original:Param1** | 8 | 10 | 9 | 11 | | | | |
| **Improved:Param2** | 11 | 2 | 11 | 11 | | | | |
| | **NAhA_1** | **NChA_1** | **NAhK_1** | **NChK_1** | **NAhA_2** | **NChA_2** | **NAhK_2** | **NChK_2** |
| **Improved2:Param3** | 18 | 8 | 16 | 22 | 21 | 20 | 15 | 27 |

| **Run** | **Norm of the error** | | | |
|---|---|---|---|---|
| | **error_ankle** | **error_ankle_dot** | **error_knee** | **error_knee_dot** |
| **Original:Param1** | 2.9411 | 30.2673 | 1.9959 | 25.1505 |
| **Improved:Param2** | 2.9161 | 26.1761 | 1.2770 | 20.1386 |
| **Improved2:Param3** | 1.9918 | 22.9543 | 1.5950 | 20.5281 |

### 4.2.1 Controller linear analysis

Using the same linearization model, the NN hidden layer incremented model (termed as Improved_2) is presented below in equations (4.10) and (4.11). We see a similar response of fitting in the ankle, while the knee response has increased from 81%, from equation (4.8), to 84% fit as shown in equation (4.10). Figure 4.7 (a) shows the faster stabilization of the improved parameter set, comparing to Fig 4.4, while Figure 4.7 (b) shows the step response of this improvement comparing to the Param1 and Param2 as explained in Section 4.1.

NAhA_1=18, NAhA_2=21, NChA_1=8, NChA_2=20, NAhK_1=16, NAhK_2=15, NChK_1=22, NChK_2=27

$$y_1(j\omega) = \frac{3295.1(j\omega+25.81)(j\omega+55.86)}{(j\omega+2969)(j\omega+57.21)(j\omega+25.47)}u_1(j\omega) + \frac{10.888(j\omega-2.927)(j\omega+2511)}{(j\omega+2969)(j\omega+57.21)(j\omega+25.47)}u_2(j\omega)$$ - 84 % fit knee (4.10)

$$y_2(j\omega) = \frac{-561(j\omega+24.24)(j\omega+100.1)}{(j\omega+2969)(j\omega+57.21)(j\omega+25.47)}u_1(j\omega) + \frac{86.615(j\omega+20.98)(j\omega+2979)}{(j\omega+2969)(j\omega+57.21)(j\omega+25.47)}u_2(j\omega)$$ - 80 % fit ankle (4.11)

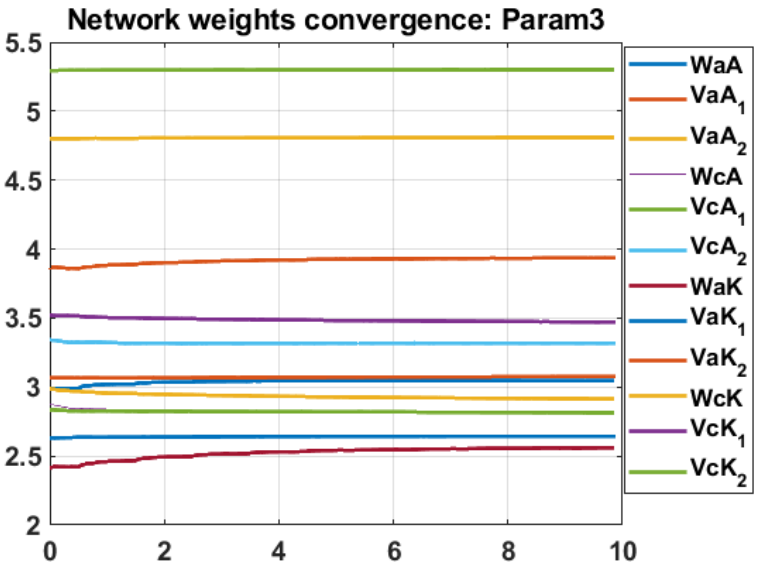


**(a)**

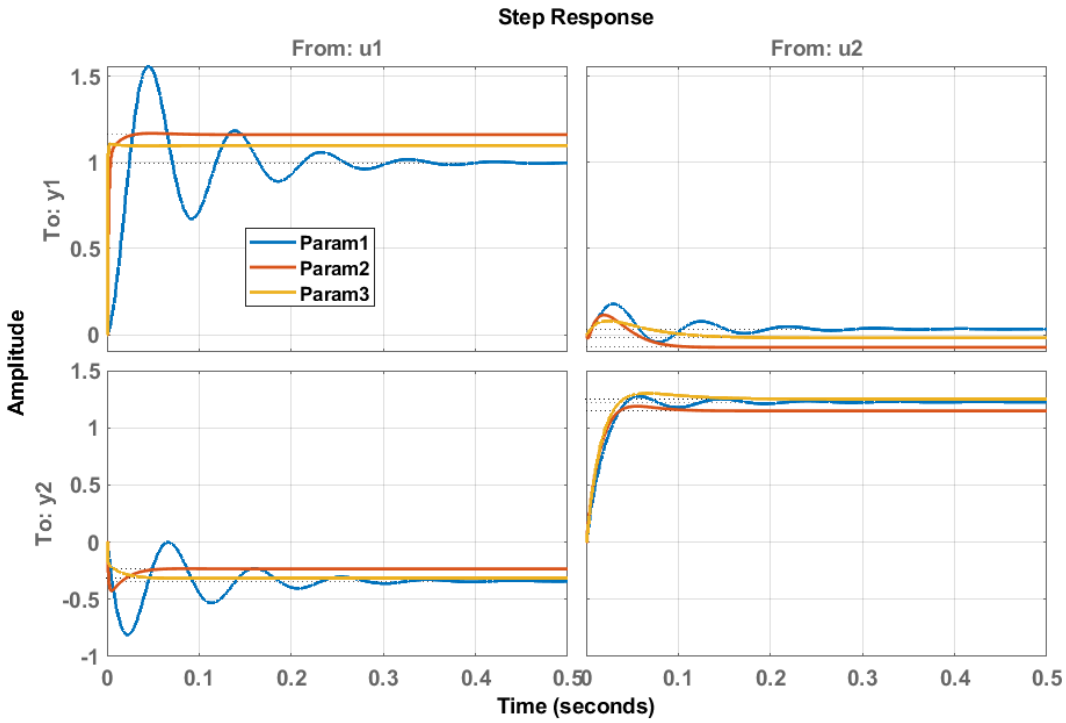


**(b)**

Figure 4.6 (a) The Frobenius norm of the model parameters - input and hidden layer weights of the improved parameter set 2, and (b) Step responses of the linear models of parameter sets from Table 4.2.

Comparing with the controllers from Sec. 4.1.1 (the Original and Improved), the transfer functions were composed of one real pole and one complex pole pair in the previous discussion. The transfer function of DNDP closed loop with two hidden layers is composed of three real poles, one of which is very far at -2979, which means its dynamics is 100 times faster than the other two which are located at -25 and -57. Hence the effect of this fast pole can be neglected except in the $W_{11}$ because there the two zeros compensate the poles in the denominator, and the fast pole is exposed. We have pure aperiodic processes without oscillation. The increase of the number of hidden layers increases the dimensionality of the hidden space, which allows performing more complex approximations. The pole drives the dominant dynamics at -25, which leads to time constant of 0.04 sec or a very fast reaction.

## 4.3 Investigation of the NN learning process to initial conditions of the hyperparameters

The learning process of the neural network is a dynamic optimization process which is based on gradient methods. Hence it is not enough to produce a minimizing solution of the cost function. In addition, it requires knowledge of how these solutions depend on data and/or assumptions. Sensitivity analysis allows assessing the effects of changes in the data values, effectively selecting the initial conditions, and enhancing the reliability. There are many ways to initialize the weight and biases of the neural network - zero initialization, random initialization etc. If all the weights or biases are initialized with 0, the derivative with respect to loss function is the same for every weight or bias value and all parameters will have the same value in subsequent iterations. Assigning random values to weights is better than just 0 (zero) assignment. However, if weights are initialized with large magnitudes and if the activation function is sigmoidal, as in this case, the input to activation function causes its output value to saturate at unity. Hence, it is

expected that the gradient changes slowly, and learning takes a lot of time. On the other hand, when the weights are initialized with low values (close to 0); there will be the “zero initialization” problem.

As examined from the simulation, the weight initialization, WaA = (rand (NAhA, 1)-0.5) *2; generates a random matrix with elements drawn from a uniform distribution ranging from -1 to 1. The function rand() uses the MATLAB random generator which is based on a pseudorandom sequence with a large enough period. However, the problem is that each time there is a slightly different result depending on the generator’s current state. So, to have reproducible results, we set the initial state of the random generator with the command rand (‘seed’, X0). The parameter X0 is a 32- bit unsigned integer number that can be fixed by the user input. However, a question arises whether the value X0 has a considerable impact on the achieved performance and result. Fixing X0 at particular value, a predefined set of parameters for the matrices is achieved WaA, VaA, WcA, VcA, WaK, VaK, WcK, VcK. The total number of hyperparameters is

Nparam =

NAhA+NAiA*NAhA+NCiA+NCiA*NChA+NAiK+NAiK*NAhK+NCiK+NCiK*NChK

To get different values for all the elements, the random generator state should be incremented with ‘Nparam’ such that X1 > X0 + Nparam. So, 130 trials have been run with the initial state of the random generator changed to 1000, which shifts the initial values of the parameters within a neighborhood in order to see the influence upon the performance of the closed-loop system. Again, we characterize performance of the system with a vector of four numbers, Perf = [Norm (ThetaA_Ref - ThetaA) Norm (Theta_Dot_A_Ref - Theta_Dot_A) Norm (ThetaK_Ref - ThetaK) Norm (Theta_Dot_K_Ref-Theta_Dot_K)]. Having smaller error and

output signals follow better the reference or desired signals, there will be smaller values in the vector performance.

Table 4-3 Changes in norm of initial states of network with changes in input initial, X0.

| Param set | Hidden network parameter | | | | | Norm of initial state of Network | | | | | | | |
|---|---|---|---|---|---|---|---|---|---|---|---|---|---|
| | NAhA | NChA | NAhK | NChK | X0 | WaA | VaA | WcA | VcA | WaK | VaK | WcK | VcK |
| 1 | 8 | 10 | 9 | 11 | 1000 | 1.8718 | 2.7665 | 2.0670 | 2.7348 | 1.5278 | 2.4535 | 1.9769 | 2.5724 |
| 1 | 8 | 10 | 9 | 11 | 4000 | 1.6830 | 1.8588 | 1.6895 | 2.4270 | 1.5449 | 2.2767 | 1.8797 | 2.3903 |
| 1 | 8 | 10 | 9 | 11 | 10000 | 1.6852 | 2.0742 | 2.0751 | 2.7259 | 1.7112 | 2.4246 | 1.7557 | 2.829 |
| 2 | 11 | 2 | 11 | 11 | 1000 | 2.0743 | 2.6775 | 0.96259 | 1.5115 | 2.249 | 1.9956 | 1.9523 | 2.545 |
| 2 | 11 | 2 | 11 | 11 | 4000 | 1.9566 | 2.0361 | 0.71062 | 1.1347 | 1.7698 | 2.5858 | 1.9558 | 2.2598 |
| 2 | 11 | 2 | 11 | 11 | 10000 | 1.7408 | 2.4664 | 1.0372 | 1.1368 | 2.1094 | 2.2093 | 1.9649 | 2.7586 |

Table 4-4 Effect of input initial, X0, on the error norm at joint angle and velocity.

| Param set | Hidden network param | | | | | Norm of the error | | | |
|---|---|---|---|---|---|---|---|---|---|
| | NAhA | NChA | NAhK | NChK | X0 | error_ankle | error_ankle_dot | error_knee | error_knee_dot |
| 1 | 8 | 10 | 9 | 11 | 1000 | 2.9411 | 30.2673 | 1.9959 | 25.1505 |
| 1 | 8 | 10 | 9 | 11 | 4000 | 2.1040 | 24.3676 | 1.5872 | 21.5751 |
| 1 | 8 | 10 | 9 | 11 | 10000 | 2.7493 | 30.9432 | 1.9312 | 22.1993 |
| 2 | 11 | 2 | 11 | 11 | 1000 | 2.2904 | 28.202 | 1.61078 | 20.9783 |
| 2 | 11 | 2 | 11 | 11 | 4000 | 2.34893 | 24.8138 | 1.47008 | 21.671 |
| 2 | 11 | 2 | 11 | 11 | 10000 | 2.63041 | 30.022 | 1.92229 | 22.5009 |

In previous section, there are two sets of parameter values for the number of neuron units in the hidden layer - the initial parameters Param1 = (NAhA=8; NChA=10; NAhK=9; NChK=11) and the best parameters Param2 or Improved case = (NAhA=11; NChA=2; NAhK=11; NChK=11). The comparisons were made for fixed state of the random generator X0 = 1000. In that case the norm of the initial state of the network for the Param1 set is [1.8718,2.7665,2.0670,2.7348,1.5278,2.4535,1.9769,2.5724] and for Param2 set is [2.0743,2.6775,0.96259,1.5115,2.249,1.9956,1.9523,2.545]. Then norm of the initial state is calculated as [norm (WaA), norm (VaA), norm (WcA), norm (VcA), norm (WaK), norm (VaK), norm (WcK), norm (VcK)].

Now the sensitivity of the performance will be compared for the initial parameters Param1 = (NAhA=8; NChA=10; NAhK=9; NChK=11) when X0 is changed from 1000 to 4000, and to 10000. In that case the norm of the initial state of the network for the X0=1000 is

[1.8718,2.7665,2.0670,2.7348,1.5278,2.4535,1.9769,2.5724], for X0=4000 set is [1.6830,1.8588,1.6895,2.4270,1.5449,2.2767,1.8797,2.3903], and for X0=10000 set is [1.6852,2.0742,2.0751,2.7259,1.7112,2.4246,1.7557,2.829]. As can be seen the change in the initial state is small enough. The performance at X0=1000 is Perf1 = [2.9411,30.2673, 1.9959,25.1505], the performance for X0=4000 is Perf2= [2.1877,24.7652,1.5400,21.1629], and the performance for X0=10000 is Perf3= [2.7493,30.9432,1.9312,22.1993]. Figure 4.7 represents the results for the Param1 set and X0 = 1000, 4000, and 10000. The error theta dot at knee error is bigger at the external points and smaller at the constant acceleration regions. The error in theta dot varies from 0.4 rad/s at the positive range and around 1.2 rad/s at the negative region. These errors are mapped to 0.05 rad and to 0.2 rad in the theta at knee signal. As can be seen it is managed to improve the error values on all coordinates only by changing the initial conditions, representing

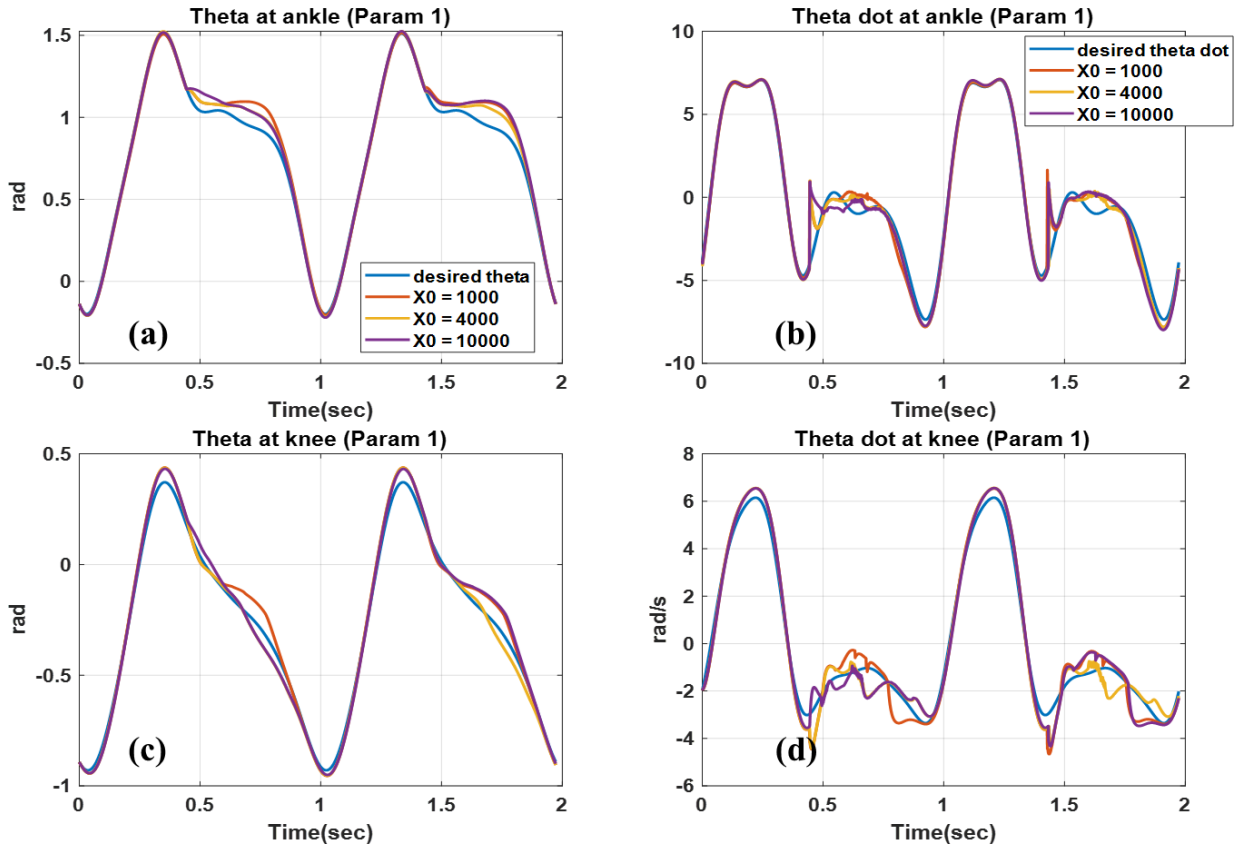


Figure 4.7 Joint angle and velocity tracking with initiation, X0 = 1000, 4000 and 10000 for hidden node values as Param1, tracking of (a) ankle angle, (b) ankle velocity, (c) knee angle, and (d) knee velocity.

the performance of the closed loop system with the initial network parameters for the number of hidden neurons and with changed initial state of the weights and biases.

Figure 4.8, represents the results for the Param2 set (from Table 4.3) and X0 = 1000. The error theta dot at knee error is bigger at the extremal points and smaller at the constant acceleration regions. The error in theta dot varies from 0.5 rad/s at the positive range and around 1 rad/s at the negative region. These errors are mapped to 0.05 rad and to 0.2 rad in the theta at knee signal. Theta dot at the ankle is tracked very well at its extremal points, and the largest errors

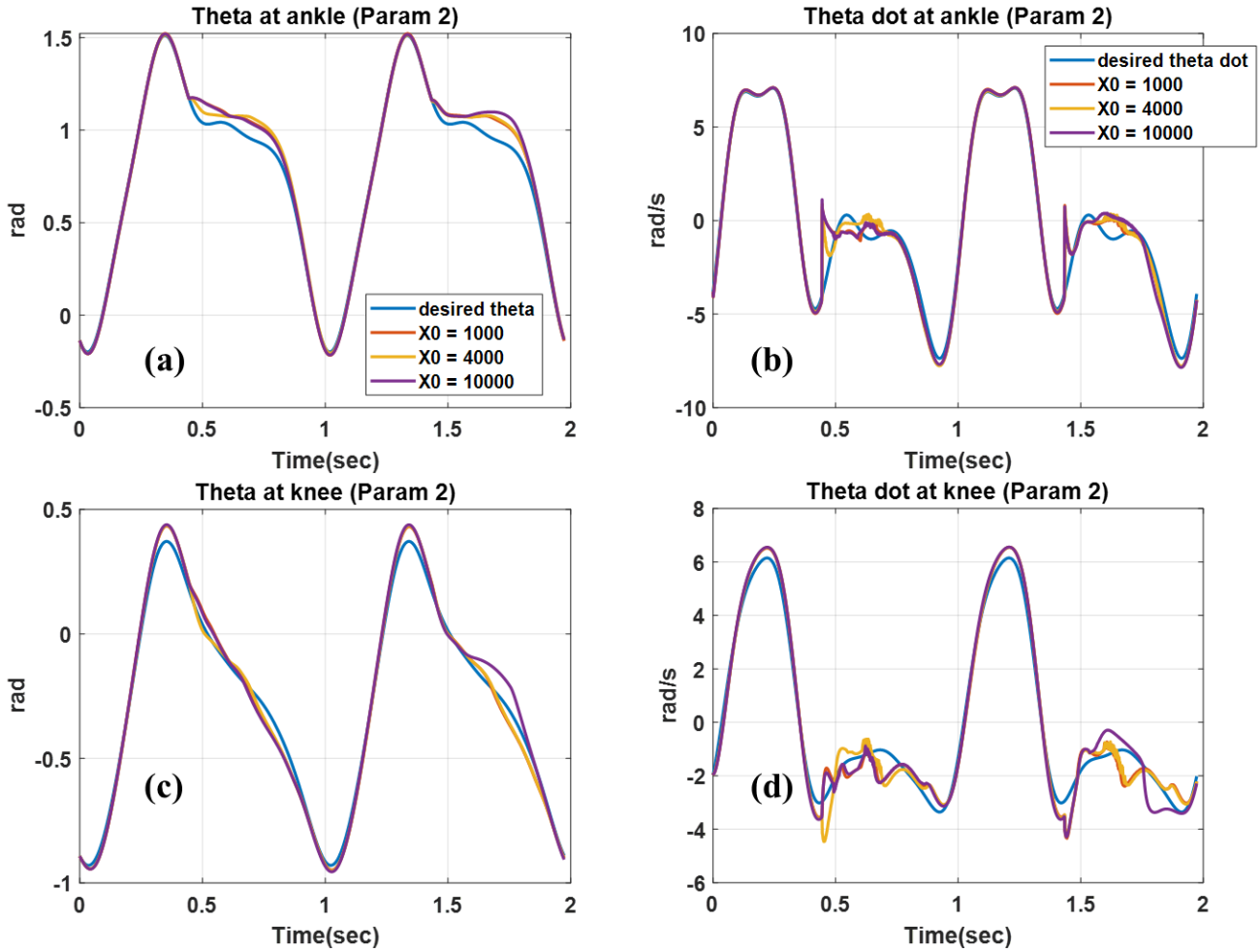


Figure 4.8 Joint angle and velocity tracking with initiation, X0 = 1000, 4000 and 10000 for hidden node values as Param2, tracking of (a) ankle angle, (b) ankle velocity, (c) knee angle, and (d) knee velocity.

appear around zero when the desired angular velocity goes for a short period above zero and drops quickly below. However, the actual theta dot goes in the opposite direction shortly after dropping below zero. The error there is around 1 rad/s. which is mapped to 0.1 rad in the theta at ankle signal. For comparing the sensitivity of the performance for the best parameters (NAhA=11, NChA=2, NAhK=11, NChK=11) when X0 is changed from 1000 to 4000 to 10000. In that case the norm of the initial state of the network for the X0=1000 is [2.0743,2.6775,0.96259,1.5115,2.249,1.9956,1.9523,2.545] and for X0=4000 is [1.9566,2.0361,0.71062,1.1347,1.7698,2.5858,1.9558,2.2598]. For X0=10000 set initial state is

[1.7408,2.4664,1.0372,1.1368,2.1094,2.2093,1.9649,2.7586]. As can be seen, Figure 4.8, the change is the initial state is small enough. The performance at X0=1000 is Perf1 = [2.2904,28.202,1.61078,20.9783], at X0=4000 Perf2 = [2.34893,24.8138,1.47008,21.671], and at X0=10000, Perf3 = [2.63041,30.022,1.92229,22.5009]. Next figure represents the results for the best param set and X0 = 10000.

Next, the sigmoidal activation function will be changed to tan-sig. Also, it will be interesting to compare the results of adaptive learning with the results of a pre-trained network. Since the biggest error is evident when the acceleration signal or torque is changing, a recurrent neural network can be designed for the action layer, which feedbacks the generated torque signal.

### 4.3.1 Controller linear analysis

As described and simulated earlier in this section, the resulting models are estimated as a state-space canonical representation (same as sections 4.1.1, and 4.2.1) in discrete Z domain with sampling frequency of 1KHz and then converted to transfer functions. So, in a sense, these are average models that capture the essentials of closed-loop dynamical constraints. Linear model fit improvements impacted by initialization value X0 variation for both Param1 and Param2, from Table 4.4, are presented below, including the step response comparison w.r.t X0 in Figure 4.10, and 4.11.

Param 1 (NAhA=8; NChA=10; NAhK=9; NChK=11)

X0 = 1000;

$y_1(j\omega) = \frac{68.315(j\omega+40.13)(j\omega+9.226)}{(j\omega+83.36)(j\omega+18.83)(j\omega+13.35)} u_1(j\omega) + \frac{24.436\ (j\omega-15.66)\ (j\omega+10.77)}{(j\omega+83.36)(j\omega+18.83)(j\omega+13.35)} u_2(j\omega)$ - 84 % fit knee (4.12)

$$y_2(j\omega) = \frac{68.421(j\omega+24.54)(j\omega+4.24)}{(j\omega+83.36)(j\omega+18.83)(j\omega+13.35)}u_1(j\omega) + \frac{53.112\ ((j\omega)^2+28.46(j\omega)+233.6)}{(j\omega+83.36)(j\omega+18.83)(j\omega+13.35)}u_2(j\omega)$$ - 74 % fit ankle (4.13)

X0 = 4000

$$y_1(j\omega) = \frac{74.434(j\omega+15.2)(j\omega+40.66)}{(j\omega+97.43)(j\omega+24.18)(j\omega+19.17)}u_1(j\omega) + \frac{20.554(j\omega-2.345)(j\omega+31.92)}{(j\omega+97.43)(j\omega+24.18)(j\omega+19.17)}u_2(j\omega)$$ - 86 % fit knee (4.14)

$$y_2(j\omega) = \frac{137(j\omega+3.563)(j\omega+13.15)}{(j\omega+97.43)(j\omega+24.18)(j\omega+19.17)}u_1(j\omega) + \frac{69.736((j\omega)^2+41.91(j\omega)+599.7)}{(j\omega+97.43)(j\omega+24.18)(j\omega+19.17)}u_2(j\omega)$$ - 84 % fit ankle (4.15)

X0 = 10000

$$y_1(j\omega) = \frac{184.44(j\omega+13.67)(j\omega+23.33)}{(j\omega+141.7)(j\omega+30.59)(j\omega+12.75)}u_1(j\omega) + \frac{-9.2961((j\omega)^2 - 5.277(j\omega) + 138.9)}{(j\omega+141.7)(j\omega+30.59)(j\omega+12.75)}u_2(j\omega)$$ - 87 % fit knee (4.16)

$$y_2(j\omega) = \frac{225.72(j\omega+13.32)(j\omega+0.1528)}{(j\omega+141.7)(j\omega+30.59)(j\omega+12.75)}u_1(j\omega) + \frac{11.741(j\omega+13.57)(j\omega+331.8)}{(j\omega+141.7)(j\omega+30.59)(j\omega+12.75)}u_2(j\omega)$$ - 75 % fit ankle (4.17)

The poles of the system are real at locations [-83 to -142], [-19 to -31] and [-12 to -19] depending on the random variation of the initial conditions. The relative locations of the poles are the same. As we proved in the last Section 4.2.1, the gain of the system is generally dependent on the number of structural parameters. In the next figures, Figure 4.9, we see the differences between transients given the variation in the initial conditions - some are more oscillatory than others and have on or another steady state value, but the settling time is approximately the same for all of them due to close locations of the respective poles.

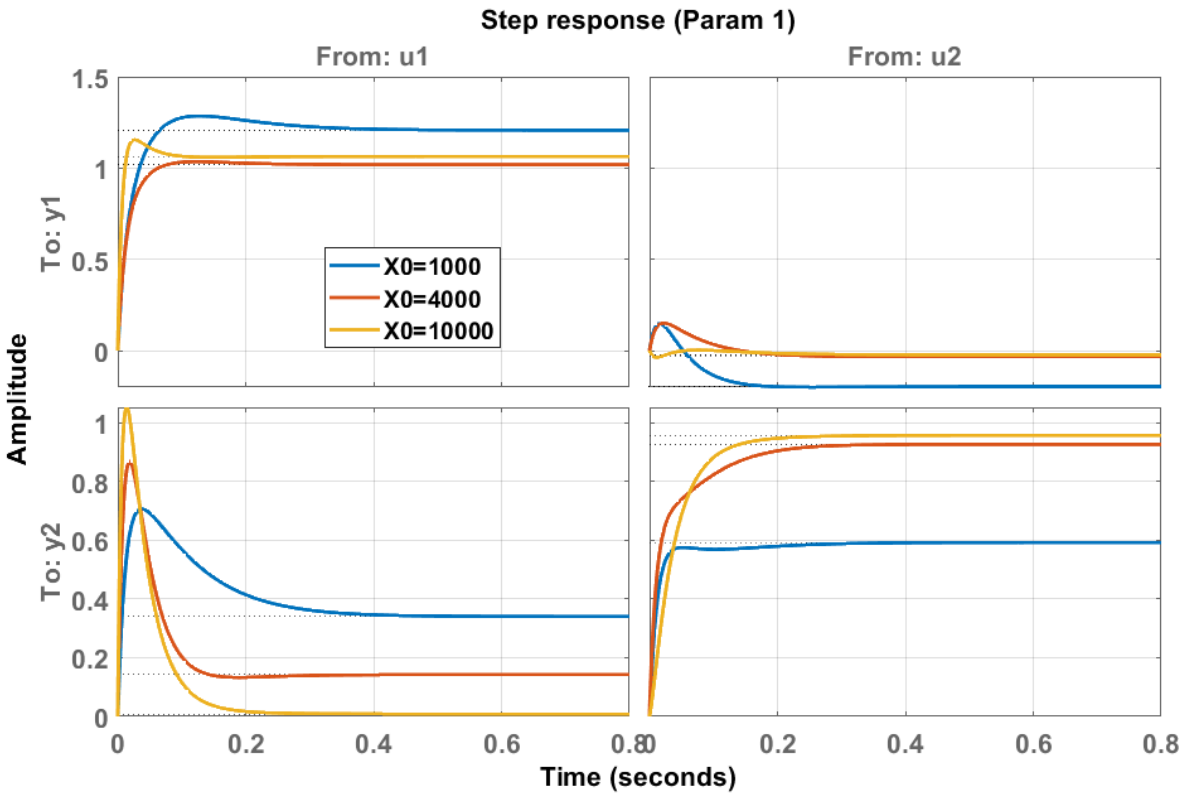


Figure 4.9 Step responses of the linear models of parameter sets from Table 4.4 (Param1).

Param 2 (NAhA=11;NChA=2;NAhK=11;NChK=11)

X0 = 1000;

$$y_1(j\omega) = \frac{286(j\omega+7)(j\omega+34)}{(j\omega+219)(j\omega+44)(j\omega+8)}u_1(j\omega) + \frac{-25(j\omega-23)(j\omega+9)}{(j\omega+219)(j\omega+44)(j\omega+8)}u_2(j\omega) \text{ - 86 \% fit knee} \quad (4.18)$$

$$y_2(j\omega) = \frac{358((j\omega)^2+12(j\omega)+52)}{(j\omega+219)(j\omega+44)(j\omega+8)}u_1(j\omega) + \frac{-4(j\omega-1802)(j\omega+7)}{(j\omega+219)(j\omega+44)(j\omega+8)}u_2(j\omega) \text{ - 78 \% fit ankle} \quad (4.19)$$

X0 = 4000

$$y_1(j\omega) = \frac{314(j\omega-1)(j\omega+46)}{(j\omega+321)(j\omega+57)(j\omega+2)}u_1(j\omega) + \frac{34(j\omega+9)(j\omega+130)}{(j\omega+321)(j\omega+57)(j\omega+2)}u_2(j\omega) \text{ - 81 \% fit knee} \quad (4.20)$$

$$y_2(j\omega) = \frac{401((j\omega)^2+9(j\omega)+72)}{(j\omega+321)(j\omega+57)(j\omega+2)}u_1(j\omega) + \frac{79(j\omega+0.7)(j\omega+205)}{(j\omega+321)(j\omega+57)(j\omega+2)}u_2(j\omega) \text{- 75 \% fit ankle} \quad (4.21)$$

X0 = 10000

$$y_1(j\omega) = \frac{158(j\omega+14)(j\omega+21)}{(j\omega+107)(j\omega+33)(j\omega+12)}u_1(j\omega) + \frac{-10((j\omega)^2-8(j\omega)+69)}{(j\omega+107)(j\omega+33)(j\omega+12)}u_2(j\omega)\text{- 87 \% fit knee} \quad (4.22)$$

$$y_2(j\omega) = \frac{199(j\omega+14)(j\omega+1)}{(j\omega+107)(j\omega+33)(j\omega+12)}u_1(j\omega) + \frac{5(j\omega+14)(j\omega+504)}{(j\omega+107)(j\omega+33)(j\omega+12)}u_2(j\omega)\text{- 75 \% fit ankle} \quad (4.23)$$

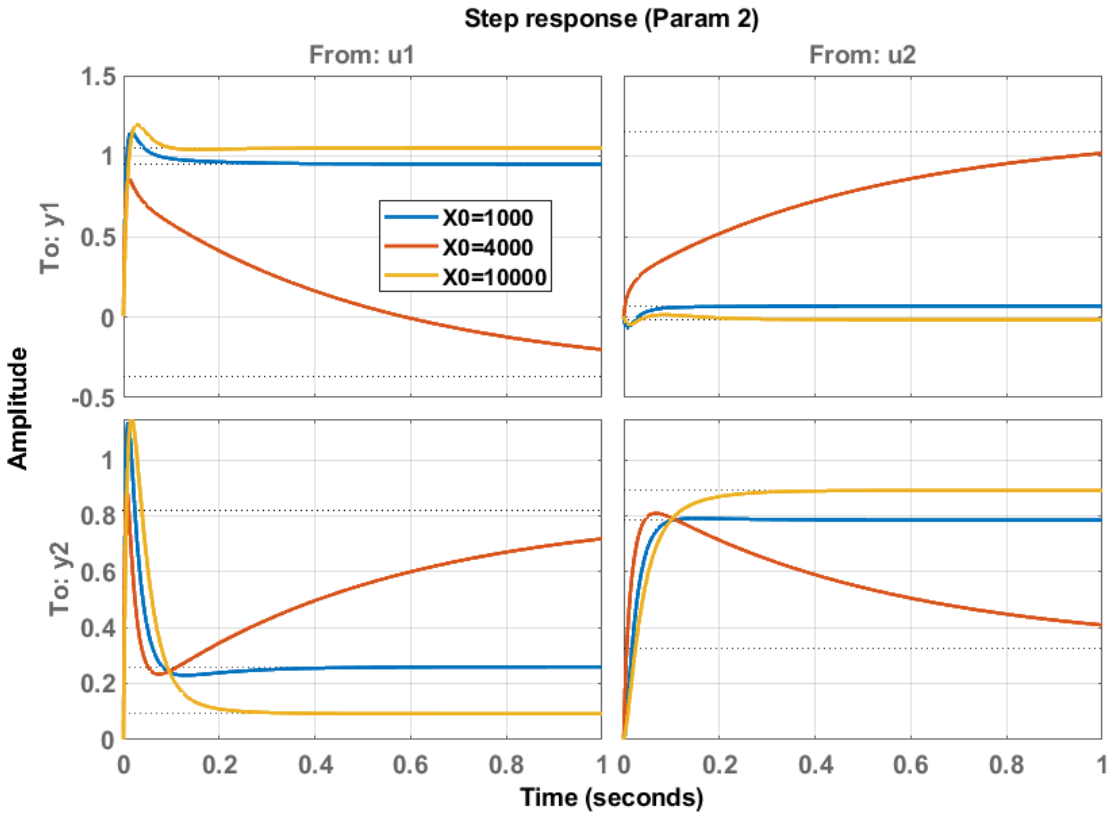


Figure 4.10 Step responses of the linear models of parameter sets from Table 4.4 (Param2).

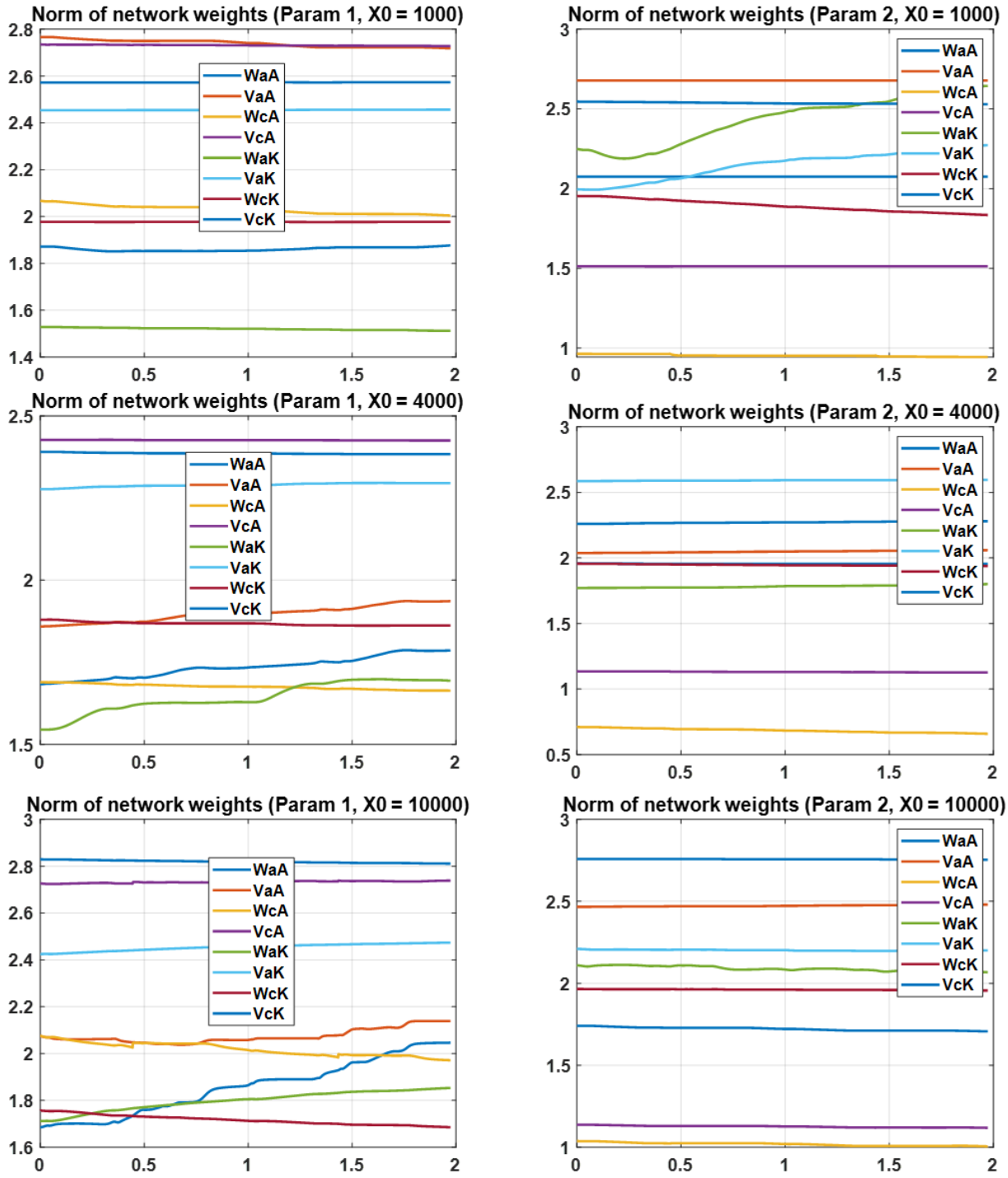


Figure 4.11 Network weight convergence, based on initialization X0.

The poles of the system are real at locations [-2 to -12], [-33 to -57] and [-107 to -321] depending on the random variation of the initial conditions. The relative locations of the poles are

the same. As we proved, in the last section, the gain of the system is generally dependent on the number of structural parameters. In the next figures, Fig 4.10, we see the differences between transients given the variation in the initial conditions – some are more oscillatory than others and have one or another steady-state value, but the settling time is approximately the same for all of them due to close locations of the respective poles.

On the other hand, the initial conditions change the behavior in the step response, for X0=4000, we have negative gain of $W_{11}$ and crossed sensitivity between channels due to large static gains in $W_{12}$ and $W_{21}$.

The difference between responses for Param 1 and Param 2 set is that can be seen in sensitivity to varying initial conditions of the network weights (Fig 4.11). In case with Param 2, its sensitivity is smaller due to smaller deviation observed mainly in $W_{21}$. Smaller sensitivity gives better predictability of network performances. Another way to state that is that increased dimension of the hidden layer leads to decreased sensitivity to the initial state of the random weight initializer.

## 4.4 Introduction of a centralized DNDP controller for synchronization

In the previous sections, certain limiting behavior of the control system is defined as two independent direct neural dynamic programming (DNDP) nodes working in parallel. The tracking performance of the ankle is improved but at the cost of tracking performance of the knee and reverse. So, to address this limiting behavior, a new level of control system called - a centralized DNDP controller is discussed in this section. The centralized controller produces a synchronization signal (**'Synk**' in the Figure 4.12) which is fed into dedicated ankle and knee controllers. The input of the synchronization controller are the tracking errors, XaL= $[\theta_a, \dot{\theta}_a, \theta_k, \dot{\theta}_k]$, at the ankle and at

the knee with respect to the reference angles. The cost function of the synchronization controller, SL, is thus formed as,

$$\text{SL} = -0.5\dot{\theta}_{,error}^{2} - 0.5\dot{\theta}_{k,error}^{2}$$

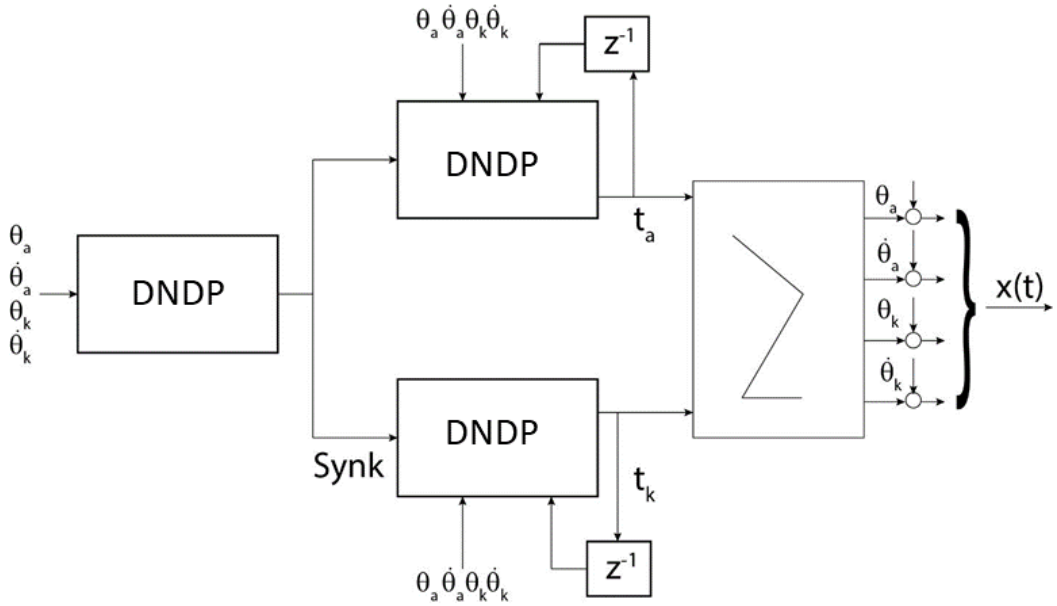


Figure 4.12 Centralized control system with synchronization signal (**Synk**) to both ankle and knee.

Again, for the local ankle and knee DNDP nodes, the recurrent configurations are used with local torque feedback from the previous variant. The idea of designing such a synchronization controller can be understood from a biological viewpoint. In the human body, the motor cortex is responsible for activating each individual joint whereas the premotor cortex is responsible for synchronization of the motion between joints. So, it seems natural to introduce this higher level of control. A relatively small random torque at the joints is presented in the next figure, Figure 4.13. The random torque term also occurs in the natural movement of humans, as there are terrain irregularities and external forces acting. White noise is with large bandwidth and the introduction of random torque helps to excite the full frequency spectrum of the underlying mechanical system.

So, this is a way to extract more information from the actual physical system, and thus the learning process of the DNDP networks is improved. In Figure 4.13, the $\mathbf{n_a}$ and $\mathbf{n_k}$ are the Gaussian random noises with unit variance. The variance can be tuned up and down depending on the effect upon the learning process. Also, when experimenting, it is good to get these random values from a predefined sequence to be sure. This can be achieved by setting the initial condition of the random number generator or saving the sequence to a file.

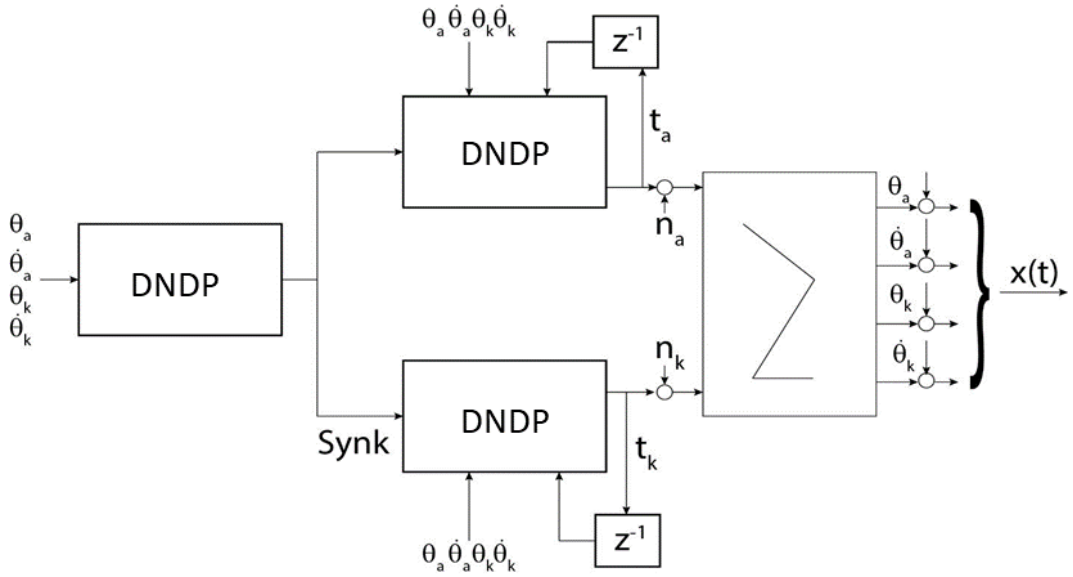


Figure 4.13 Centralized control system with synchronization signal (Synk) to both ankle and knee, with the presence of random torque $\mathbf{n_a}$ and $\mathbf{n_k}$ added to ankle and knee, respectively.

Around 250 experiments with different settings for the 6 tunable parameters NAhA - number of hidden layer neurons for the action network of the ankle, NChA - number of hidden layer neurons for the critic network of the ankle, NAhK - number of hidden layer neurons for the action network of the knee, NChK - number of hidden layer neurons for the critic network of the knee, NAhL - number of hidden layer neurons for the action synchronization network and, NChL - number of hidden layer neurons for the critic synchronization network is done. The tracking performance by the 2-norm of the ankle and knee angular errors is considered. First parameter set presented in this report is, Param1 =

[NAhA=11,NChA=2,NAhK=11,NChK=11,NAhL=30,NChL=1]. It is interesting to note that to achieve better tracking, we set the number of hidden layer neurons of the action synchronization network as relatively high, and the number of hidden layer neurons of the critic synchronization network is relatively small. The vector with errors for the Param 1 is [1.9645,22.7545,1.6980,22.4143] which comparing with experiments from the previous sections where the first error (the ankle angle) was never below 2.

The next interesting experiment is Param2 = [NAhA=11,NChA=2,NAhK=11,NChK=11,NAhL=36,NChL=5], where there is higher number of neuron in the action synchronization network and lower number of neurons in the critic synchronization network. The errors achieved with that settings are [1.8998,24.4013,1.6534,21.7345]. That param set is selected because the norm of tracking error is below 2 for the ankle. The following experiment is from the original system without the synchronization DNDP node, where Param 3 = [NAhA=11, NChA=2, NAhK=11, NChK=11] where resultant errors are [2.2904, 28.2020, 1.6108, 20.9783]. The norm of the ankle error is higher compared to results for Param 1 and Param 2. Next figure, 4.14 (a-e) presents a comparison among simulations with Param sets 1, 2 and 3.

Table 4-5 Comparison of three cases with added synchronization to action and critic networks, NahL and NChL, respectively.

| **2-cases with hidden network param** | | | | | | | **Norm of the error** | | | |
|---|---|---|---|---|---|---|---|---|---|---|
| **Param set** | **NAhA** | **NChA** | **NAhK** | **NChK** | **NAhL** | **NChL** | **error_ankle** | **error_ankle_dot** | **error_knee** | **error_knee_dot** |
| 1 | 11 | 2 | 11 | 11 | 30 | 1 | 1.9645 | 22.7545 | 1.6980 | 22.4143 |
| 2 | 11 | 2 | 11 | 11 | 36 | 5 | 1.8998 | 24.4013 | 1.6534 | 21.7345 |
| 3 | 11 | 2 | 11 | 11 | N/A | N/A | 2.2904 | 28.2020 | 1.6108 | 20.9783 |

Figure 4.14 presents the tracking results for Param1 and 2 along with no synchronization signal with respect to the reference signal (as per Table 4.5). The effect of the additional torque is

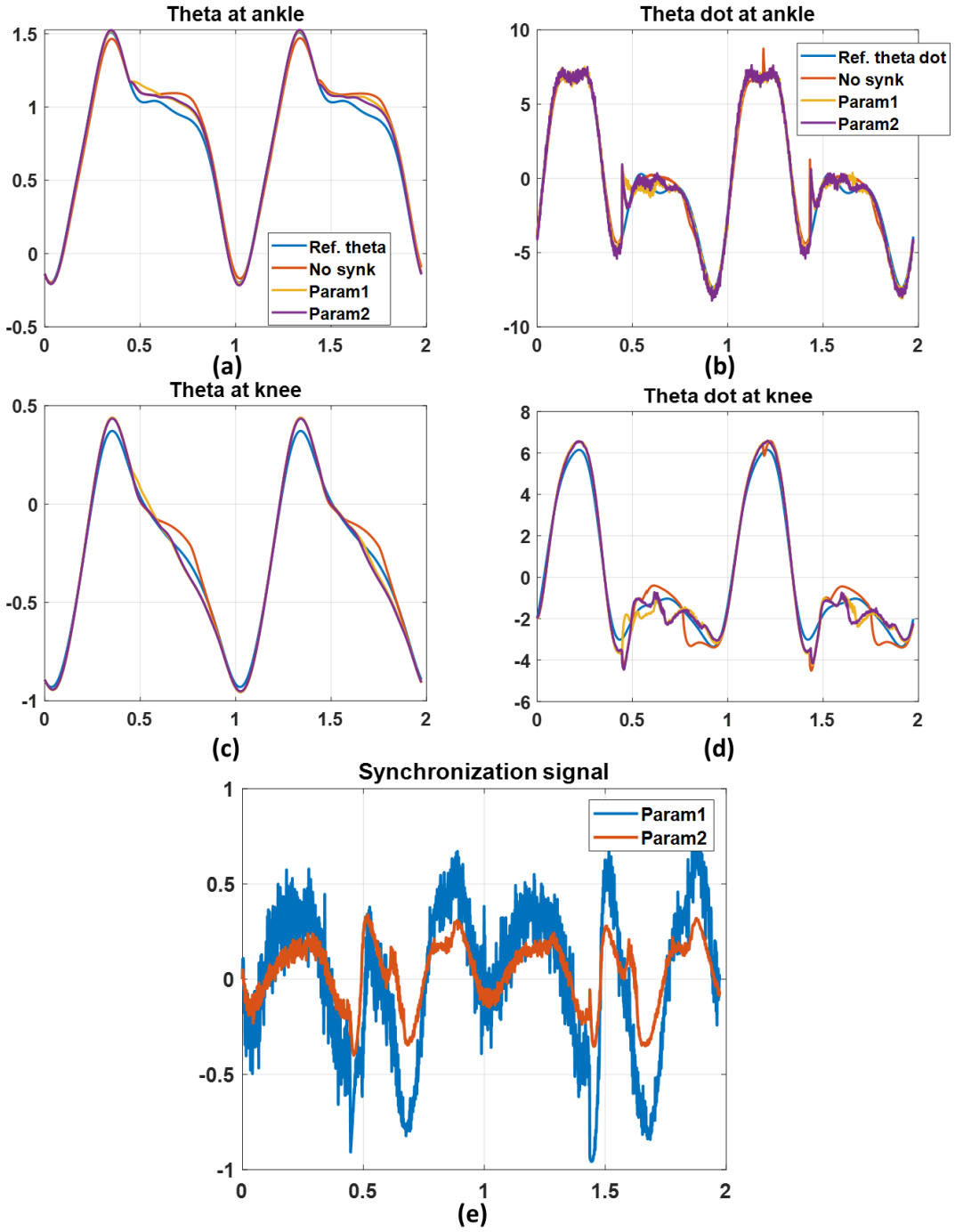


Figure 4.14 Performance of centralized DNDP network, comparison of 3 parameter sets from Table 4.5, with/without added synchronization to action-critics networks.

most evident in the angular velocity of the ankle which is expected because it has the smallest moment of inertia. The level of fit is improved to the reference, of course at the cost of increased random variation around it. Even the near zero region, which was problematic, is better tracked.

### 4.4.1 Controller linear analysis

The resulting models, as described and simulated earlier in this section, are estimated as a state-space canonical representation (same as sections 4.1.1, and 4.2.1) in discrete Z domain with sampling frequency of 0.001s and then converted to transfer functions. So, in a sense, these are average models that capture the essentials of closed-loop dynamical constraints.

Param 1 (NAhA=11;NChA=2;NAhK=11;NChK=11;NAhL=30;NChL=1)

$$y_1(j\omega) = \frac{61(j\omega+26)(j\omega+34)}{(j\omega+81)((j\omega)^2+40(j\omega)+627)}u_1(j\omega) + \frac{15(j\omega-7.4)(j\omega+26)}{(j\omega+81)((j\omega)^2+40(j\omega)+627)}u_2(j\omega)$$ - 87 % fit knee

(4.24)

$$y_2(j\omega) = \frac{109(j\omega+3.5)(j\omega+15)}{(j\omega+81)((j\omega)^2+40(j\omega)+627)}u_1(j\omega) + \frac{59((j\omega)^2+37(j\omega)+807)}{(j\omega+81)((j\omega)^2+40(j\omega)+627)}u_2(j\omega)$$ - 84 % fit ankle

(4.25)

A third-order model is used to approximate the dynamics of the closed-loop. In this approximation, one real pole exists at -6, which gives a time-constant around 0.01 sec, natural frequency of 25 rad/sec, and damping of around 0.8 which is higher than the original controller which was analyzed in Section 4.1. Hence, the only introduction of the centralized node causes some improvement in the damping, which generally leads to smaller oscillations and dynamic error. However, the dominant pole of the closed loop system is too close to the imaginary axis making the system response slow.

Param 2 (NAhA=11;NChA=2;NAhK=11;NChK=11;NAhL=36;NChL=5)

$$y_1(j\omega) = \frac{85(j\omega+12)(j\omega+50)}{(j\omega+107)(j\omega+48)(j\omega+11)}u_1(j\omega) + \frac{26(j\omega+2)(j\omega+48)}{(j\omega+107)(j\omega+48)(j\omega+11)}u_2(j\omega)\text{- 84 \% fit knee} \quad (4.26)$$

$$y_2(j\omega) = \frac{155(j\omega+4)(j\omega+16)}{(j\omega+107)(j\omega+48)(j\omega+11)}u_1(j\omega) + \frac{84(j\omega+15)(j\omega+41)}{(j\omega+107)(j\omega+48)(j\omega+11)}u_2(j\omega)\text{ - 84 \% fit ankle} \quad (4.27)$$

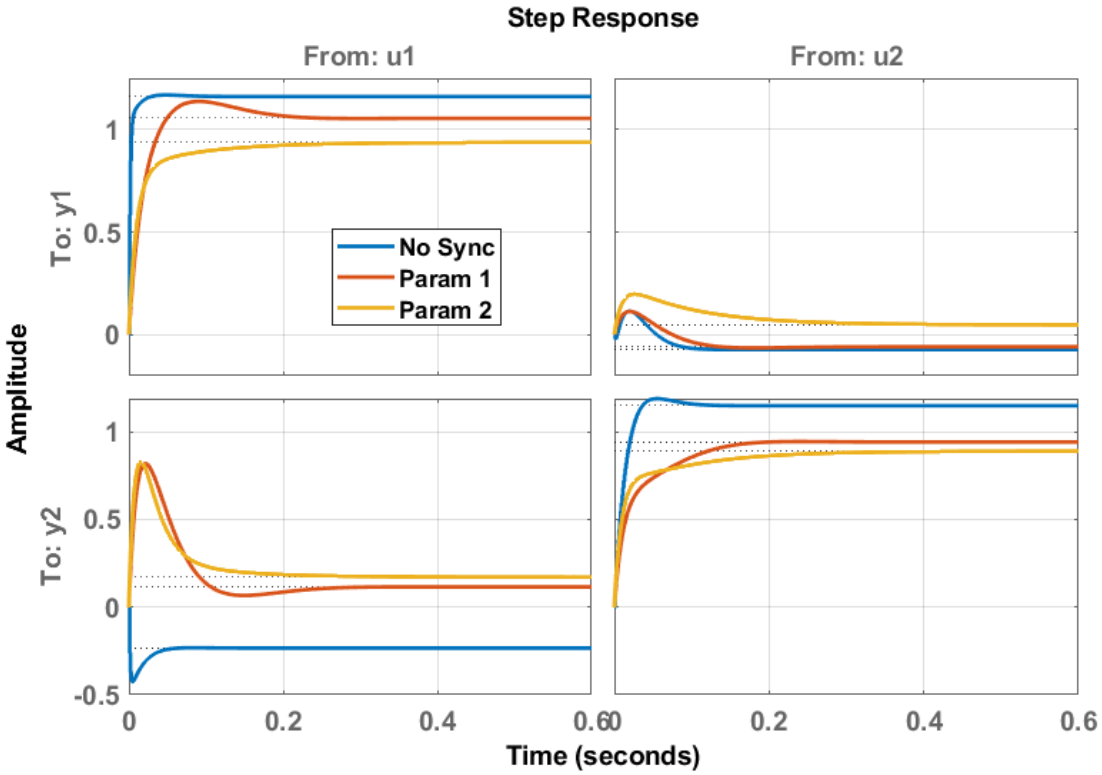


Figure 4.15 Step responses of the linear models of parameter sets from Table 4.5.

The step response of the two-parameter sets in the system with synchronization being added, is shown in Figure 4.15. With the increase of the number of elements in the hidden layer or the synchronization network, the real pole begins to shift left from -81 to -111 making its response faster in time. Also, the natural frequency of complex pair becomes real pair with poles at -48 and -11. Hence the processes are no longer oscillating but aperiodic.

## 4.5 Effect of centralized Neural Network distribution on Ankle and Knee Gait

An interesting and new development of the (so far) presented dynamic closed-loop control system is described below, where the distributed structure with two DNDP systems is substituted with a single centralized DNDP. The structure is shown in Figure 4. 16. motivation for this decision is the observation that when having separate controllers, some limitation is observed in closed-loop performance where when improving tracking performance of one joint leads to degraded tracking performance in the other joint. According to the DNDP structure, we have an action network and a critic network. The action network is responsible for producing the current torque as a function of the current state.

Torque from DNDP:

$$\tau = W_{act}\sigma(V_{act}X_{act}(t)) + u(t) \qquad W_{act} \in R^{NAhC\times 2} \qquad V_{act} \in R^{8\times NAhC} \tag{4.28}$$

And the critic network tries to optimize the performance of the action network expressed with the total future cost R(t). However, since the R(t) is unobservable and its approximation J(t) - the output of the critic network. The hyperparameters of the critic network are optimized with respect to minimizing the prediction error between R(t) and J(t). The inputs to the action network are the angular position and angular velocities of the joints together with the reference tracking error. However, in this case, the output of the action network is the ankle and knee torque.

Input to action network:

$$X_{act}(t) = (e_a(t), \dot{e}_a(t), \theta_a(t), \dot{\theta}_a(t), e_k(t), \dot{e}_k(t), \theta_k(t), \dot{\theta}_k(t))^T \tag{4.29}$$

Input to critic network:

$$X_{crit}(t) = (X_{act}(t)^T, \tau^T)^T \tag{4.30}$$

Estimate of the cost function:

$$J(t) = W_{crit}\sigma(V_{crit}X_{crit}(t)) \tag{4.31}$$

Error of critic network:

$$e_{crit}(t) = (J(t - T_S) - S(t)) - \alpha J(t) \tag{4.32}$$

Error terms:

$$e_a(t) = r_a(t) - \theta(t), \tag{4.33a}$$

$$\dot{e}_a(t) = \dot{r}_a(t) - \dot{\theta}_a(t) \tag{4.33b}$$

$$e_k(t) = r_k(t) - \theta(t) \tag{4.33c}$$

$$\dot{e}_k(t) = \dot{r}_k(t) - \dot{\theta}_k(t) \tag{4.33d}$$

Error of the action network:

$$e_{act}(t) = -J(t) \tag{4.34}$$

Gradient of the cost with respect to input torque for the critic network:

$$\partial J/\partial\tau = 0.5V_{crit}W_{crit}(1 - \sigma^2(V_{crit}X_{crit}(t)))E_\tau \quad E_\tau = (0_{2,6}, I_2)^T \tag{4.35}$$

Weight updates, critical network

$$\Delta W_{crit} = -F_{crit}\sigma(V_{crit}X(t))e_{crit}(t)\sigma(V_{crit}X(t)) - K_{reg}\sigma(V_{crit}X(t))\sqrt{e_{crit}(t)}W_{crit} \tag{4.36}$$

$$\Delta V_{crit} = -e_{crit}(t)X_{crit}(t)G(W_{crit}0.5(1 - \sigma(V_{crit}X_{crit}(t)))) - K_{reg}G\sqrt{e_{crit}(t)}V_{crit} \tag{4.37}$$

Weight updates

$$\Delta W_{act} = -\partial J/\partial\tau\, F_{act}\sigma(V_{act}X(t))e_{act}(t)\sigma(V_{act}X(t)) - K_{reg}\sigma(V_{act}X(t))\sqrt{e_{act}(t)}W_{act} \tag{4.38}$$

$$\Delta V_{act} = -\partial J/\partial\tau\, e_{act}(t)X_{act}(t)G(W_{act}0.5(1 - \sigma(V_{act}X_{act}(t)))) - K_{reg}G\sqrt{e_{act}(t)}V_{act} \tag{4.39}$$

Applying updates:

$$W_{crit}(t) = W_{crit}(t - T_S) + 0.0025\Delta W_{crit} \tag{4.40}$$

$$V_{crit}(t) = V_{crit}(t - T_S) + 0.0025\Delta V_{crit} \quad (4.41)$$

$$W_{act}(t) = W_{act}(t - T_S) + 0.0025\Delta W_{act} \quad (4.42)$$

$$V_{act}(t) = V_{act}(t - T_S) + 0.0025\Delta V_{act} \quad (4.43)$$

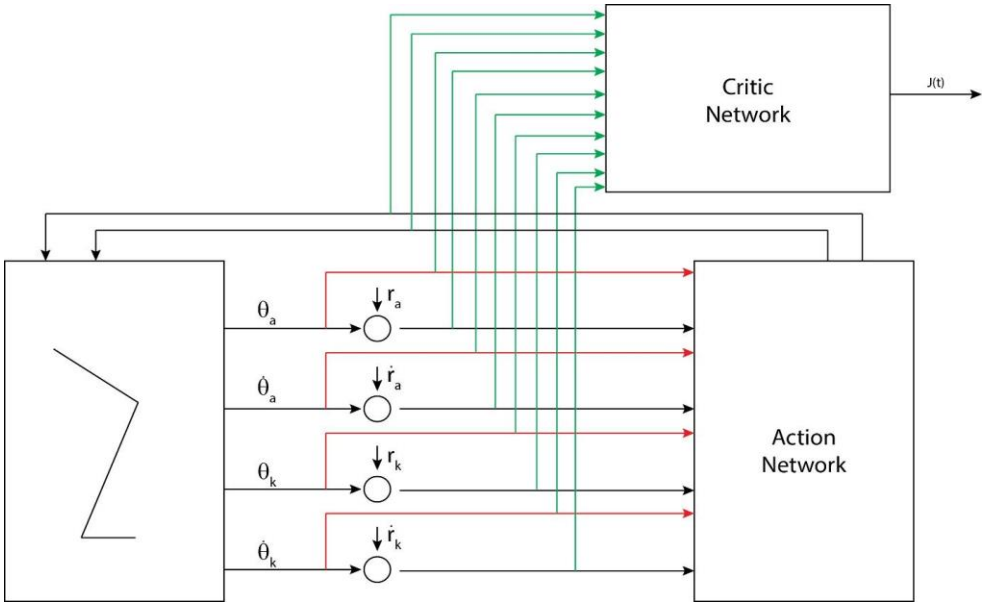


Figure 4.16 Distributed DNDP system with separate controllers for Ankle and knee,

Figure 4.16 presents the proposed control structure as in this section. Both networks are generalized from the standard single-input single-output DNDP model. The action network is constructed as a sigmoidal input layer with 8 inputs and a hidden layer with NAhC neurons. The critic network is constructed as an input sigmoidal layer with 10 inputs and a hidden layer with NChC neurons. For the presented experiments, three parameters - NAhC, NChC and the initial seed of the random generator are tuned. Previously, the initial conditions of the matrix lead to a large deviation in the tracking performance. This can be explained from the employment of the gradient descent method, which guarantees the determination of the local extreme. However, can easily miss a global extreme if the cost function is non-convex. The tracking performance is evaluated again with the 2-norm of the angular errors - [Norm(ref_a - ank) Norm(ref_a_dot - ank_dot) Norm(ref_k - knee) Norm(ref_k_dot - knee_dot)] during 2 sec period. Around 200 tuning

of the parameters have been tested. Below results, as in Table 4.6 and Figure 4.17, are presented and compared (three of the results which give best performance). For Param 1, NahC = 18, NChC = 4 and initial random generator seed is 5000. The obtained error norms are [1.8252, 27.8556, 1.6540, 20.2595]. For Param 2 where NAhC is 18, NChC is 49 and initial seed of the random generator is 5000. The error norms are as follows [3.2069, 27.2515, 1.1388, 15.9213]. This is an interesting case because a very low level is reached at the knee angular position and angular velocity however at the cost of increased error at the ankle joint. For Param 3 where NAhC is 18, NChC is 37, and initial seed of the random generator is 4012; the error norms are as follows [1.3734, 26.3890, 2.3723, 28.1191]. This case is kind of opposite to the simulation with Param 2 because it is low error at the ankle angular position and angular velocity, but relatively elevated errors in the knee joint. Hence, this limiting property observed with the distributed system is still present in a centralized system. However, it is a bit more attenuated since it is a combination of parameters and initial conditions, which lead to better balance in the tracking performance, as shown in comparative plots in Fig 4.17. In addition, the comparative improvement from Section 4.1 with hidden neurons in ankle and knee, Param1 set, is also presented in the Table 4.6 and the ankle/knee angle/velocity tracking plots.

Table 4-6 Comparison of three cases with centralized DNDP control.

| **Hidden network param** | | | | **Norm of the error** | | | |
|---|---|---|---|---|---|---|---|
| **Param set** | **NAhC** | **NChC** | **X0** | **error_ankle** | **error_ankle_dot** | **error_knee** | **error_knee_dot** |
| **Original**: Section 4.1: Param1 (NAhA=8, NChA=10, NAhK=9, NChK=11 | | | | 2.9411 | 30.2673 | 1.9959 | 25.1505 |
| 1 | 18 | 4 | 5000 | 1.8252 | 27.8556 | 1.6540 | 20.2595 |
| 2 | 18 | 49 | 5000 | 3.2069 | 27.2515 | 1.1388 | 15.9213 |
| 3 | 18 | 37 | 4012 | 1.3734 | 26.3890 | 2.3723 | 28.1191 |

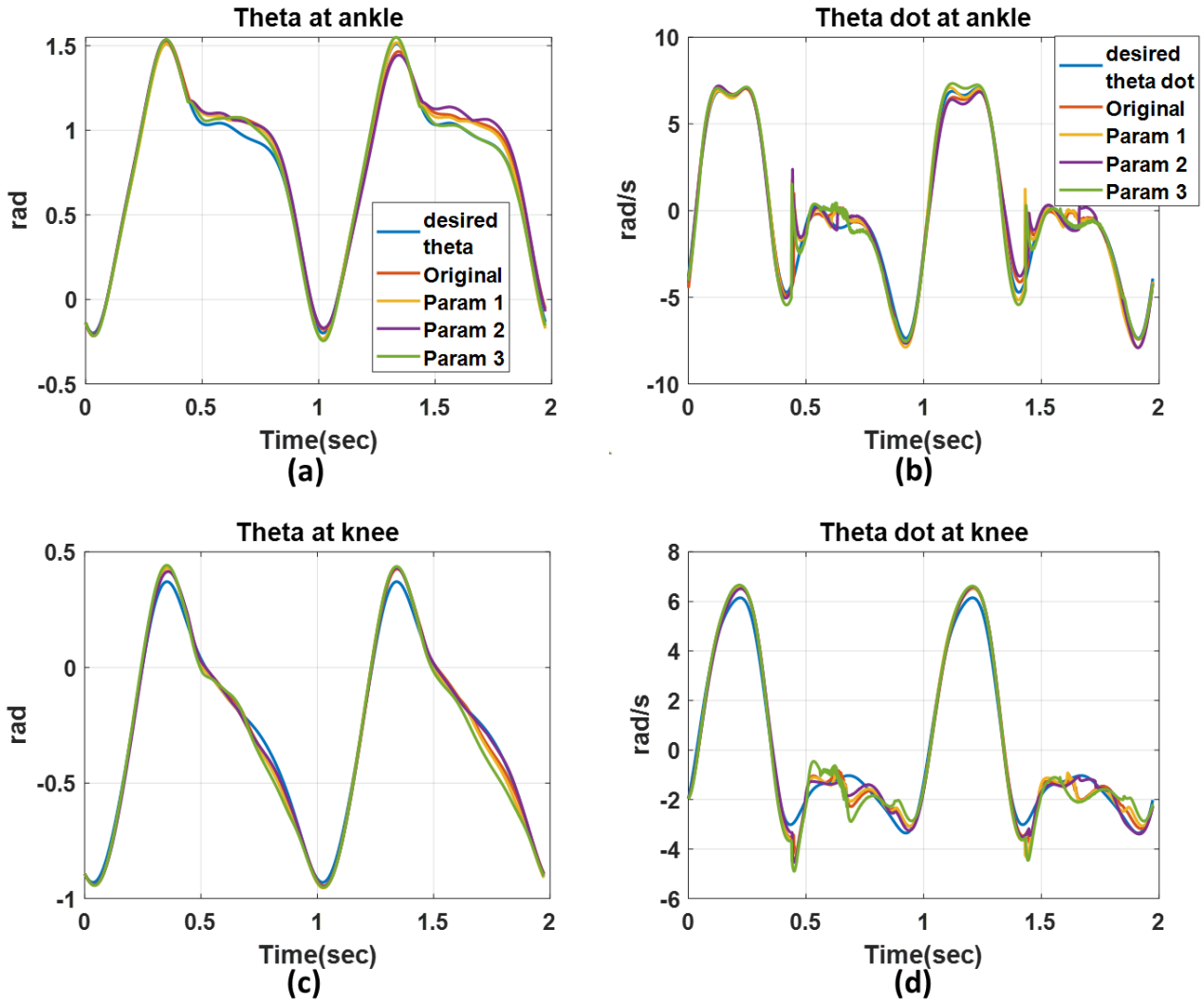


Figure 4.17 Effect of centralized DNDP control system (comparison among three parameter sets from Table 4.6): tracking of (a) ankle angle, (b) ankle velocity, (c) knee angle, and (d) knee velocity.

### 4.5.1 Controller linear analysis

The resulting models are estimated as a state-space canonical representation (same as sections 4.1.1, and 4.2.1) in discrete Z domain with sampling frequency of 0.001s and then converted to transfer functions. So, in a sense, these are average models that capture the essentials of closed-loop dynamical constraints.

Param 1 (NAhC=18, NChC=4, Xrnd=5000)

$$y_1(j\omega) = \frac{133.39((j\omega)^2+98.24(j\omega)+3916)}{(j\omega+102.1)((j\omega)^2+51.98(j\omega)+4231)}u_1(j\omega) + \frac{-23.826((j\omega)^2-24.25(j\omega)+2190)}{(j\omega+102.1)((j\omega)^2+51.98(j\omega)+4231)}u_2(j\omega)$$ - 85 % fit knee (4.44)

$$y_2(j\omega) = \frac{-139.35((j\omega)^2+7.64(j\omega)+951.4)}{(j\omega+102.1)((j\omega)^2+51.98(j\omega)+4231)}u_1(j\omega) + \frac{92.772((j\omega)^2+60.1(j\omega)+5664)}{(j\omega+102.1)((j\omega)^2+51.98(j\omega)+4231)}u_2(j\omega)$$ - 77 % fit ankle (4.45)

It is interesting to see that it is needed in this model to increase the order of the linear approximation model to third, i.e. adding one additional real pole that makes the closed-loop dynamics more complex. This complexity is related to higher order error terms in tracking performance. For Param 1, we have a real pole at -102 or time-constant around 0.01 sec. Also, the model is characterized by an oscillatory mode with natural frequency around 65 rad/sec and damping around 0.4. So that oscillation will be quite evident in data. Also, on all the channels, the Param1 model is characterized by complex zeros.

Param 2 (NAhC=18, NChC=49, Xrnd=5000)

$$y_1(j\omega) = \frac{107.3(j\omega+57.41)(j\omega+24.55)}{(j\omega+24.87)((j\omega)^2 + 129.2(j\omega) + 5551)}u_1(j\omega) + \frac{23.53(j\omega+23.52)\,(j\omega-8.416)}{(j\omega+24.87)((j\omega)^2 + 129.2(j\omega) + 5551)}u_2(j\omega)$$ – 90 % fit (4.46)

$$y_2(j\omega) = \frac{-30.211((j\omega)^2 + 9.155(j\omega) + 1138)}{(j\omega+24.87)((j\omega)^2 + 129.2(j\omega) + 5551)}u_1(j\omega) + \frac{42.001(j\omega+88.31)(j\omega+41.18)}{(j\omega+24.87)((j\omega)^2 + 129.2(j\omega) + 5551)}u_2(j\omega)$$- 73 % fit (4.47)

With the increase of the hidden layer critic network elements from 4 to 49, the linear approximation model changes. The real pole is slowed down from -102 to -25, corresponding to a time-constant of 40ms. Also, the oscillating poles' natural frequency is increased to 75 rad/sec and damping is increased to 0.86. So, with the radical increase of the total gain of the critic network, we can relatively expect a more dampened response with less overshot. This is because the critic network is focused on minimizing long-term system error.

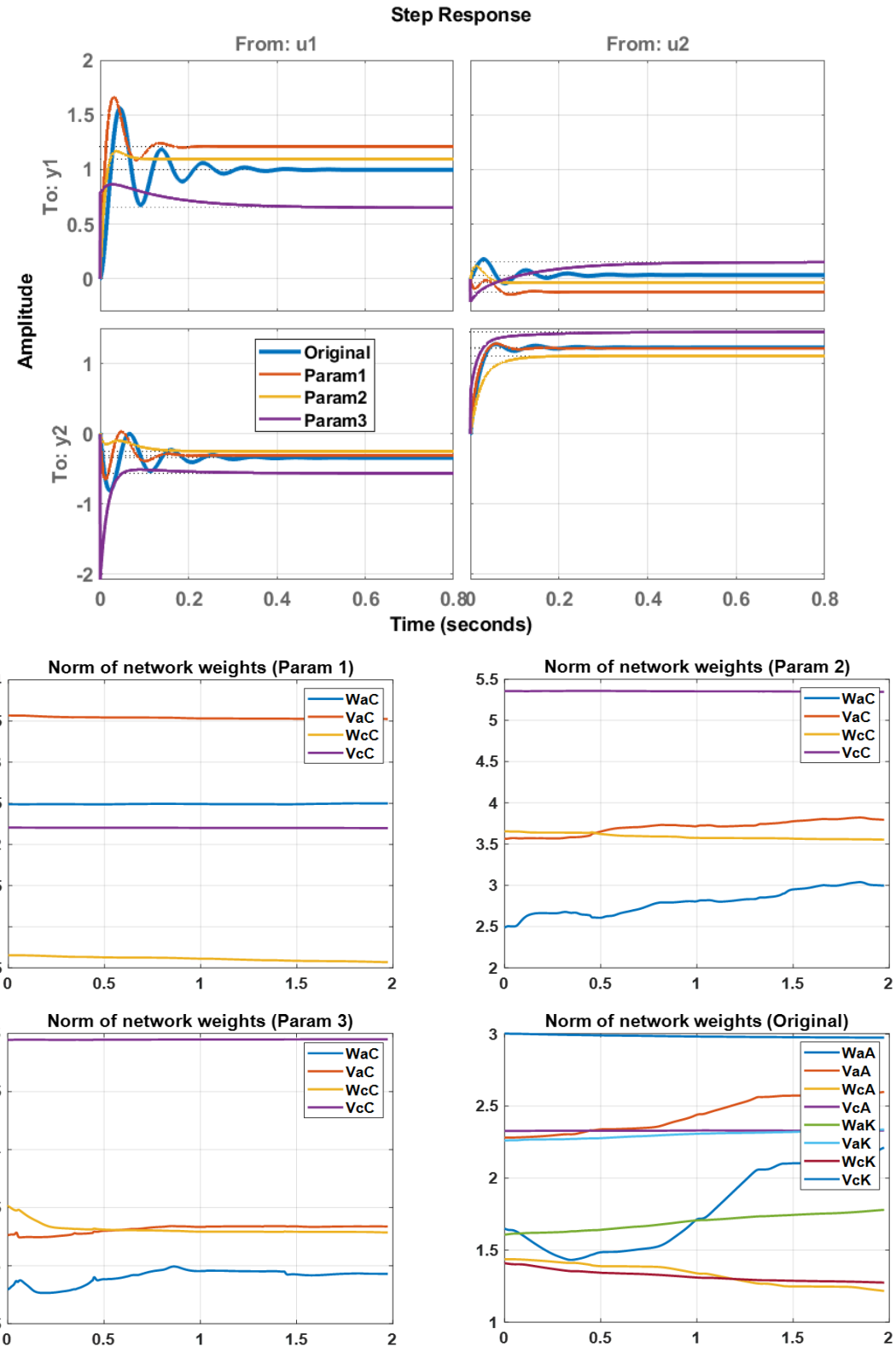


Figure 4.18 a) Step responses of the linear models of parameter sets from Table 4.6. b) Weight convergence of three parameters along with original parameter.

Param 3 (NAhC=18,NChC=37,Xrnd=4012)

$$y_1(j\omega) = \frac{20346(j\omega+7.19)(j\omega+78.27)}{(j\omega+25920)(j\omega+64.63)(j\omega+7.986)}u_1(j\omega) + \frac{-5584.4(j\omega-1.168)(j\omega+45.34)}{(j\omega+25920)(j\omega+64.63)(j\omega+7.986)}u_2(j\omega)$$ - 68 % fit

(4.48)

$$y_2(j\omega) = \frac{-56632(j\omega+9.387)(j\omega+13.74)}{(j\omega+25920)(j\omega+64.63)(j\omega+7.986)}u_1(j\omega) + \frac{15647(j\omega+8.344)(j\omega+145)}{(j\omega+25920)(j\omega+64.63)(j\omega+7.986)}u_2(j\omega)$$ - 63 % fit

(4.49)

Also, for Param 3 with varying the random generator, we can achieve fully aperiodic behavior of the linear approximation model by obtaining three real poles instead of complex conjugate poles. In Figure 4.18, we can compare the step response of the linear models (constant of 1 is set to one of the inputs while the other input is held zero). As expected, the reference on the first channel (ankle) is most strongly reflected in the first output (ankle) and the reference on the second channel (knee) is dominantly reflected in the second (knee) output. While the figure allows comparing the models with respect to their linear dynamics.

## 4.6 Effect of centralized Neural Network distribution with integral angular error control

At this stage, the structure will be extended as a single unified DNDP network with additional channels that account for the integral joint angular error. The action network has 10 inputs - ankle angular velocity, ankle angular position, ankle angular velocity error, ankle angular position error, integral of ankle angular position error, knee angular velocity, knee angular position, knee angular velocity error, knee angular position error and integral of knee angular position error. These two integral error terms are included in the network input in comparison with the previous experiments. A common technique in control is to include information about integral errors to improve the accuracy of the closed-loop system in addition to stability. The outputs of the action network are torque for both ankle and knee joints. The critic network has 12 inputs - all

10 inputs of the action network and two torque control inputs from the action network output layer. The critic network output is the approximation J(t) of the weighted future cost function, $R(t) = (t) + \alpha r(t+1) + \alpha^2 r(t+2) + \ldots$. Action network and critic network are composed of a single hidden layer respective with NAhC and NChC number of sigmoidal units. Action network weights are tuned with respect to minimizing the approximation J(t) of the cost function, and the critic network weights are tuned with respect to minimizing the approximation error between J(t) and R. However, after careful examination of the control model it is observed that the original structure includes additional feedforward and PD feedback terms which also can be tuned. This PD feedback will have strong influence upon the controller performance, and the sensitivity to its parametrization will be examined next.

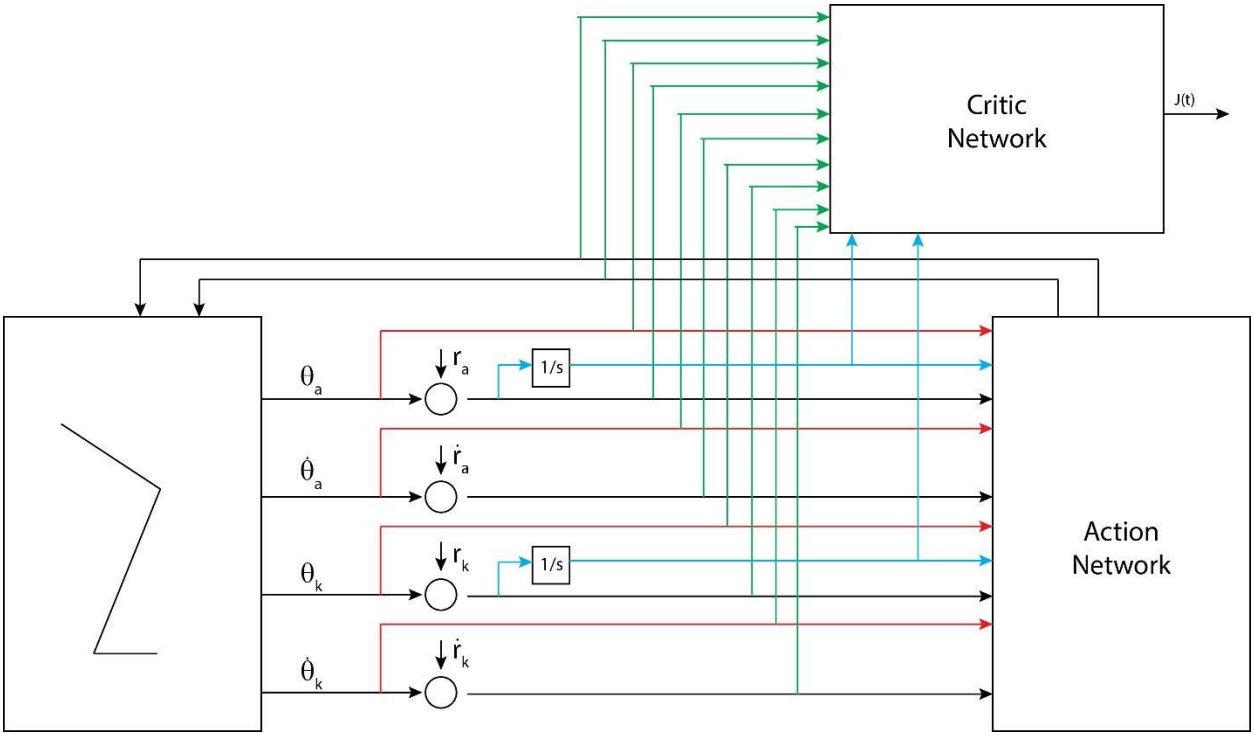


Figure 4.19 Centralized DNDP control system with integral angular error control.

The torque at hip joint $\tau_h$ which is not controlled with DNDP is given by

$$\tau_h = M(\theta)\left(\dot{\theta}_{ref,h} + k_p e_\theta + k_d e_{\dot{\theta}}\right) + C\left(\theta, \dot{\theta}\right)\dot{\theta}_h + G(\theta) + F(\theta)a_{xy} - D_{toe}F_{toe} \qquad (4.50)$$

As can be seen, the torque depends on the parameters of the dynamic model (M, C, G, F) and also there is integrated a PD regulator with terms $k_p e_\theta + k_d e_{d\theta/dt}$. DNDP controller is applied to the ankle and knee joints and is based on the errors $e_a = \theta_{ref,a} - \theta_a$ and $e_k = \theta_{ref,k} - \theta_k$ between the desired and actual joint angles. The input vector of the proposed DNDP model has the form.

$$X_c = \left(I_{e,a}, e_a, \dot{e}_a, \theta_a, \dot{\theta}_a, I_{e,k}, e_k, \dot{e}_k, \theta_k, \dot{\theta}_k\right)^T \quad (4.51)$$

where $I_{e,a} = \int_0^t e_a dl$ and $I_{e,k} = \int_0^t e_k dl$ are the integral errors at ankle and at the knee. The output of the action network which is applied to the limb is composed of two scalar signals $u = (z_a, z_b)$. However, by examining the structure, these signals are not directly applied to the limb as torques $\tau_a$ and $\tau_b$, but they are further processed according to the expressions.

$$\tau_a = z_a + R_{v,a}(e_a + \lambda_a de_a/dt) \quad (4.52)$$

$$\tau_k = z_k + R_{v,k}\,(e_k + \lambda_k de_k/dt) \quad (4.53)$$

The calculated signals from the action networks are corrected by a PD controller which multiplies the respective joint angle error and joint angular error. The control structure is the combination of two regulators.

Adding PD terms: $u_a(t) = K_{V,a}(\dot{e_a}(t) + \lambda_a\, e_a(t))$, $u_k(t) = K_{V,k}(\dot{e_k}(t) + \lambda_k\, e_k(t))$ (4.54)

Success indication: $S(t) = -0.5(e_a(t)/\theta_{a,max})^2 - 0.5(\dot{e}_a(t)/\dot{\theta}_{a,max})^2 - 0.5(e_k(t)/\theta_{k,max})^2 - 0.5(\dot{e}_k(t)/\dot{\theta}_{k,max})^2$ (4.55)

A matrix of 30x30 combinations for the number of hidden layer neurons (NAh, NCh) for the action and the critic network is used for simulations. This will give a complete picture of the structural sensitivity of the neural architecture to the 2-norm of the 4 error terms (ankle angular error, ankle angular velocity error, knee angular error, and knee angular velocity error) used to compare all the variants of the network.

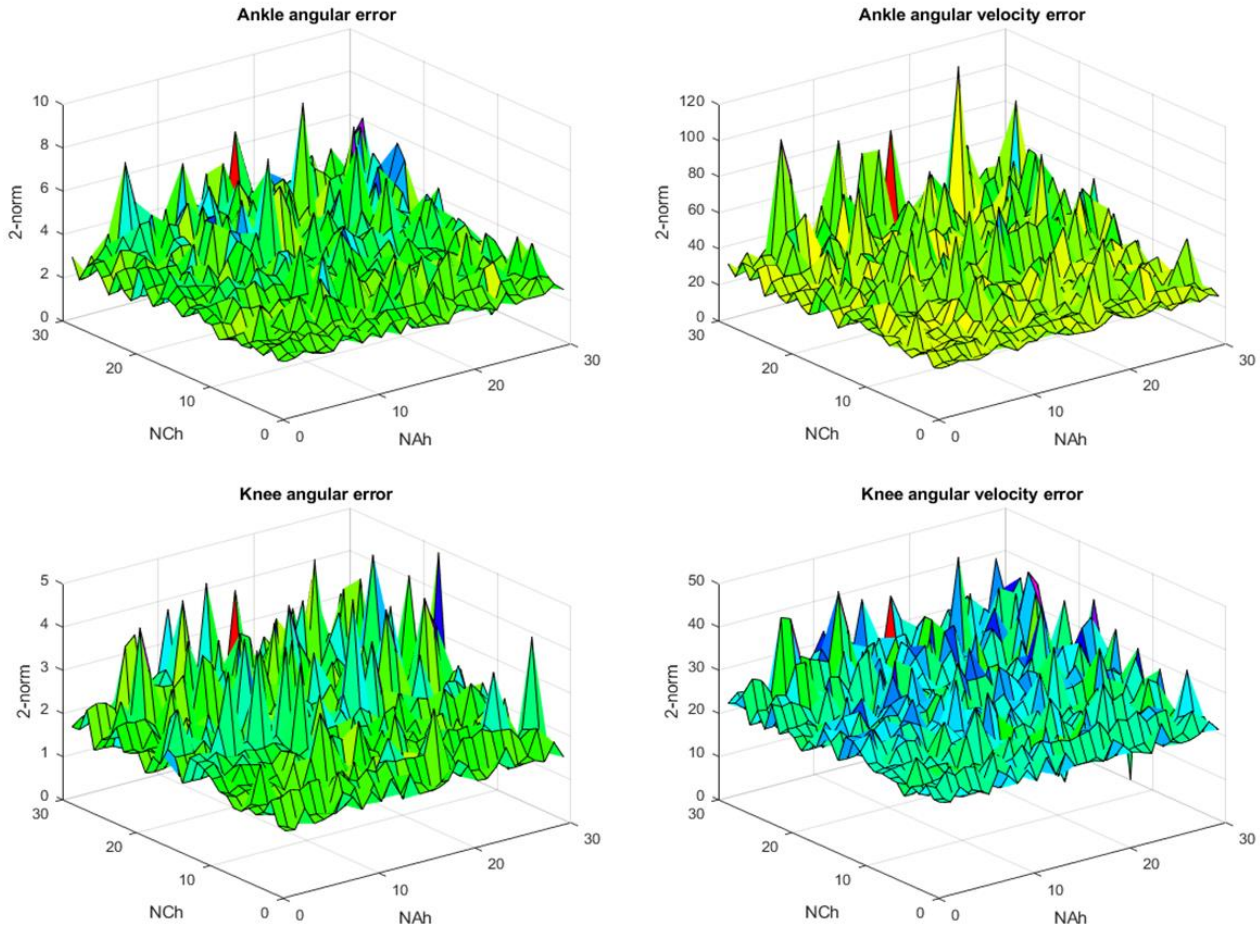


Figure 4.20 Effect of centralized DNDP control system with error integral control.

From Figure 4.20 it is observed that there is not clear dependence between the number of hidden neurons in the hidden layer of the action and critic networks. Some combinations can give lower error levels, and other combinations may give larger errors. A strong dependence of error on the initial conditions of the examined network is shown earlier. Generally, it is expected that the increased number of neurons would lead to better-fitting, more accurate tracking, and lower errors. However, the experimental results contradict this. As can be seen from the figures lowest error levels are achieved when one of the networks (action or critic) has a relatively higher number of hidden neurons, and the other network (critic or action) has a relatively low number of hidden neurons. This is an interesting conclusion because it is not much investigated in earlier literatures. The explanation for such dependence can be searched in relation to the fact that low complexity

hidden layers can approximate only local features associated with high frequency components in the input signal, and higher complexity hidden layers tend to approximate global features associated with low-frequency components in the input signal. Hence combining low and high number of neurons either in action or critic network results in achieving network response in a larger frequency range and eventually improve the bandwidth of the closed loop system. In the figure below, the tracking results are shown for four parameter sets - Param 1, Param 2, Param 3 and Param 4. The results for Param 1 and Param 2 give a balanced response in terms of angle and knee tracking performance. The next parameter sets Param 3 and Param 4 give either a bias in tracking performance improvements at the ankle joint (Param 3), however at the cost of degradation in knee joint, or a bias in tracking performance improvements at the knee joint (Param 4), however at the cost of degradation in ankle joint. As can be seen the 2-norm of the tracking error for Param 3 at ankle is 1.3159; however the norm of the tracking error at knee is increased to 2.16. Also, in Param 4 we have norm at the knee error as small as 0.8765, however the norm of the ankle tracking error is increased up to 5.6778.

Table 4-7 Case responses with centralized DNDP control associated with error integral control.

| **Hidden network param** | | | | **Norm of the error** | | | |
|---|---|---|---|---|---|---|---|
| **Param set** | **NAhC** | **NChC** | **Time (s)** | **error_ankle** | **error_ankle_dot** | **error_knee** | **error_knee_dot** |
| 1 | 10 | 3 | 2 | 1.7907 | 23.8696 | 1.6781 | 21.5087 |
| 2 | 30 | 2 | 2 | 1.6730 | 25.9209 | 1.7919 | 23.6386 |
| 3 | 30 | 9 | 2 | 1.3159 | 24.3612 | 2.1622 | 24.7696 |
| 4 | 20 | 28 | 2 | 5.6778 | 46.2120 | 0.8765 | 14.1049 |
| 1 | 10 | 3 | 10 | 4.1190 | 49.0349 | 4.1708 | 46.7270 |
| 2 | 30 | 2 | 10 | 4.4462 | 61.2846 | 4.4078 | 51.5780 |
| 3 | 30 | 9 | 10 | 3.2032 | 56.8412 | 5.6559 | 56.6401 |
| 4 | 20 | 28 | 10 | 9.7639 | 89.5974 | 2.7497 | 41.7029 |

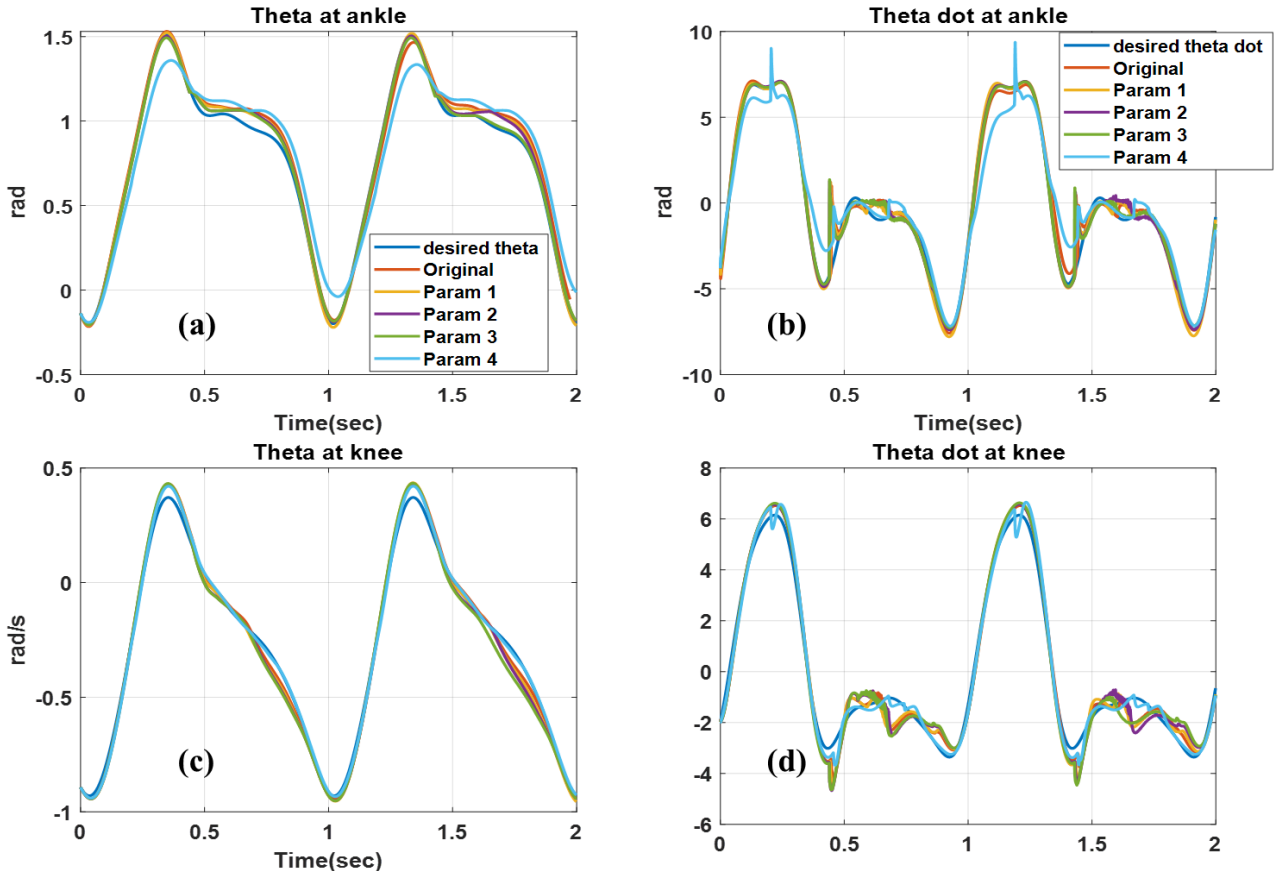


Figure 4.21 Effect of centralized DNDP control system with error integral control (comparison among param sets 1 and 2 from Table 4.7): tracking of (a) ankle angle, (b) ankle velocity, (c) knee angle, and (d) knee velocity. Training time = 2 sec.

An interesting comparison for the four parameter sets (from Table 4.7) is to observe the approximation of the future cost function J(t). As we know from the DNDP theory, it is expected that the J(t) decreases with time as the action network learning progresses. This can be observed in Figure 4.22, which plots the J(t) for the four parameter sets. It can be seen that with time elapses, all the network variants tend to minimize the maximal amplitude of the J(t).

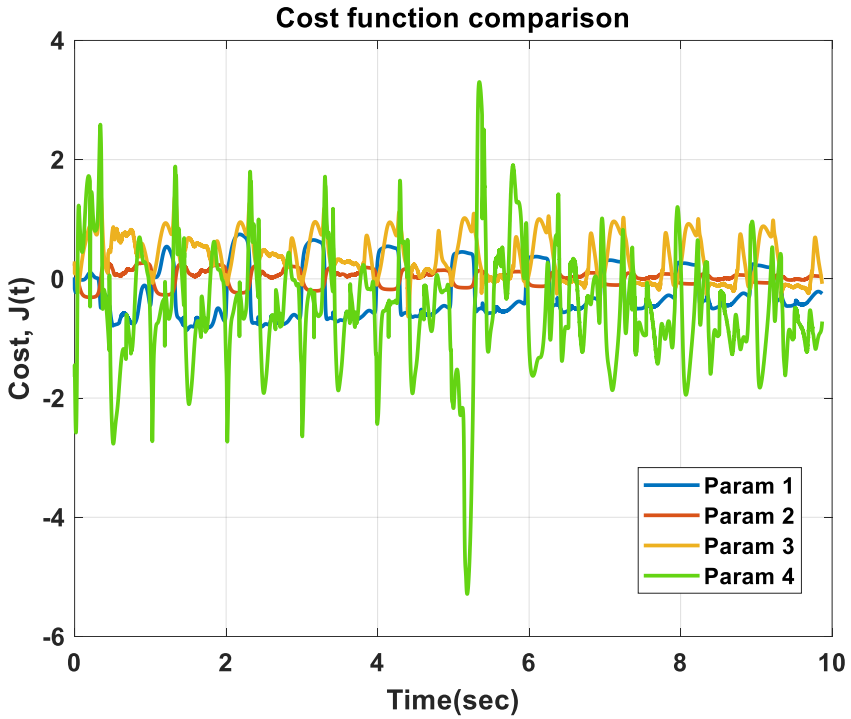


Figure 4.22 Effect of centralized DNDP control system with error integral control on the cost function, J(t), for four parameter sets from Table 4.7.

## 4.6.1 Controller linear analysis

The resulting models are estimated as a state-space canonical representation in discrete Z domain with sampling frequency of 0.001s and then converted to transfer functions, as below, for the parameter sets as presented in Table 4.7,

Param 1 (NAhC=10, NChC=3)

$$y_1(j\omega) = \frac{-0.06(j\omega-2000)(j\omega+44.6)(j\omega+3.675)}{(j\omega+4.33)(j\omega+70.33)(j\omega+100.9)}u_1(j\omega) + \frac{-0.013(j\omega-2000)(j\omega+70.04)(j\omega+4.628)}{(j\omega+4.33)(j\omega+70.33)(j\omega+100.9)}u_2(j\omega)$$

– 84.77 % fit (4.56a)

$$y_1(j\omega) = \frac{-0.1(j\omega-2000)(j\omega+13.06)(j\omega+6.57)}{(j\omega+4.33)(j\omega+70.33)(j\omega+100.9)}u_1(j\omega) + \frac{-0.032(j\omega-2000)(j\omega+69.92)(j\omega+4.183)}{(j\omega+4.33)(j\omega+70.33)(j\omega+100.9)}u_2(j\omega)$$

– 83.46 % fit (4.56b)

Param 2 (NAhC=30, NChC=3)

$$y_1(j\omega) = \frac{-3.73(j\omega-2000)(j\omega+40.5)(j\omega+1.33)}{(j\omega+3.91)(j\omega+40.5)(j\omega+6383)}u_1(j\omega) + \frac{0.6(j\omega-2000)(j\omega+22.33)(j\omega-19.42)}{(j\omega+3.91)(j\omega+40.5)(j\omega+6383)}u_2(j\omega)$$

– 84.4 % fit (4.57a)

$$y_2(j\omega) = \frac{1.22(j\omega-2000)(j\omega+40)(j\omega+0.46)}{(j\omega+3.91)(j\omega+40.5)(j\omega+6383)}u_1(j\omega)$$

$$+\frac{-0.22(j\omega-2000)(j\omega+713)(j\omega+3.204)}{(j\omega+3.91)(j\omega+40.5)(j\omega+6383)}u_2(j\omega)$$

- 65.74 % fit (4.57b)

Param 3 (NAhC=30, NChC=9)

$$y_1(j\omega) = \frac{-0.8(j\omega-2000)(j\omega+41.61)(j\omega+1.771)}{(j\omega+2.802)(j\omega+44.39)(j\omega+1137)}u_1(j\omega)$$

$$+\frac{-0.11(j\omega-2000)(j\omega+27.24)(j\omega-24.53)}{(j\omega+2.802)(j\omega+44.39)(j\omega+1137)}u_2(j\omega)$$

- 70.17 % fit (4.58a)

$$y_2(j\omega) = \frac{-0.52(j\omega-2000)((j\omega)^2-1.835(j\omega)+4.938)}{(j\omega+2.802)(j\omega+44.39)(j\omega+1137)}u_1(j\omega)$$

$$+\frac{0.049(j\omega-2000)(j\omega+2.146)(j\omega-646.9)}{(j\omega+2.802)(j\omega+44.39)(j\omega+1137)}u_2(j\omega)$$

- 79 % fit (4.58b)

Param 4 (NAhC=20,NChC=28)

$$y_1(j\omega) = \frac{-0.063(j\omega-2000)(j\omega+23.62)(j\omega+12.5)}{(j\omega+170.2)(j\omega+18.09)(j\omega+11.82)}u_1(j\omega)$$

$$+\frac{-0.0207(j\omega-2000)(j\omega+13.39)(j\omega+1.103)}{(j\omega+170.2)(j\omega+18.09)(j\omega+11.82)}u_2(j\omega)$$

- 85.89 % fit (4.59a)

$$y_2(j\omega) = \frac{-0.077(j\omega + 2.975)(j\omega + 24.38)(j\omega - 2000)}{(j\omega + 170.2)(j\omega + 18.09)(j\omega + 11.82)} u_1(j\omega)$$

$$+ \frac{-0.0207(j\omega - 2000)((j\omega)^2 + 28.6(j\omega) + 405.3)}{(j\omega + 170.2)(j\omega + 18.09)(j\omega + 11.82)} u_2(j\omega)$$

- 70.69 % fit (4.59b)

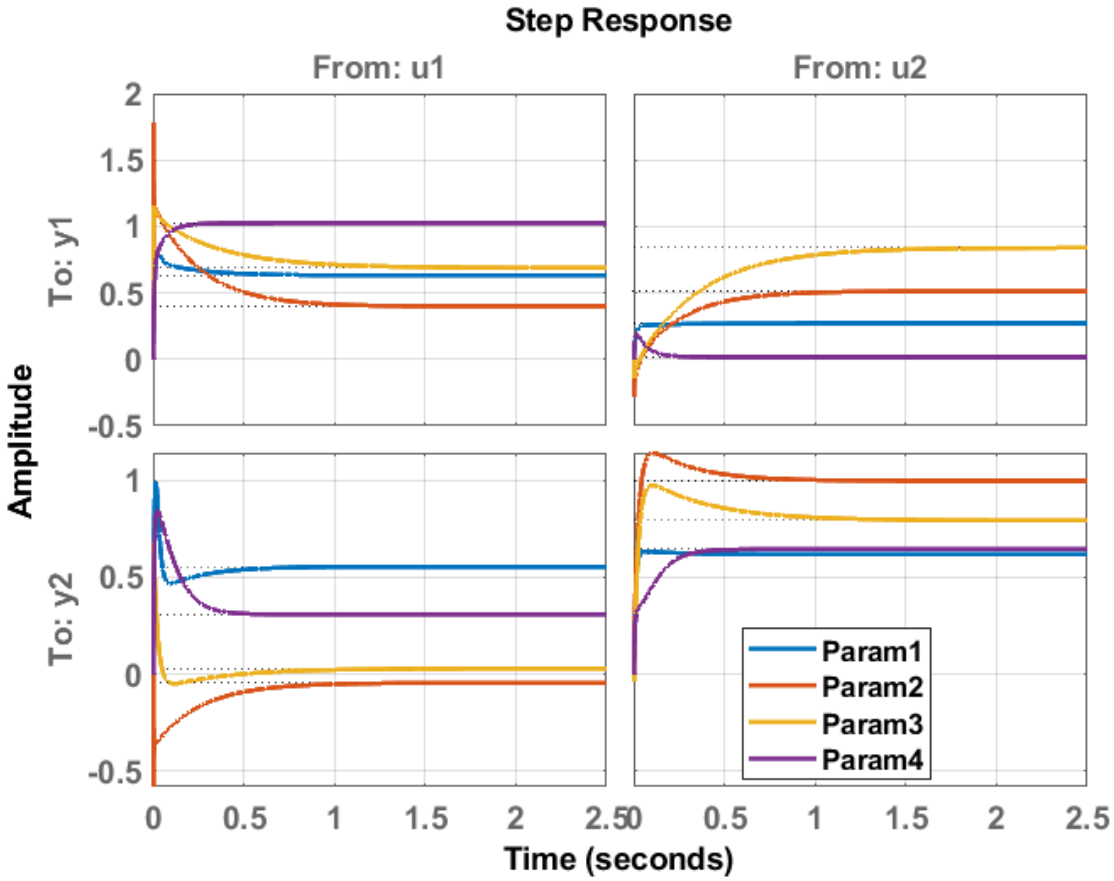


Figure 4.23 Step responses of the linear models of parameter sets from Table 4.7.

Figure 4.23 compares the step response of the linear models (constant of 1 set to one of the inputs while the other input is held zero). As expected, the reference on the first channel (ankle) is most strongly reflected in the first output (ankle) and the reference on the second channel (knee) is dominantly reflected in the second (knee) output. However, the figure allows to compare the models with respect to their linear dynamics. The goal of the centralized structure is to minimize the interdependence between channels i.e. $W_{12} = 0$ and $W_{21} = 0$. This decoupling between

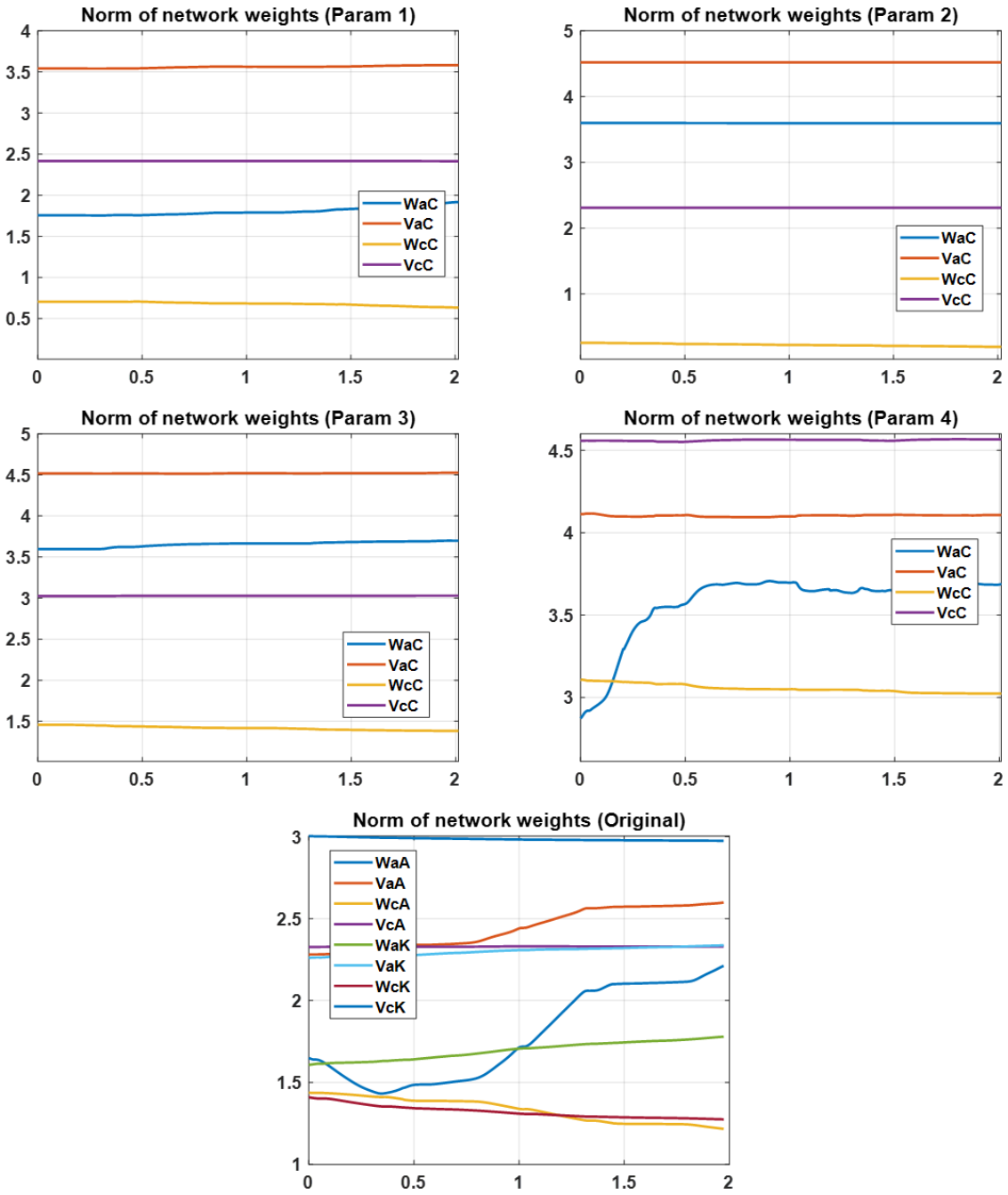


Figure 4.24 Weight convergence of four parameters along with original parameter.

channels are achieved best with the Param 4 where NChC is higher. For the other cases, the interdependence between channels is higher for effect of the ankle reference on the knee angle. However, the smallest error is achieved for Param 2 model where $W_{11}(j0) = W_{22}(j0) = 1$ and

NAhC=30 (highest) but NChC=3 (lowest). This observation about error is confirmed also from the nonlinear model.

Now considering the control signal calculation as,

$$\tau_{knee} = \sigma(X_{act}V_{at})W_{act,knee} + K_{d,knee}d_t\theta_{knee} + K_{p,knee}\theta_{knee} = \sigma(X_{act}V_{act})W_{act,knee} + \tau_{knee,pd} \quad (4.60)$$

$$\tau_{ankle} = \sigma(X_{act}V_{act})W_{act,ankle} + K_{d,ankle}d_t\theta_{ankle} + K_{p,ankle}\theta_{ankle} = \sigma(X_{act}V_{act})W_{act,ankle} + \tau_{ankle,pd} \quad (4.61)$$

The number of hidden layer neurons NAhA of the action network determine the controller gain corrections $\sigma(X_{act}V_{act})W_{act,knee}$ and $\sigma(X_{act}V_{act})W_{act,ankle}$. When the NAhA is higher the dimensions of the matrices $V_{act}$ and $W_{act}$ increase. Since they are initialized with random numbers according to [85] for a random gaussian matrix $A$ initialized with random numbers we have

$$s\sqrt{dim(A)} < E(||A||_2) < 2s\sqrt{dim(A)} \quad (4.62)$$

where $s$ is the standard distribution from which the elements of the matrix are drawn and for $dim(A) = max(m, n)$, where $m$ and $n$ are the row and column dimensions. The E() is the mean value operator. As seen, with the increase of the dim(A) = NahA, the average gain $E(||A||_2)$ increases too.

$$\sigma(X_{act}V_{act})W_{act} = (\sigma(0) + \sigma'(0\ \ )X_{act}V_{act} + \xi(||X_{act}V_{act}||_2^2))W_{act} \quad (4.63a)$$

$$E(||\sigma(X_{act}V_{act})W_{act}||_2) \propto E(||X_{act}V_{act}W_{act}||_2) \quad (4.63b)$$

or considering the upper and lower bound of the random matrix we get

$$E(||\sigma(X_{act}V_{act})W_{act}||_2) \propto s\sqrt{dim(V_{act})}||X_{act}||_2 \quad (4.64)$$

Hence, the norm of the torque gain with respect to robot state is proportional to the standard deviation of the Gaussian initializer and proportional to NAhA. Assuming following linearized model of ankle or knee joints,

$$d_{tt}(r_\theta - \theta) = \tau/J + \eta(X_{act}) \tag{4.65}$$

This means that the second derivative of the angular position is proportional to the torque plus some disturbance signal depending on the current robot configuration, which can be obtained from the nonlinear equations if needed. Hence, it is observed that increasing the torque gain with respect to current state will lead to smaller error due to increased feedback gain. However, the rest of the dynamical terms need to be considered for more precise analysis. But from experiments with tuning the PD regulators, same conclusion was obtained that increasing the gains of the PD controller leads to smaller error. Similarly, increasing the equivalent gain of the DNDP action network will lead to smaller error. The above expressions prove that the equivalent gain of action network given a random initializer is proportional to network dimensions, or by increasing the NAhA that will amount to smaller error.

The role of the action network training is to modify the weights of the action network, hence making the feedback loop nonstationary with $V_{act}(t)$ and $W_{act}(t)$. The training rules are as follows,

$$dW_{act} = [dW_{act,knee}; dW_{act,ankle}] \tag{4.66a}$$

$$dW_{act,knee} = -\gamma_F \, \partial_{\tau_{knee}} J(t) \, E_{act} \sigma(X_{act} V_{act}) + \eta(W_{act}) \tag{4.66b}$$

$$dW_{act,ankle} = -\gamma_F \, \partial_{\tau_{ankle}} J(t) \, E_{act} \sigma(X_{act} V_{act}) + \eta(W_{act}) \tag{4.66c}$$

$$dV_{act} = -\gamma_G \, X_{act}^T \, d\sigma(X_{act} V_{act})(\partial_{\tau_{knee}} J(t), \partial_{\tau_{ankle}} J(t)) W_{act} \, E_{act} + \eta(V_{act}) \tag{4.66d}$$

However, the regularization terms $\eta(M)$ put a upper bound on $||M||_2$, where $M$ is the respective network weight matrix, or $||V_{act}(t)||_2 < B_V$ and $||W_{act}(t)||_2 < B_W$, for all $t > 0$. The resulting weights from training will exist with a Gaussian distribution of variance $s(t)$, which will fit to instantaneous matrix values. Considering the results from above,

$$E(||\sigma(X_{act}V_{act})W_{act}||_2) \propto s(t)\sqrt{dim(V_{act})}||X_{act}||_2 \quad (4.67)$$

It can be observed that during training, the gain of the torque controllers will depend on the variance of the elements in the matrix.

## 4.7 Effect of centralized Neural Network distribution with integrated proportional differential (PD) controller

In the previous section, an additional feedforward and PD feedback are included in torque calculation which was not mentioned in the literature. This PD feedback will have a strong influence upon DNDP the controller performance, which will be demonstrated here. The figure (Figure 4.25) shows the structure of feedforward correction with PDa and PDk controllers respectively for minimization of ankle and knee dynamics error. PD control is a special case of PID control, a well-known classical control algorithm employed a lot in robotics. The performance of DNDP will be examined with and without the PD compensations. Below its effect will be examined on the total performance of the system.

As mentioned earlier, in Section 4.6, the output of the action network which is applied to the limb is composed of two scalar signals $u = (z_a, z_b) = net_a(x_a)$, the weight of the action network are obtained by minimizing the output of critic network $J_t = net_c(x_c)$, which is tuned according to the prediction error $e_c = (J_{k-1} - V) - J_t\alpha$, where the instantaneous cost function is given by

$$V = -\frac{1}{2}\frac{I_{e,a}^2}{\theta_{max,a}^2} - \frac{1}{2}\frac{\theta_a^2}{\theta_{max,a}^2} - \frac{1}{2}\frac{\dot{\theta}_a^2}{\dot{\theta}_{max,a}^2} - \frac{1}{2}\frac{I_{e,k}^2}{\theta_{max,k}^2} - \frac{1}{2}\frac{\theta_k^2}{\theta_{max,k}^2} - \frac{1}{2}\frac{\dot{\theta}_k^2}{\dot{\theta}_{max,k}^2} \quad (4.68)$$

These signals $z_a$ and $z_b$ are not directly applied to the limb as torques $\tau_a$ and $\tau_b$, but they are further processed according to the expressions, as previously presented in equations 4.52 and 4.53,

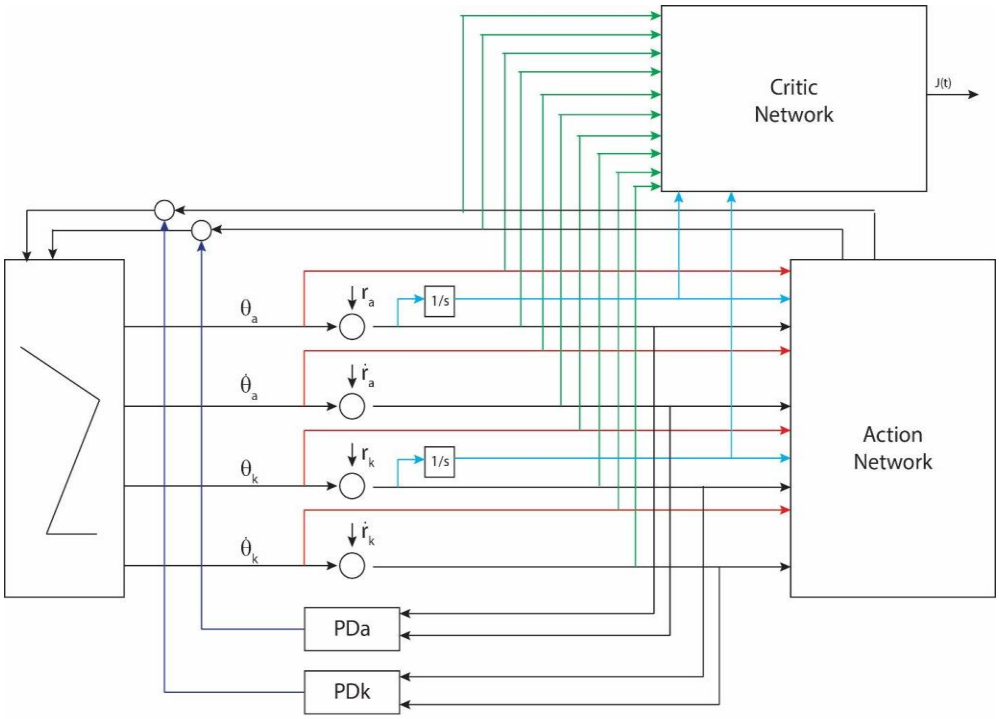


Figure 4.25 centralized Neural Network distribution with integrated proportional differential (PD) controller.

$$\tau_a = z_a + R_{v,a}(e_a + \lambda_a de_a/dt)$$

$$\tau_k = z_k + R_{v,k}\,(e_k + \lambda_k de_k/dt)$$

The parameters of the ankle PD controller $R_{v,a}$ and $\lambda_a$ for the ankle (or $R_{v,k}$ and $\lambda_k$ for the knee), have well known physical meaning. Increasing of proportional gain $R_{v,a}$ leads to increase of the bandwidth of the closed-loop system and eventually to faster transient response which is a basis for minimization of tracking error. However, if the proportional gain is too high, the system may become oscillatory due to amplification of internal resonance frequencies of the limb structure or due to amplification of sensor measurement noise. In this simulation, measurement noise is not included, so theoretically, very low levels of errors are achieved. A main disadvantage of the proportional gain is that it acts on the whole frequency band. The differential gain $\lambda_a$multiplies the

first derivative of the tracking error - or equivalently the velocity tracking errors. It is commonly interpreted as a prediction action of the controller, but technically it increases the high frequency response of the system and attenuates the low frequencies. This is advantageous because it acts as forcing the system performance (if the control constraints allow that). In this section, the effect of the proportional gain is investigated.

Table 4-8 Case responses with centralized DNDP control with integrated PD control.

| **Hidden network param** | | | | | **Norm of the error** | | | |
|---|---|---|---|---|---|---|---|---|
| **Param set** | **NAhC** | **NChC** | **Rk** | **Ra** | **error_ankle** | **error_ankle_dot** | **error_knee** | **error_knee_dot** |
| 1 | 10 | 3 | 79 | 5 | 2.5617 | 31.9127 | 0.2029 | 4.1333 |
| 2 | 10 | 3 | 13 | 9 | 1.4914 | 19.4795 | 1.7466 | 22.6957 |

For example, the following combination of parameters, Rk = 79, Ra = 5, NAhC=10, NChC=3 (as from Table 4.8), results the following 2-norm of the tracking errors: [2.5617, 31.9127, 0.2029, 4.1333]. The normed error achieved for the knee angular error and knee angular velocity error are small. By varying only, the hidden number dimension and DNDP structure, knee joint error is as small as 0.89, but at the cost of a big increase in ankle tracking error. With tuning the PD controller for the knee joint by increasing its gain from 5 to 79 we improved its performance without degrading the performance of the ankle. As can be seen from Figure 4.26, the error in the knee joint angle tracking and angular velocity tracking is minimized to a level, for both param1 and 2, which was difficult to achieve with the DNDP network alone. While Fig 4.26(e) also presents the predicted cost function from the critic network over a 10 second interval, for both the parameter sets. A balanced result where both ankle and knee tracking errors are improved is achieved for Rk = 13 and Ra = 9 (Param2 set in Table 4.8), the tracking errors achieved are [1.4914,19.4795,1.7466,22.6957]. Walking dynamics for these parameters are presented in the figure, Figure 4.26, representing better tracking as well as better 2-norm error (as from simulation), comparing to Param1.

The tracking performance of the knee joints was further improved. Proportional gains as high as Ra = 200 is experimented and as a result, the 2-norm of the ankle tracking error fell to 0.071. When trying to go beyond that limit with Ra> 200 the noise is amplified coming from rounding errors which is a computational limit. However, it was not easy to get same level of performance for ankle joints because both channels of the system are interconnected dynamically. It is actually a common problem when one tries to control multi-input multi-output systems with single-input single-output controllers like PID. The problem is that when both channels of a system are connected dynamically at a high enough level, improving the performance in the one channel limits the achievable performance in the other channel. There are many strategies in control theory to cope with this situation - design of lead-lag compensators, design of centralized controllers, design of multivariable PID, etc. Hence here it can be seen that the role of the proposed DNDP exactly as a decoupling compensator between both control channels because it integrates information from both channels. However, selection of the optimal configuration of the DNDP is important. For these experiments, the number of hidden neurons in the centralized action network is 10 and the number of hidden neurons in the centralized critic network is 3.

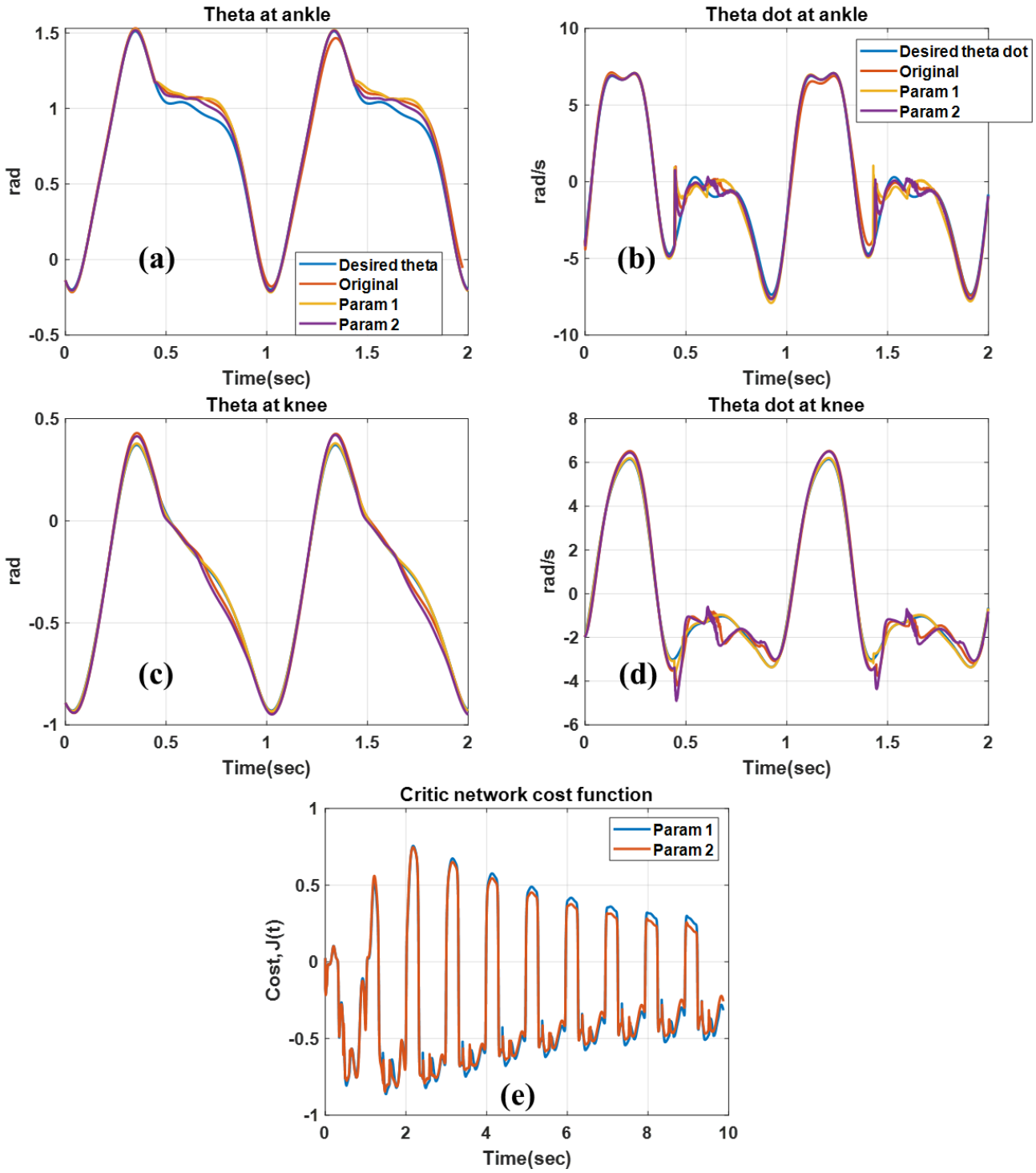


Figure 4.26 Effect of centralized DNDP control system with integrated proportional differential (PD) controller: tracking of (a) ankle angle, (b) ankle velocity, (c) knee angle, (d) knee velocity, and critic network cost function J(t): for 10 sec.

### 4.7.1 Controller model

The controller is defined with its weight matrices of the action network given by,

$W_{crit}(t) \in R^{N_{crit,h} \times 1}$ - output weights matrix of the critic network

$V_{crit}(t) \in R^{N_{crit,i} \times N_{crit,h}}$- input weights matrix of the critic network

$N_{crit,h}$ - number of hidden neurons in the critic network

$N_{crit,i}$- number of inputs of the critic network

The critic network has single output - the optimization criteria $J(t)$ which is an approximation of reinforcement cost, $R(t) = \sum_{k=1}^{\infty} \alpha^{k-1} r(t+k)$ with $0 < \alpha < 1$ and $r(t)$- the reinforcement signal measuring level of success. The purpose of the controller is to reduce the vector of angular errors denoted with, $e(t) = (r_{hip} - \theta_{hip}, r_{knee} - \theta_{knee}, r_{ankle} - \theta_{ankle})^T$ together with the integral terms of the angular errors at the knee and ankle joints according to the proposed control structure above in the introduction. These integral terms can be defined as, $I[e(t)] = \int_0^t e(w)dw \approx \sum_{k=0}^{t/T_S} e(kT_S)T_S$- integral of the error, where $T_S$ is sampling interval. Equivalently, $I[e(t)] = I[e(t - T_S)] + e(kT_S)T_S$.

The control system produces three signals - hip, knee, and ankle torques. According to the original approach we use a computed torque for the hip segment obtained from model inversion

$$\tau_{hip} = M(\theta)(d_{tt} r_{hip} + K_{p,hip} e_{hip}(t) + K_{d,hip} d_t e_{hip}(t)) + C(\theta) d_t \theta + G(\theta) + F(\theta) a_{xy} - D_{toe} F_{toe} \quad (4.69)$$

This approach is good if the inertial and geometric parameters of the models are good, but in practice, that cannot be guaranteed, since, additional PD gains are introduced to minimize the error between the programmed trajectory and the actual one. These gains are $K_{p,hip}$ and $K_{d,hip}$. Finally, the input vector to the action network is given by, $X_{act} = (I[e_{ankle}], e_{ankle}, \dot{e}_{ankle}, \theta_{ankle}, \dot{\theta}_{ankle}, I[e_{knee}], e_{knee}, \dot{e}_{knee}, \theta_{knee}, \dot{\theta}_{knee})$. And the output of the

action network is described with $(u_{knee}, u_{ankle}) = \sigma(X_{act}V_{act})W_{act}$, where $\sigma$ - sigmoidal activation function. Control signals calculated from the action network are added to the torque signal applied to the knee and ankle joints together with the PD corrections, as below,

$\tau_{knee} = u_{knee} + K_{d,knee}d_t e_{knee} + K_{p,knee}e_{knee}$ - torque applied to the knee (4.70)

$\tau_{ankle} = u_{ankle} + K_{d,ankle}d_t e_{ankle} + K_{p,ankle}e_{ankle}$ - torque applied to the ankle (4.71)

The criteria for training of the action network is the quadratic polynomial containing integral error, joint error and the joint angular velocity,

$$S_{act} = -k_1(I[e_{ankle}])^2 - k_2(I[e_{knee}])^2 - k_3(e_{ankle})^2 - k_4(e_{knee})^2 - k_5(d_t e_{ankle})^2 - k_6(d_t e_{knee})^2 \quad (4.72)$$

The input to the critic network is the same as the input to the action network but extended with the output of the action network to accommodate the amplitude of the control signal in critic network decision,

$X_{crit} = (X_{act}, u_{knee}, u_{ankle})$ - input to the critic network

The output of the critic network is an approximation the reinforcement learning criteria,

$J(t) = \sigma(X_{crit}V_{crit})W_{crit}$ - output of the critic network

Then,

$E_{crit} = (J(t - T_S) - S_{act}) - \alpha J(t)$ - performance of the critic network, where $\alpha J(t)$ is the predicted value of reinforcement cost, $R(t)$, and $J(t - T_S) - S_{act}$ is the actual value of the reinforcement cost,

$E_{act} = -J(t)$ - performance of the action network

Thus, weight updates of the critic network:

$dW_{crit} = -\gamma_F E_{crit}\sigma(X_{crit}V_{crit}) + \eta(W_{crit})$, $\eta(W_{crit})$ - quadratic regularization term

$dV_{crit} = -\gamma_G X_{crit}^T d\sigma(X_{crit}V_{crit})W_{crit} E_{crit} + \eta(V_{crit})$

And, weight updates of the action network:

$\partial_{X_{crit}} J(t) = V_{crit} d\sigma(X_{crit} V_{crit}) W_{crit}$ - derivatives of the output of the critic network with respect to the inputs of the critic networks, as needed to backpropagate $E_{crit}$.

From this matrix we use only derivatives with respect to action network outputs $\partial_{\tau_{knee}} J(t)$ and $\partial_{\tau_{ankle}} J(t)$,

$$dW_{act} = [dW_{act,knee}; dW_{act,ankle}] \quad (4.73a)$$

$$dW_{act,knee} = -\gamma_F \, \partial_{\tau_{knee}} J(t) \, E_{act} \sigma(X_{act} V_{act}) + \eta(W_{act}) \quad (4.73b)$$

$$dW_{act,ankle} = -\gamma_F \, \partial_{\tau_{ankle}} J(t) \, E_{act} \sigma(X_{act} V_{act}) + \eta(W_{act}) \quad (4.73c)$$

$$dV_{act} = -\gamma_G \, X_{act}^T \, d\sigma(X_{act} V_{act}) (\partial_{\tau_{knee}} J(t), \partial_{\tau_{ankle}} J(t)) W_{act} \, E_{act} + \eta(V_{act}) \quad (4.73d)$$

## 4.7.2 Leg model

A well-known nonlinear leg model from analytic mechanics can be described as, $X(t) = (\theta_{hip}, \theta_{knee}, \theta_{ankle}, \dot{\theta}_{hip}, \dot{\theta}_{knee}, \dot{\theta}_{ankle})^T$ - state vector of the leg.

Then the equation of motion can be described as,

$$M(\theta) \, d_{tt}\theta + C(\theta, d_t\theta) \, d_t\theta + G(\theta) + F(\theta) a_{xy} - D_{toe} F_{toe} = \tau \quad (4.74)$$

$$\theta = (\theta_{hip}, \theta_{knee}, \theta_{ankle})^T, \tau = (\tau_{hip}, \tau_{knee}, \tau_{ankle})^T \quad (4.75)$$

This is a parameter varying linear system. Since, the reference trajectory is fixed, we may represent it as linearized around the reference trajectory.

The hip segment is controlled by a computed torque method as

$$\tau_{hip} = M(\theta)(d_{tt} r_{hip} + K_{p,hip} e_{hip}(t) + K_{d,hip} d_t e_{hip}(t)) + C(\theta) d_t\theta + G(\theta) + F(\theta) a_{xy} - D_{toe} F_{toe} \quad (4.76)$$

Hence, substituting that in the equation above,

$\theta_{hip} = r_{hip}$, considering that parameters of the robot are identified without error. This assumption is not fulfilled in practice, and $K_{p,hip}$ , $K_{d,hip}$ terms should compensate for the difference. Assuming hip error is small enough to be neglected, the remaining in the model dynamics can be considered as a system of the following equations,

$$m_{11}d_{tt}\theta_{knee} + m_{12}d_{tt}\theta_{ankle} + c_{11}d_t\theta_{knee} + c_{12}d_t\theta_{ankle} + \xi_{knee}(t) = \tau_{knee} - \tau_{ankle} \quad (4.77a)$$

$$m_{21}d_{tt}\theta_{knee} + m_{22}d_{tt}\theta_{ankle} + c_{21}d_t\theta_{knee} + c_{22}d_t\theta_{ankle} + \xi_{ankle}(t) = \tau_{ankle} \quad (4.77b)$$

$$\tau_{knee} = \sigma(X_{act}V_{act})W_{act,knee} + K_{d,knee}d_t\theta_{knee} + K_{p,knee}\theta_{knee} \quad (4.77c)$$

$$\tau_{ankle} = \sigma(X_{act}V_{act})W_{act,ankle} + K_{d,ankle}d_t\theta_{ankle} + K_{p,ankle}\theta_{ankle} \quad (4.77d)$$

Where most of the parameters $M(\theta)$, $C(\theta,\dot{\theta})$, $G(\theta)$, $V_{act}(t)$,$W_{act}(t)$,$V_{crit}(t)$ and $W_{crit}(t)$ are varying around their stationary values in time according to the leg trajectory. In conclusion, the controller structure is generally linear however with parameters varying in some range; hence, there exists an equivalent set of linear models corresponding to the parameter variation.

### 4.7.3 Characterization of the closed loop sensitivity

Using system identification methods, the closed loop system can be described with various linear structures. For the purpose of comparison, it is enough to consider the following system

$$\theta_{knee}(j\omega) = W_{11}(j\omega)r_{knee}(j\omega) + W_{12}(j\omega)r_{ankle}(j\omega) \quad (4.78a)$$

$$\theta_{ankle}(j\omega) = W_{21}(j\omega)r_{knee}(j\omega) + W_{22}(j\omega)r_{ankle}(j\omega) \quad (4.78b)$$

Where, $\theta_{knee}(j\omega) = F[\theta_{knee}(t)]$, and, $\theta_{ankle}(j\omega) = F[\theta_{ankle}(t)]$ are the Fourier transforms of the angular signals during leg movement, while, $r_{knee}(j\omega)$ and $r_{ankle}(j\omega)$ are transforms of the

respective reference trajectories and $W_{mn}(j\omega)$ are transfer functions giving the linear dependence between the Fourier transforms.

For the case of **Param1**, from Table 4.8, a nonlinear model of 70% level of fit (knee) and 46% of fit (ankle) can be estimated.

Param 1 (NAhC=10, NChC=3, Rk=79, Ra=5)

$$y_1(j\omega) = \theta_{knee}(j\omega) = \frac{23.327\ (j\omega + 32.41)}{(j\omega)^2\ +\ 63.14(j\omega)\ +\ 1007} r_{knee}(j\omega) + \frac{6.4412\ (j\omega + 30.16)}{(j\omega)^2\ +\ 63.14(j\omega)\ +\ 1007} r_{ankle}(j\omega)$$

- 70 % fit (4.79a)

$$y_2(j\omega) = \theta_{ankle}(j\omega) = \frac{-44.307\ (j\omega + 13.08)}{(j\omega)^2\ +\ 63.14(j\omega)\ +\ 1007} r_{knee}(j\omega) + \frac{38.104\ (j\omega + 37.12)}{(j\omega)^2\ +\ 63.14(j\omega)\ +\ 1007} r_{ankle}(j\omega)$$

- 46 % fit (4.79b)

For the case of **Param2**, from Table 4.8, a nonlinear model of 68% level of fit (knee) and 70% of fit (ankle) can be estimated.

Param 2 (NAhC=10, NChC=3, Rk=13, Ra=9)

$$y_1(j\omega) = \theta_{knee}(j\omega) = \frac{-2.3142\ (j\omega - 302.1)}{(j\omega + 27.75)(j\omega + 36.66)} r_{knee}(j\omega) + \frac{30.152\ (j\omega + 9.926)}{(j\omega + 27.75)(j\omega + 36.66)} r_{ankle}(j\omega)$$

- 68 % fit (4.80a)

$$y_2(j\omega) = \theta_{ankle}(j\omega) = \frac{-44.307\ (j\omega+13.08)}{(j\omega)^2 + 63.14(j\omega) + 1007} r_{knee}(j\omega) + \frac{38.104\ (j\omega+37.12)}{(j\omega)^2 + 63.14(j\omega) + 1007} r_{ankle}(j\omega)$$

- 70 % fit (4.80b)

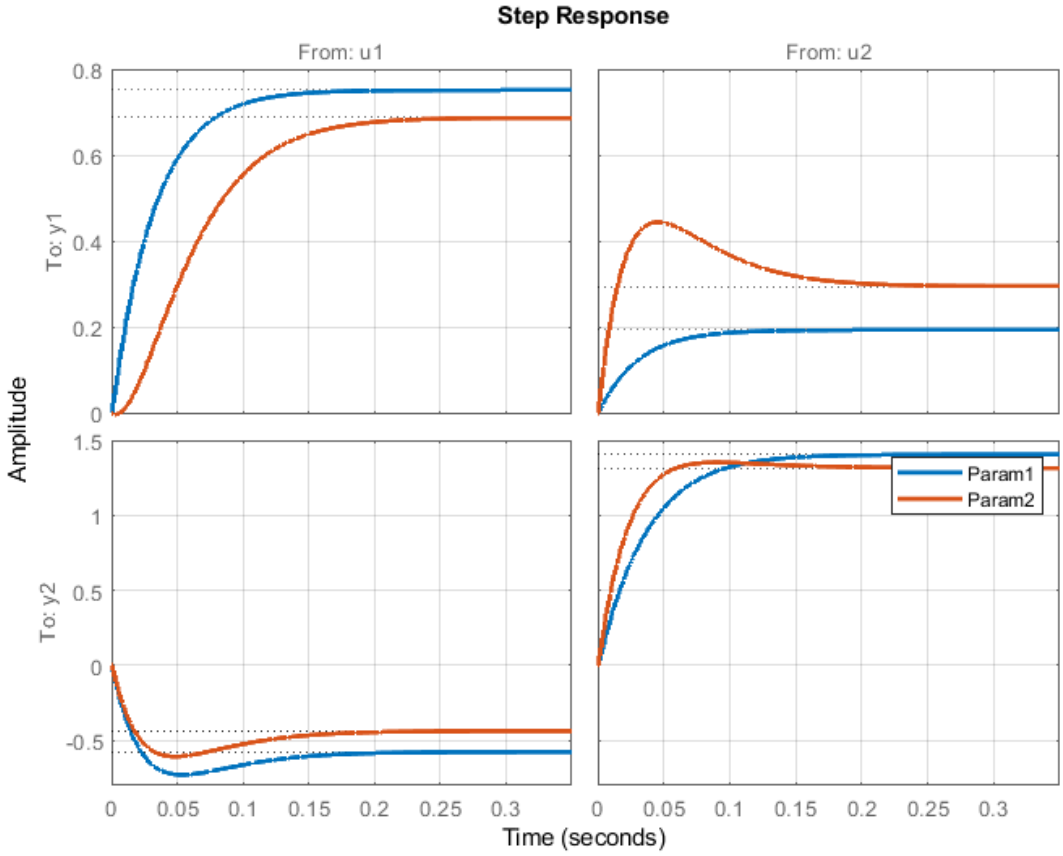


Figure 4.27 Step responses for a centralized DNDP control system with integrated proportional differential (PD) controller.

Now, calculating the steady state gains of both cases by substituting, $j\omega \rightarrow 0$, we obtain, $\theta_{knee} = r_{knee}$, and $\theta_{ankle} = r_{ankle}$ as $t \rightarrow \infty$. The level of fit between simulated data with the nonlinear model and the transfer functions can be easily increased to 90% and more by increasing the order of the model, but that appears to be overfitting situation. There are several differences between the transfer functions of the models:

- Param2 model has two poles at -37 and -28 with the one at -28 being dominating, so the time constant of the model is around 0.03sec. For the Param 1 model we have a complex pole with resonance frequency of 10 rad/s giving a time constant of 0.1 sec.

- In both cases, there is negative correlation between ankle and knee channels due to $W_{12}$ and $W_{21}$ which are non-negative. Moreover, they contribute to achieving the steady-state gain of 1 to the respective reference signal. However, the Param 2 model has non minimum phase in $W_{12}$ channel due to positive pole at 302. Presence of such a pole in the closed loop transfer function means that it will be present in the open loop too (more accurately in the DNDP controller because we don't see it in Param 1), and such poles are not compensable. So, the Param 2 case has some fundamental limitations of achieving better performance which explains partially the empirical observation in this section that, "improving the performance in the one channel limits the achievable performance in the other channel."

The following Figure 4.28 shows the weight convergence of the two centralized DNDP parameters sets in comparison to the original parameter set.

## 4.8 Controller performance summary

This chapter describes dynamic optimization control based on artificial neural network for development of gait restoration devices. Controlling of these devices can be complicated due to numerous challenges such as actuator redundancy, mixed actuator dynamics, electromechanical delay (EMD) and muscle fatigue. The system under investigation is a 2DOF model of a human gait controller using DNDP algorithm composed of a critical and action network trying to solve the optimal control problem in real-time. Initially, the critic and action network for both knee and ankle joints are sigmoid based feed-forward networks with a single hidden layer. In general, with the increase of the number of neurons in each network we would expect that the performance of the desired trajectory tracking will be improved too. However, the problem with gradient based NN learning is that only local extrema of the cost function is achieved which may differ a lot from the global extrema. This difference depends on several factors - initial values of the model

parameters, dimension of the hyperspace, learning rate, constraints, clipping options, regularization, cost function weights, etc. We calculated 4 signal errors and their 2-norms which allows us to investigate the performance of the system by 4 numbers representing the magnitude of these errors.

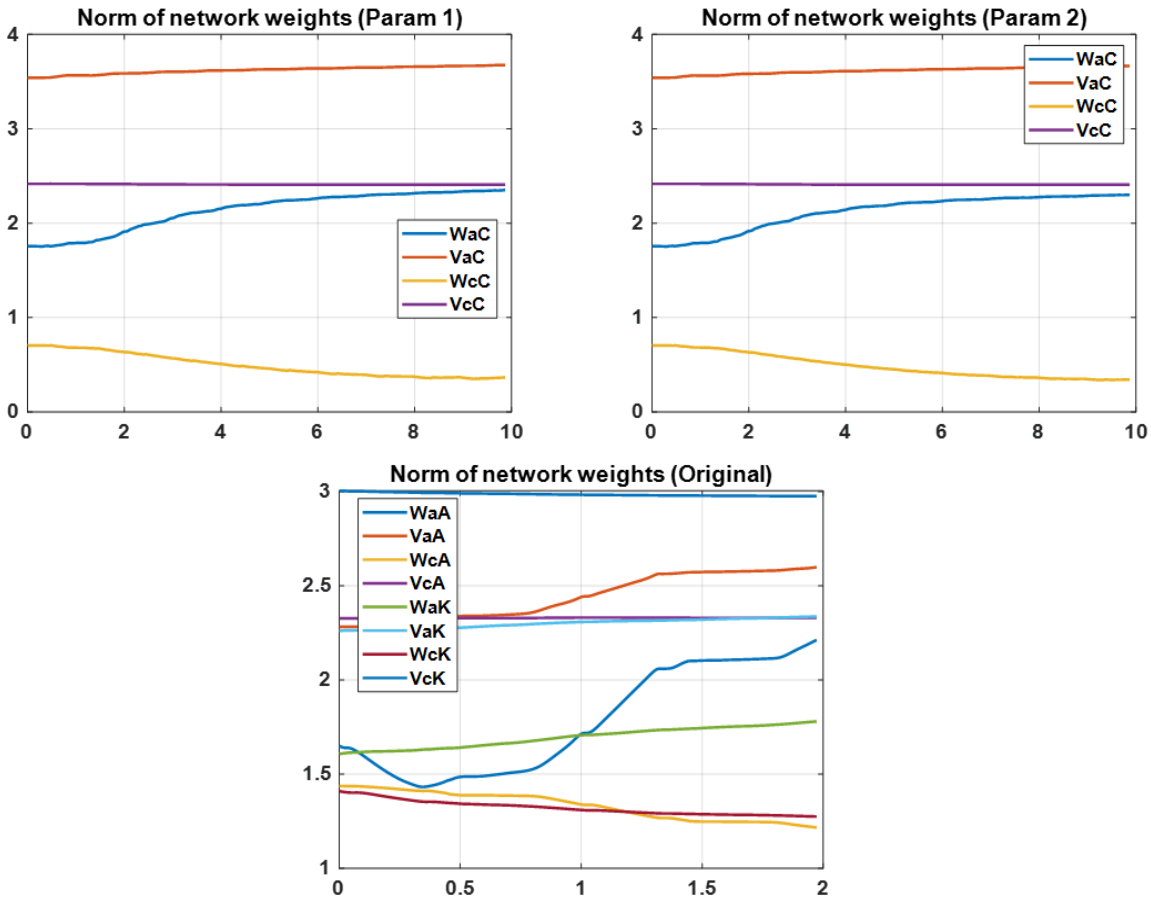


Figure 4.28 Weight convergence of the two centralized DNDP parameters sets in comparison to the original parameter set.

Next, we increased the number of hidden layers in each of the networks. The critic and action network for both knee and ankle joint was extended from a single sigmoid based feed-forward hidden layer to networks with two hidden sigmoidal layers. As can be seen, the dimension of the parameter space is increased considerably with respect to the initial case where we had a single hidden layer on each network. By working in a hyperspace with a higher dimension, we get

fine tuning of the multivariate nonlinear function defined with a particular network. Extending the number of hidden layers or making the network deeper is a common approach to minimize loss and increase accuracy. However, finding the optimal parameter values which lead to maximization of network performance is not an easy task.

Later, we dealt with the sensitivity to initial conditions. There are many ways to initialize weight and biases of the neural network - zero initialization, random initialization, He initialization etc. If all the weights or biases are initialized with 0, the derivative with respect to loss function is the same for every weight or bias value and all parameters will have the same value in subsequent iterations. Assigning random values to weights is better than just 0 assignment. If weights are initialized with big magnitudes and if the activation function is sigmoidal as in our case; the input to activation function causes its output value to saturate at unity. Hence, we can expect that the gradient changes slowly, and learning takes a lot of time. When the weights are initialized with low values close to 0; we fall back to the zero-initialization problem. In these experiments, we encountered a certain limiting behavior of the control system as defined as two independent deep learning dynamic programming (DLDP) nodes working in parallel for two different joints. The central controller was introduced to improve the tracking performance of the ankle but more or less at the cost of tracking performance of the knee and reverse. In order to overcome this limiting behavior, we decided to introduce a new level of control system called - a centralized DLDP controller. The centralized controller produces a synchronization signal (sync in the figure) that is fed into dedicated ankle and knee controllers.

According to the DNDP structure, the action network is responsible to produce the current torque as a function of the current state. And the critic network tries to optimize the performance of the action network expressed with the total future cost R(t). However, the hyperparameters of

the critic network are optimized with respect to minimizing the prediction error between R(t) and J(t). Both networks are generalized from the standard single-input single-output DNDP model. For the presented experiments we tune three parameters - NAhC, NChC and the initial seed of the random generator. We have proved that the initial conditions of the matrix lead to large deviation in the tracking performance. When we have very low error at the knee angular position and angular velocity, we also have relatively elevated errors in the ankle joint. Hence, this limiting property is still present in a centralized system. As it is a bit more attenuated, we are able to find a combination of parameters and initial conditions which lead to better balance in the tracking performance.

In fully centralized controller with integrators, two integral error terms are included in the network input in comparison with the previous experiments. A common technique in control is to include information about integral errors to improve the accuracy of the closed-loop system in addition to stability. The outputs of the action network are both torques - for the ankle and knee joints. For this investigation, we have decided to examine a matrix of 30x30 combinations for the number of hidden layer neurons (NAh,NCh) for the action and critic network. It gives us a complete picture of the structural sensitivity of the neural architecture to the 2-norm of the 4 error terms we use to compare all the variants of the network. We observed that there is no clear dependence between the number of hidden neurons in the hidden layer of the action and critic networks. Some combinations can give lower error levels and some combinations may give larger errors. Also, we have shown a strong dependence of error on the initial conditions of the examined network. Generally, we would expect that the increased number of neurons would lead to better fitting, more accurate tracking and lower errors. However, the experimental results contradict this. As can be seen from the figures, lowest error levels are achieved when one of the networks (action or critic) has relatively higher number of hidden neurons and the other network (critic or action)

has relatively lower number of hidden neurons. The explanation for such dependence can be searched in relation to the fact that low complexity hidden layers can approximate only local features associated with high frequency components in the input signal and higher complexity hidden layers tend to approximate global features associated with low frequency components in the input signal. Hence, combining low and high number of neurons either in action or critic network; we achieved network response in a larger frequency range and eventually improved the closed-loop system's bandwidth.

Lastly, we investigated the application of PD controllers in torque calculation. It shows the structure of feedforward correction with PDa and PDk controllers respectively for minimization of ankle and knee dynamics error. Increment of proportional gain $R_{v,a}$ leads to increased bandwidth of the closed-loop system and eventually faster transient response which is a basis for minimization of tracking error. However, if the proportional gain is too high, the system may become oscillatory due to amplification of internal resonance frequencies of the limb structure or due to amplification of sensor measurement noise.

The first three of the controllers are not centralized, the last three controllers are centralized, and the 4th controller is semi-centralized (or hybrid). The last approach that investigates the PD controller tunings can be applied to each of the previous 6 control structures, because that PD controller is present in all of them and eventually its tuning can improve their performances. So, the centralized controller used here has fewer tunable parameters, smaller norm of the angle and angular velocity errors and can be easily extended to higher dimensions (i.e. more joints or layers). But at the same time, it has limitations like - higher dimension of the input and output weight matrices, less degrees of freedom, dependence on initial conditions and interdependence between joints. The decentralized controller can tune independently the performance on each joint, more

degrees of freedom and more flexible for specific modification. It has some constraints like, harder to select the structural parameters of the network due to the large number of iterations to be executed. The joints are ignorant of each other. Again, it has dependence on initial conditions. The Hybrid controller introduced synchronization signal. It has more complex hierarchical organization. Increasing the complexity of the synchronization network improves the performance of the hybrid controller. This has the limitation of increased number of structural parameters to select compared to decentralized case. Like the other two, it is also dependent on initial conditions.

The next chapter will focus on the expansion of the scopes of this dissertation outlining the initial requirement and design approaches for data collection and clinical procedure.

# Chapter 5 Initial measurement requirements and design

In chapter 4, different controllers are discussed with their structure, results, and performance for improvement of the tracking performance of the amputated leg and minimize the difference between amputated and intact leg of the unilateral transfemoral individual. Simulation was done and the analysis was described based on fundamental control theory and linear analysis. It gives us a basic idea of how the controllers should behave with real dynamic locomotion. But data collection from the unilateral transfemoral amputee is a vital part of consideration for this type of research. The contact force and pressure of the residual limb inside the prosthetic socket, ground reaction force measurement and pressure on the ground created by the foot are the important ones to be considered. For a lower limb amputee, these forces are created between the residual limb and the prosthetic socket and are not readily evident using visual gait analysis or kinematic gait analysis. Researchers obtained these measurements by using strain-gauges, accelerometers and surface EMG electrodes attached directly to the muscles. At the same time, the procedure should be clinically approved, hassle-free, and physically comfortable for the patients. In this chapter, the Data acquisition system and protocol designed to investigate the interaction forces that include interfacial socket forces and EMG muscle forces of a transfemoral amputee is proposed which can give us a clearer view of how to get the measurements of interest.

## 5.1 Importance of measurements

Quantitative gait analysis provides information to supplement qualitative gait analysis and helps to evaluate the effectiveness of the rehabilitation treatments of the amputee, thereby improving the gait functionality to a great extent. Quantitative measurements usually include determining one or more gait parameters which can be employed in kinetic gait analysis. In kinetic gait analysis, the actual biomechanical forces play an important role in locomotion like Ground

Reaction Forces (GRF), Joint Moments and Powers that is accountable for the movement of the body, are measured. The overall scenario cannot be figured out ignoring these measurements. In addition, a comparative analysis can be done between the residual muscle activity of the transtibial amputee and transfemoral amputee. Comparative gait analysis can be done between healthy and amputee individuals. These comparative studies form the basis to assess the clinical outcomes of the amputee's treatment procedure. Based on that, a suitable rehabilitation plan along with best suited prosthetic socket and prosthesis type can be selected for the rest of the life. Next, dynamic control strategies can be implemented to improve the design of prosthetic devices and mimic the more natural human like locomotion. The prosthetic socket is the most important part of the prosthesis since it provides a coupling contact point of the prosthetic leg and residual limb. Considering an artificial prosthetic design perspective, it is very important to sense the contact forces generated inside the socket in real time as it increases the possibility of extracting signals to control a powered prosthetic joint. The distinct characteristics of each gait pattern can then be used to improve the performance of the prosthesis to account for different gaits, surface terrain and inclinations. From clinical point of view, the elongation and contraction of the muscles related with the gait activity, play an important role in pumping blood back to the heart and in the overall health of the vascular system.

The lack of understanding of amputees' gait coordination slows the prosthetic device design improvement and thus impact badly in the clinical rehabilitation process. The performance of a prosthetic device should not be compromised at the expense of the health of the intact and residual limb. Studies have shown that there is a high incidence of pathological problems in the intact limb, such as knee arthritis as the intact limb is adversely affected by the prosthetic gait [86]. Moreover, the muscle coordination of the intact limb is another manifestation of gait coordination, which

enables us to better understand the characteristics of amputees' motor control. To investigate these effects, the residuum-socket interface pressure and gait characteristics in amputee subject with transfemoral amputation can be studied for work related gait activities. Understanding the overall distribution of the pressure and shear stress on the contact interface is very important for prothesis designing of an artificial leg such as substantial performance for prolonged using, reduction of soft tissue damage and comfortable walking.

## 5.2 Background of current data collection instruments

Qualitative gait analysis involves the physical examination and functional assessment, vision-based measurements are made by trained personnel using visual observation or through the use of cameras or motion capture video cameras. [86]. Passive marker based optical system is also used in similar experiments recently [87]. Although qualitative gait analysis is widely used and appears to be a promising clinical tool for the therapist to evaluate the amputee's gait, it was shown to be unreliable as visual observations do not provide adequate information to improve the rehabilitation process of the amputee. Energy expenditure profile is also used by some researchers as a comparative index parameter for comparing the performance of different prosthesis. It refers to the amount of energy consumption by the amputee during locomotion and is directly related to overall walking efficiency. But significant inconsistencies were observed though it is a powerful indicator of overall individual gait cycle performance.

Figure 5.1 Data collection during self-pace walking healthy subject and unilateral transtibial amputee [69, 88].

In some previous studies, the temporal-spatial parameters are studied to observe the effect of different types of prosthesis on the amputee's gait . Temporal-spatial parameters provide timing and position measurements of the human gait using simple tools such as stop-watch, foot switches, gait pressure mats, active or passive markers, etc. The most widely used temporal-spatial parameters are velocity of walking, step length, stride length, cadence, etc. Temporal spatial parameters are widely used for gait analysis as they are simple to acquire and easier to obtain.

The major drawback of the existing Data acquisition system to monitor the interfacial force between the residual limb and the prosthetic socket developed by different manufacturers is the limited functionality and cost. The traditional devices allow the monitoring of key parameters of amputee's gait such as activity level, number of steps, energy expenditure but they do not address

the distribution of the body weight at the interface between the residual limb and the socket. Combination of EMG and force measurements of a lower limb amputee can be valuable to clinicians and researchers to provide a suitable rehabilitation. A clinically approved procedure and preparation should be followed for collection of EMG and force measurements along with combination of reliable, stand-alone electronic devices and viable data acquisition system. Harish et al developed and validated a reliable, light weight, portable and stand-alone device called as Prosthetic Activity Monitor (PAM) which can measure and record these interaction forces for healthy and unilateral transtibial amputee.

Similar DAQ system for studying the sheer pressure and interfacial force of unilateral transfemoral amputee is proposed for the intact and residual muscles of interest. Surface Electromyography has been proved significantly important for recording the muscle activity from superficial muscles whereas intramuscular electrodes are used for measuring muscle activity from the inner muscles during the activation of muscles. EMG sensing devices were used to detect electrical signals from various muscles starting from 1980 [89]. EMG electrodes are developed over the last few decades to contribute to the large-scale use of EMG signals in the medical field. At the same time, there was a tremendous improvement in understanding the properties of surface EMG recording [89, 90]. Electricity could initiate muscle contractions [91] and initially EMG was recorded using an oscilloscope. Between 1930 and 1950, researchers started using improved EMG electrodes for measuring the muscle activity, hence improving the detection of EMG signals [92].

Different type of transducers, pneumatic devices, fluid-filled sensors and strain-gauge beams have been widely used for obtaining the force measurements at the prosthetic socket. These type of force sensors are capable of normal and shear stress measurement. Earlier research studies used either accelerometers or transducers as sensors and were not able to create an overall picture

of the force distribution at different points inside the prosthetic socket [86]. Now a days, the advanced force measuring systems use more accurate, reliable, high resolution, flexible and very thin force sensors. These sensors can be easily placed on muscles of interest and can be integrated into any force measurement application without creating any additional physical inconvenience.

For gait analysis purpose, several prosthetic activity monitors are commercially available. These devices are capable to capture steps and energy expenditure in both amputee and intact subjects. Ossur® developed a PAM called patient monitoring device which could track the position of an amputee by measuring step length, maximum speed, distance traveled, average speed, active time, and inactive time [93]. This device also generates an activity index that can aid clinicians in comparing the gait performance of different individuals. Another commercial prosthetic activity monitor is the StepWatch Activity Monitor (SAM) developed by Orthocare Innovations™ [94] which is used for long term monitoring of gait of an amputee by recording the number of steps. The step watch technology helps to collect data of an amputee's activity and displays it on a smartphone via the Galileo app. The app provides insight into the amputee's activity by providing statistical analysis of the collected data. The company also developed a device for measuring prosthetic socket reaction forces called Smart Pyramid. This device helps in assessing the performance of the prosthesis over time.

As for the protocol described here, two PAMs were used. The first one is the Minisun™ IDEAA (Intelligent Device for Energy Expenditure and Physical Activity) [95]. This device records temporal-spatial parameters (Step length, Stride length, Stance time, Gait duration, Cadence etc.) with the combination of foot switches and accelerometers. It comes along with a software package that analyses the data collected and estimates the gait activity and the energy expenditure of the subject during the gait activity. It is also capable of recording EMG signals.

Figure 5.2 MiniSun IDEAA [95].

**GaitView** is a Windows program that shows the raw data. These raw data include work related activity and detailed gait in the form of histograms, data tables or statistical analysis. We can review any activity of interest at any moment, detailed to every step of walking. The recorded histogram results can be displayed, processed, and analyzed later as needed with suitable software.

The second PAM proposed here for data collection is the extended OU-PAM (University of Oklahoma Prosthetic Activity Monitor). The existing OU-PAM is designed to capture Residuum socket interface (RSI) force and EMG from muscles of the transtibial amputee. It is consisted of signal conditioning and Data acquisition board along with two tubes carrying the cables that connect to the sensors inside the prosthetic socket of the transtibial amputee. The Atmel® Extension board ATEVK525 (8-bit microcontroller AT90USBxxxx) forms the core of the OU-PAM that includes an SD-Card slot for data storage. The OU PAM has a data acquisition rate of 1000Hz which is sufficient to capture variations in EMG signals for the human gait in real

time. OU-PAM can capture data from up to 16 channels. 10 of these channels are used for capturing RSI force data and the rest are used to capture EMG data. All the three boards and the power source are enclosed in a light weight, sturdy box that can be strapped on as a backpack of the amputee thereby not bothering his regular physical motion during gait.

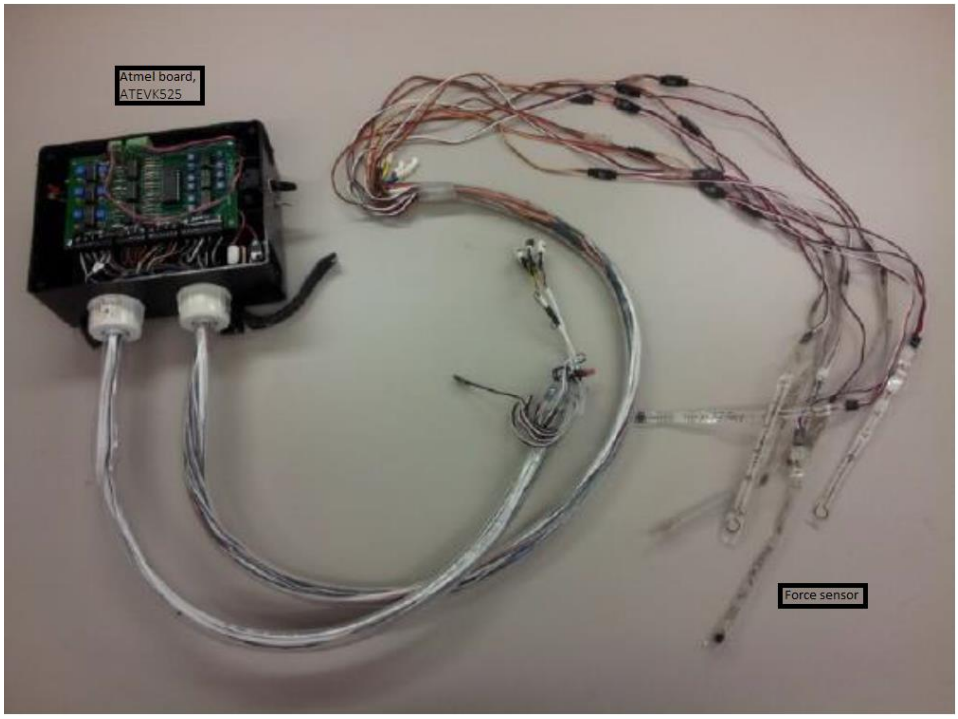


Figure 5.3 Existing OU Patient Activity Monitor [69].

The physical ability of the subject to carry out the normal gait activities (as listed below) in the clinical protocol unhindered by the PAM will also be investigated. Thus, the data acquired using this PAM is not in a laboratory setting but rather in regular conditions for work related activities. The output connectors and LED indicator mounted of the PAM allow the user to verify the functioning of the sensors and the signal conditioning circuits. Potentiometers installed on the PCB will facilitate the gain adjustment of the amplifier by varying the resistance of the channels making sure that the sensor output is not saturated. The final assembly of the Prosthetic Activity Monitor proposed to be used in this research will combine these features altogether.

Clinical studies have shown that the factors that lead to increasing the risk of biomechanical residuum injury have significantly related to weight bearing forces at the distal end of the residuum prosthetic socket [96]. In this process, the residuum socket force is measured using the Flexiforce® A201 Piezo-resistive sensor [97]. These sensors are cheap, thin and comfortable to use as attached to the socket. The sensors are attached securely inside the prosthetic socket with the help of adhesive tape at specific locations as shown in the figure. The sensors are thin and do not result in any discomfort or change in the prosthetic fit. The force sensors are calibrated each time before use so that the measurements are correct. The force detected by the sensor is converted to voltage with the help of amplifier circuit.

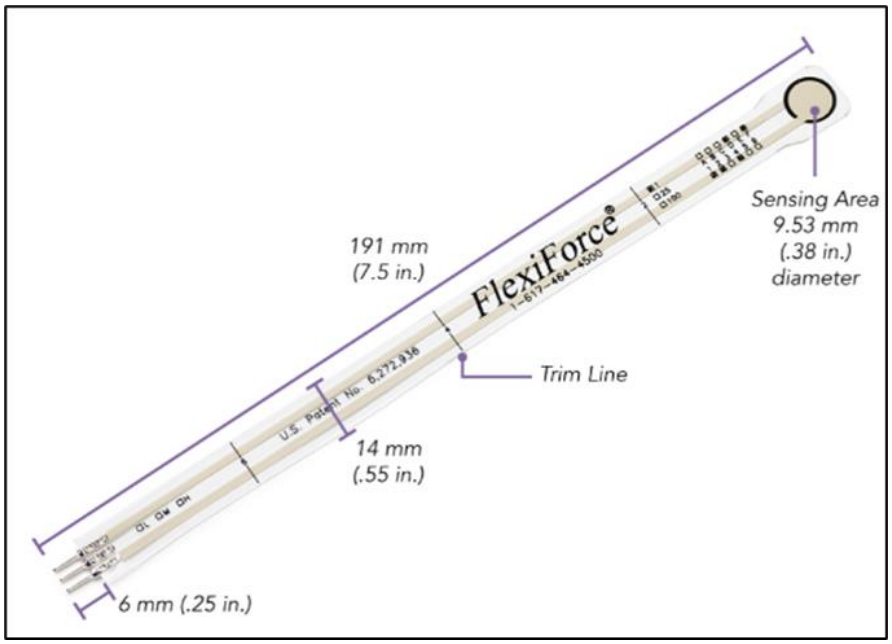

Figure 5.4 Flexiforce® A201 Piezo-resistive sensor [97].

The study of EMG signals can provide insight into how the muscular systems generate joint moments generation and limbs stabilization in both normal and pathological gait [98]. For lower limb amputees, the study of EMG signals of residual muscle provides significant impact in gait recognition and prosthetic device development [99]. Thus, studying changes in muscle activity

and especially residual muscle activity during locomotion is crucial. Most of the studies have focused on the contraction of intact muscles in amputees [100]. The study of residual muscles requires sensors with higher sensitivity and minimal thickness to enable placement inside the prosthetic socket to ensure accurate data acquisition and physical comfort at the same time while collecting data. Surface electrodes can be categorized into three main types: wet, dry contact, and dry noncontact. Some researchers have developed sEMG acquisition systems that use highly accurate, expensive, wet Ag/AgCl for signal recording [101]. They require prior skin preparation like- washing, alcohol rubbing, or even shaving. But due to higher price, they are not used for disposable purpose. For this dissertation, disposable surface stimulating Ag/AgCl electrodes with a sensing area of 1.44 $cm^2$ are used [102]. These electrodes are placed along the targeted muscles 2.5 cm apart longitudinally.

Figure 5.5 EMG sensors attached as a part of data collection from transtibial amputee [69].

Detailed study of residual socket interface forces also allows us to evaluate the maximum loading and distribution of forces inside the prosthesis during varied walking tasks instead of just during regular gait. Prosthetic socket is the human-machine interface for amputees. Such information can be used to improve the socket design for end bearing and for improved comfort for the user and thereby positively impact the health of the amputee. The development of an ideal

prosthetic socket for lower limb amputees is a challenging issue, which needs to address a complex interplay of factors affecting the durability, comfort, and overall performance of the prosthesis. These factors act in a synergistic way to determine the socket success or failure for the amputee subject. Interfacial stresses are one of the most important factors to be mentioned as an altered stress distribution can cause skin problems and pain, affecting the whole comfort and, consequently, the gait biomechanics [103].

A convenient prosthetic socket must ensure efficient fitting, appropriate load transmission, stability and control and it often plays a significant role for the success or failure of the prosthesis [103]. Most of the lower limb amputees wear a TSB (total surface bearing) socket which will lead to uniform force distributions at four proximal locations (anterior, posterior, lateral, and medial). So, the force sensors are placed at the distal location of the socket at four specific locations, anterior, medial, posterior, and lateral. Figure shows the location of the force sensors inside the prosthetic socket. These sensors can be used to capture the distal forces and confirm end weight bearing in the lower limb amputees. The resistance change of the force sensors is converted into a voltage by passing it through the circuit. High-frequency noises are eliminated by using a low pass filter of 3Hz. The force sensor readings during stance phase are considered as substantial as the leg is in contact with the ground. The readings from the force sensors during swing phase is ignored as the readings are negligible as the leg is in the air. The total distal RSI force is calculated by adding up all the four distal force sensors' normalized mean. Once the distal force curve is obtained for each type of gait; the maximum value of the distal force curve was recorded. This value is considered as the peak distal loading observed during that gait. The PAM is powered by a reliable, durable as well as cheaper power supply.

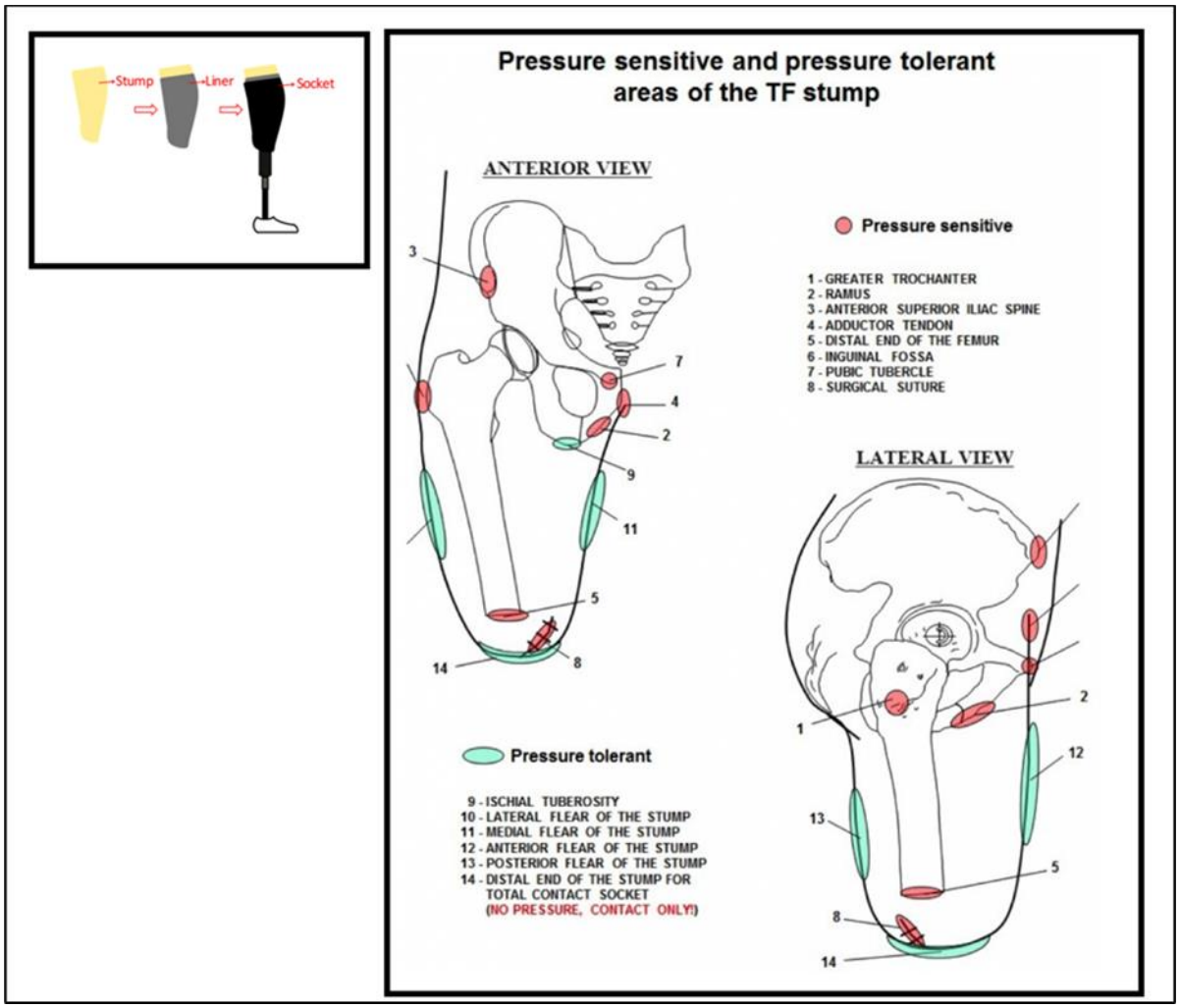


Figure 5.6 Prosthetic Stump of Transfemoral amputee [104].

## 5.3 Requirements and protocol design

Electromyography signals captured on the muscles from the lower limbs can provide us some insight into how the muscular systems generate joint movements during locomotion. The magnitude of electrical signals generated by muscles is very small in magnitude. The measurement

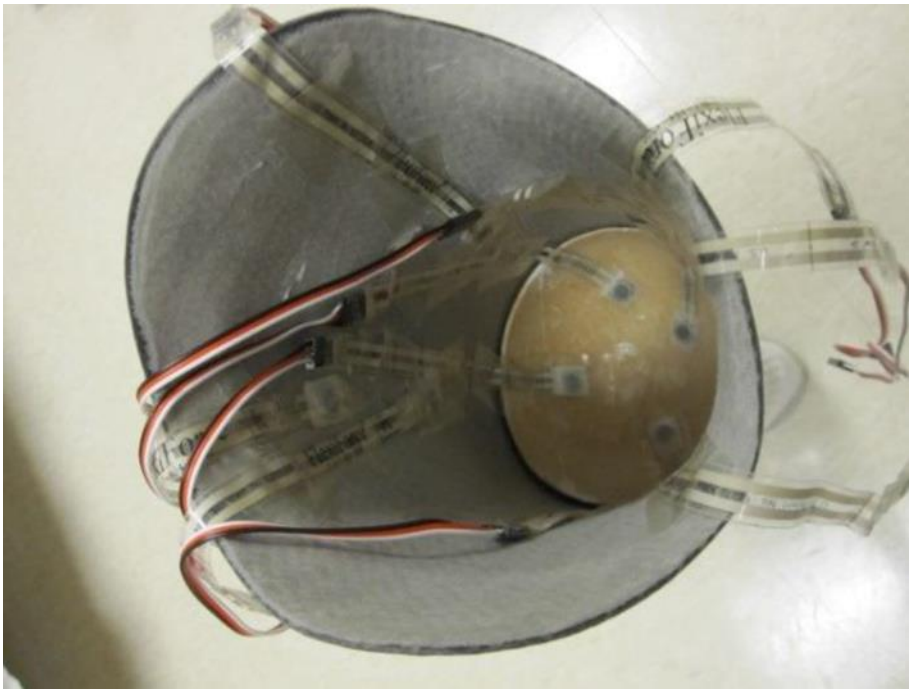

Figure 5.7 Force sensors attached to the prosthetic socket [13].

and processing of EMG signals from muscles require specialized DAQ system. Muscle contraction profiles captured from muscles explain the variation of energy consumption during different stages of gait and speed. It describes the dependence of walking speed on energy consumption. For lower limb amputees, during different phases of walking, energy distribution of lower limb muscles compared to the healthy individuals indicate the compensation strategies for the missing limb. The force is evident at distinct locations inside the prosthetic socket, part from this force is due to muscle contraction. The data obtained from the sensors indicate contact forces at specific forces at specific points in the socket in earlier literatures [15]. Few studies showed that the residual tibialis anterior muscle was more active compared with its activity at lower distal RSI force variation [102].

The PAM (patient activity monitor) in the Figure 5.3 can be used to examine weight-bearing loads at 8 locations at the residuum-prosthetic socket interface. It can be used to see the muscle activity profile in the distal residuum during the work-related activities that include

different speed of walking conditions, weightlifting, and carrying. It will be interesting to examine the relationship between average peak load and muscle activity in specific locations on the distal residuum during different walking conditions, lifting, and carrying, and comparing the muscle activity between the intact limb and the controlled one from the collected data. For unilateral transfemoral amputees, the specific locations of interest for the EMG performance are rectus femoris, hamstrings, gluteus medius, gluteus maximus and adductor for both limbs. This helps in realizing the effect of amputation on residual muscle activity and builds the foundation for understanding the effect of amputation on residual limb health. It is expected to see considerable residual muscle activity in the transfemoral amputation. Furthermore, the co-relation between residuum socket interface (RSI) force and EMG to the type of gait can be studied in future. Kotamraju et al. tested a group of unilateral transtibial amputee with the similar protocol and it was observed that RSI force and EMG activity increased during self-selected gait, brisk gait and weight carry gait [13]. In next section, the data collection framework for unilateral transfemoral amputee is described which is like this process used for data collection from transfemoral amputee in OHSU. Transfemoral amputees have shorter muscle length, and their leg is amputed above-knee, so the number of force and EMG sensors are different, the biological positions of interest are different, and the core hardware should be selected so that it can acquire data accordingly.

The calibration process eliminates DC bias and modify the range of each of the measured. Data from all channels of the PAM will be collected over the entire test protocol described in the next section and can be saved to a physical storage media. The gait data will also be investigated to determine the presence and effect of noise in the signals.

## 5.4 Transfemoral Amputation Procedure

Traditional transfemoral amputation procedure ensures that the femoral shaft axis is left as close to normal by preservation of the adductor magnus and by the myodesis (traditional amputation process where dissected muscle groups are attached directly to the bone) process of the muscle to the residual femur. By following established biomechanical principles, and satisfactory surgical techniques, patients undergo transfemoral amputation followed by suitable rehabilitation to remain able to ambulate.

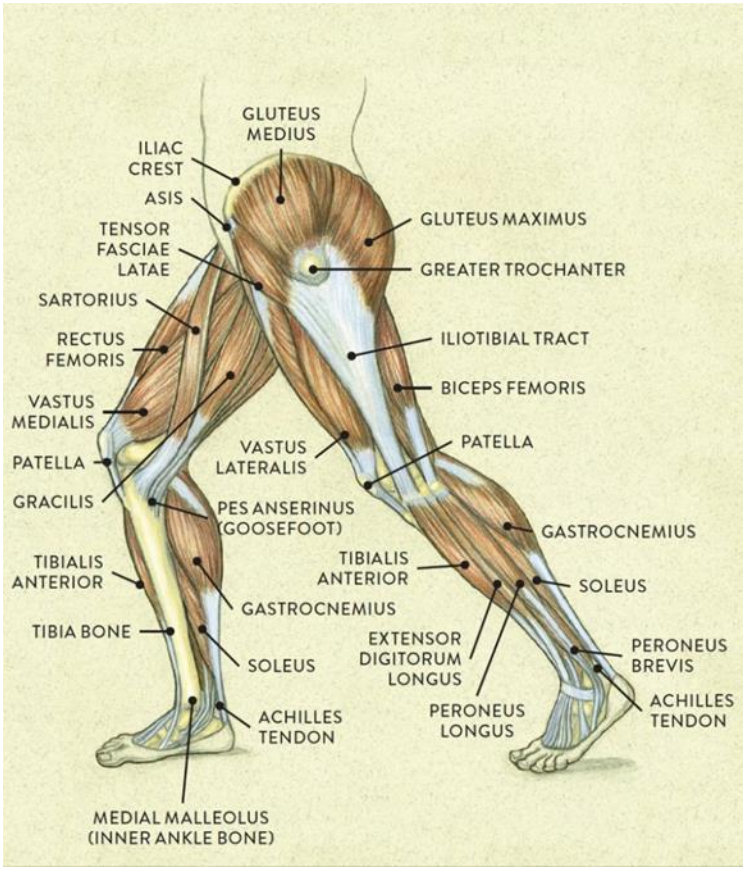


Figure 5.8 Muscles of Lower limb involved in locomotion [105].

Transfemoral amputees treated with conventional amputation show alteration of mechanical and anatomic alignment as the residual femur no longer has its normal alignment with the tibia, leaving the femoral shaft axis in abduction as compared with the intact limb. The smaller

mass of amputated adductor muscle must generate a larger force to hold the femur in its earlier position and is unable to generate sufficient force leading to an abducted position of the femur which leads to an increased energy consumption for locomotion. In stance phase of healthy gait, the mechanical axis of the lower limb moves from the center of the femoral head through the center of the knee to the midpoint of the ankle, and measures 3 degrees apart from the vertical axis [106]. The femoral shaft axis measures 9 degrees apart from the vertical placing the normal anatomic alignment of the femur in adduction. This allows the hip stabilizer muscles (gluteus medius and minimus) and abductors (gluteus medius and tensor fasciae latae) to function properly and reduce the lateral motion of the center of mass of the body, resulting in energy efficient, smoother gait [106].

The basic goal of surgery should be the preservation of the adductor magnus and maintaining the muscle balance between adductors and abductors. Surgeries are recommended following a muscle preserving technique whereby the distal insertions of the muscles are resected from the original bony attachment and reattached at a new level, maintaining greater muscle tension. Thus, a dynamically balanced residual limb with good motor control and sensation can be ensured.

1. The buttock of the surgically treated side should be elevated to allow full hip extension and adduction during the amputation procedure.
2. Skin flaps should be marked properly before the skin incision. It is recommended that the medial flap should be kept long in the sagittal plane. The most viable soft tissue (if any) is recommended to be used as the flap.

3. The muscles are identified to be sectioned. Retaining some of the tendinous portion, the quadriceps is detached just proximal to the patella. The vastus medialis is separated from the intermuscular septum.
4. The adductor magnus is detached from the adductor tubercle and reflected medially to expose the femoral shaft. Additional 2 to 3 cm of adductor magnus from the linear aspera (group of muscles) is detached depending on the length of the leg. The smaller muscles may be transected approximately 1 to 2 inches longer than the targeted bone to facilitate their inclusion.
5. The femur is exposed approximately 12 to 14 cm above the condylar level and approximately 12 cm above the joint line. Few holes are made on the lateral cortex of the distal femur and additional holes are made anteriorly and posteriorly approximately 1 to 1.5 cm apart from the cut end.
6. The adductor magnus tendon then is sutured with nonabsorbable suture material to the lateral aspect of the femur through the small drill holes.
7. To maintain the tension of amputated femur at the distal residual end, the femur is held in maximum adduction while the adductor magnus is brought across the cut end of the femur.
8. Additional anterior and posterior sutures (suture is a medical device that is used to hold body tissues together during surgery) are done to prevent the muscles from sliding forward or backward and makes it tight and more supportive.
9. The quadriceps muscle is drawn over the end of the bone anchored adductor magnus and is sutured to the posterior femur through the posterior drill holes, the remaining posterior muscles are anchored to the posterior area of the adductor

magnus. The hip should be extended during this process to prevent creating a hip flexion contracture.

Myoplasty procedure alone does not seem to restore normal muscle tension, nor does it allow for adequate muscle control or strength of the femur for regular locomotion. Advanced surgical procedure along with rehabilitation has been developed so that the amputee can have a better and controlled gait.

## 5.5 Framework for experimental gait study

It is expected that for transfemoral amputees; residual and intact muscles, in general, show more muscle activity when the speed of the gait increases. Earlier researches show that during gait activities, significant force is observed at distal area (end-bearing) of the residual limb (under the bony bridge which stabilized the residual limb anatomy) as well as middle posterior point (where the length-tension relationship of the residual gastrocnemius muscle was retrieved) for unilateral transtibial amputee [15]. The relationship between the residual and intact muscles and the forces measured at the residuum-socket interface during the gait related activity are of particular interest as they are indicators of muscle health and can provide insight into the effectiveness of gait. From previous research it is revealed that, the residual muscle on the intact limb showed deviation in activation pattern asserting the change in the biomechanics of gait after amputation [107]. The gait speed is found to be directly proportional to the magnitude of the muscle activation. It would be interesting to test the similar hypothesis for transfemoral amputee. This can be useful for the development of smart prosthetic devices that can adapt to dynamic variations or inclination in gait. It is expected and proved in earlier literatures that the activity of the residual muscle groups differs considerably in comparison to the similar muscles in the intact limb. Again, some muscle in amputee subjects is more active during the early stance phase and end of swing phase. The

researchers believe that this happens as the residual muscle no longer retains the same relationship to gait cycle, but rather triggers to stabilize the residual limb during gait. In this dissertation, we address the details of the experimental setup such as criteria for subject selection and protocol below. During the walk test, each subject was asked to perform three work related activity tasks.

These tasks include:

a) Walking at self-selected pace for a duration of 2 minutes.

b) Walking at brisk pace for a duration of 2 minutes.

c) Walking (distance of 25 feet) while carrying a load.

### 5.5.1 Criteria for subject selection

All the subjects for this clinical study should be recruited from the unilateral transfemoral amputee population residing in USA. The following criteria can be followed to establish a successful comparative study:

1. The amputees should have undergone the amputation procedure at least 6 months prior to the day of participation in the study.
2. Initially, the study should be limited to the study of the non-diabetic, male population (age group 18-64).
3. All the subjects should be capable of walking independently without any help from assistive devices except their own prosthesis.
4. The recruited subjects should be primarily English speaking and capable of giving written consent to the participation in the study.
5. It would be interesting to see the performance of different type of prosthesis for the same amputee and same gait activity.

6. Intact individuals can be recruited for this study to serve as a control group to have a better comparison.

### 5.5.2 Protocol for Clinical Study

The clinical study protocols proposed in this study have been approved by the Institutional review board at the University of Oklahoma Health Science Center (OUHSC) for the protection of human subjects [108, 109]. All the amputee subjects should use their own prosthesis during the period of the study so that the data collected would be representative of their daily usage. A certified prosthetist should be present on site for the whole duration of the study to ensure socket alignment and fit to ensure protection from any unwanted injury or discomfort. Furthermore, the primary health index data on heart rate, pulse, blood oxygen levels and the Borg index of participants should be collected by the certified medical personnel.

After the proper placement of the force and EMG sensors, the subject is required to stand upright and the signal on each data acquisition channel is measured using an oscilloscope. The overall assembly is ensured to be comfortable for the subjects thus eliminating the interference of the wiring harness during the gait activities. However, four force sensors are placed under left heel, left toe, right heel, and right toe to indicate the heel strike and toe off events. These events can be used to distinguish between the stance and swing phases of the gait cycle.

The data collection will be controlled and initiated by the switch mechanism provided in the PAM. The collected data from the sensors using the PAM is analyzed to verify the successful capture of the gait data. The status of data collection and the power supply are also monitored visually. The software protocols to download, view, and analyze the raw data information will be verified.

# Chapter 6 Conclusion and Future Research

This dissertation is aimed to develop the human gait modelling and advanced neural network control to use it for transfemoral amputee. With the comparative control design and results, it is expected to show better performance with longer training time and repeated iterations. Human gait consists of stance and swing phases, most of the controllers (targeted for prosthetic use) to the date are not capable of having similar performance level over the whole gait cycle. Not only that, different speed, terrain, and reactive forces during locomotion make it complex to control in real time. The controller design is primarily subjected to unilateral transfemoral amputee; considering the amputated leg will follow the trajectory according to the intact leg as it should be (like a healthy human gait). To address the challenges with noisy data labels from real-time terrain, I have evaluated the controller as a set of neural network and PD controller to achieve improvement of the performance. Similarly, I have changed different design parameters and controller combinations performance so that the energy consumption and the tracking error have a balance.

The following are some of the results of the research presented in this dissertation:

1. We proposed a mathematical modeling for the real time gait analysis, considering the sagittal human leg model (with three main segments). This model is kinematically flexible with more degrees of freedom to allow a versatile gait pattern.
2. We proposed optimizations and resultant improvements with neural network layer designs focusing on both the action and critic network improvement. The proposed control designs work as an extension of the existing classical control levels. The above-knee amputee prosthetics must be considered as a hierarchical control task, where each consecutive control level contributes by

fine tuning the reference trajectory for the level below or by directly introducing a correction signal over the calculated torques. In this view the goal of the adaptive neural controller is to progressively correct the control actions calculated by the basic control loops by learning specific motion behaviors of the amputee individual.

3. We proposed a centralized neural network distribution with integral error control unit. For unilateral transfemoral prosthetic applications, the controlling is more challenging than that of a transtibial amputee. The proposed single unified DNDP has additional channels which can account for integral joint angular errors, and it improves the accuracy and stability of the closed loop system as an efficiency requirement. The control structure was carefully designed with additional feedforward and PD feedback tuning for better performance.
4. Transfemoral prosthesis gait analysis is a project that can be extended into field data collection. This would require the existing PAM to be improved and tested and thus employed in field to collect gait data from human subjects with clinically approved procedures. We presented the outline for this task in the later portion of this dissertation.

## Scopes for improvement

Even though we explored an improved and optimized control approach for TF gait analysis and prosthesis device improvement, our approaches are facilitated with some assumptions that need to be further explored for better optimization, stability, and reliability, on top of what we achieved in this dissertation. Our models are developed on reported healthy human gait data and

establishing NN-based control algorithm applied to the TF prosthetic gait tracking to mimic the healthy one. A holistic approach from fault tolerance in sensor systems to contextual association of data-driven models improves the robustness of sensor driven models of human physiology in real-world settings. While the common knowledge about modeling tells us that larger volume of real data points help improving model performance significantly. Instead of using more samples or real data points, we tried to achieve robust performance through incorporation of supplemental information with the available data samples. The modeling tells us that more data helps with system performance, and this will reflect on the TF prosthesis performance in tracking the intact leg. To explore this model for practical applications, it requires both a robust sensing system to acquire data for long periods continuously from real people, and a method to utilize the real data without reliable continuous labels for model improvement. So, we present our approaches toward achieving these goals. In future, with advanced microprocessor and wireless connectivity and high-performance cloud computation capabilities, the neural network can be embedded in light weight, cheap systems as a wearable device to ensure faster adjustment and flexible performance with efficacy.

## Future work

It is expected that the embedded control system must generate comfortable, robustly stable walking gaits that can overcome the mechanical limits of the exoskeleton (such as joint and torque limits), initiate smooth foot contact with the ground, and satisfy ground contact constraints that avoid slipping.

- Further investigation of the properties of the developed controllers can be done with respect to robust stability and performance. We assumed the system properties will

be uniform with respect to initial conditions. Hence, modification of the learning rule can be done by combining pretraining with dynamic optimization.

- Testing another control structure for DNDP – LSTM (Long short-term memory) layers, different activation functions, encoder-decoder structures, and recurrent layers can be used.
- Replacement of the lower-level PD controller with a centralized algorithm – LQR (Linear quadratic regulator) or model predictive can be done.
- Comparison against alternative control approaches for biped robots or active prosthetic devices can be made.
- Generating C code for the controller can be investigated and performance testing can be evaluated experimentally (hardware in the loop simulation or on a prototype if available).

The research framework enables a quick evaluation of the performance of prosthetic devices under different operating conditions over the complete gait cycle. The controller performance is impressive based on simulation but designing a controlled prosthetic leg is a challenging task and several milestones need to be addressed before the proposed approach can be applied. Appropriate and realistic bio-mechanical design which satisfy the required rigidity, mobility and power need to be built. The dynamic model of the knee ankle joint needs to be verified with actual gait measurement. The control approach will then be tested and adjusted on the refined model. Additional issues such as accuracy of gait recognition, parameterization of the gait patterns, real-time approximation of the ground reaction force should be addressed. Finally, performance of the controlled prosthetic leg should be tested through both bio-mechanical property testing and

quantitative gait analysis. The research can be extended to bilateral transfemoral amputation and further limb loss in future.

# Bibliography


[1] C. L. Vaughan, B. Davis, and J. C. O'Connor, "Dynamics of human gait," 1992.

[2] R. Gage and R. Hicks, "Gait analysis in prosthetics," *Clinical Prosthetics & Orthotics,* vol. 9, no. 3, pp. 17-21, 1989.

[3] J. P. Ertl. "Lower-Extremity Amputations." https://emedicine.medscape.com/article/1232102-overview#a0104 (accessed.

[4] A. P. Singh. "Normal Biomechanics of Knee and Movements." https://boneandspine.com/normal-biomechanics-of-knee/#:~:text=The%20knee%20joint%20has%20biomechanical,and%20transmits%20forces%20across%20it. (accessed.

[5] N. D. Clement and D. J. Deehan, "Knee biomechanics: Will we ever know the truth?," (in eng), *Bone Joint Res,* vol. 7, no. 5, pp. 325-326, 2018, doi: 10.1302/2046-3758.75.BJR-2017-0360.

[6] L. Zhang *et al.*, "Knee Joint Biomechanics in Physiological Conditions and How Pathologies Can Affect It: A Systematic Review," (in eng), *Appl Bionics Biomech,* vol. 2020, pp. 7451683-7451683, 2020, doi: 10.1155/2020/7451683.

[7] C. W. Chan and A. Rudins, "Foot biomechanics during walking and running," in *Mayo Clinic Proceedings*, 1994, vol. 69, no. 5: Elsevier, pp. 448-461.

[8] E. M. Arnold, S. R. Hamner, A. Seth, M. Millard, and S. L. Delp, "How muscle fiber lengths and velocities affect muscle force generation as humans walk and run at different speeds," (in eng), *J Exp Biol,* vol. 216, no. Pt 11, pp. 2150-2160, 2013, doi: 10.1242/jeb.075697.

[9] M. F. Ghazali, N. A. Abd Razak, N. A. Abu Osman, and H. Gholizadeh, "Awareness, potential factors, and post-amputation care of stump flexion contractures among transtibial amputees," (in eng), *Turk J Phys Med Rehabil,* vol. 64, no. 3, pp. 268-276, 2018, doi: 10.5606/tftrd.2018.1668.

[10] J. E. Sanders and C. H. Daly, "Normal and shear stresses on a residual limb in a prosthetic socket during ambulation: comparison of finite element results with experimental measurements," *Journal of rehabilitation research and development,* vol. 30, pp. 191-191, 1993.

[11] E. A. Al-Fakih, N. A. Abu Osman, and F. R. Mahmad Adikan, "Techniques for interface stress measurements within prosthetic sockets of transtibial amputees: a review of the past 50 years of research," *Sensors,* vol. 16, no. 7, p. 1119, 2016.

[12] E. Boutwell, R. Stine, and K. Tucker, "Effect of prosthetic gel liner thickness on gait biomechanics and pressure distribution within the transtibial socket," *Journal of rehabilitation research and development,* vol. 49, no. 2, p. 227, 2012.

[13] B. Kotamraju, S. Commuri, A. Mai, C. Dionne, J. Day, and W. Ertl, "Residuum Muscle Activation During Gait in Individuals with Traditional and Osteomyoplastic Amputation," *Journal of Prosthetics and Orthotics,* vol. 30, p. 1, 08/01 2018, doi: 10.1097/JPO.0000000000000207.

[14] V. Rajtukova, R. Hudak, J. Zivcak, P. Halfarova, and R. Kudrikova, "Pressure Distribution in Transtibial Prostheses Socket and the Stump Interface," *Procedia Engineering,* vol. 96, pp. 374-381, 2014/01/01/ 2014, doi: https://doi.org/10.1016/j.proeng.2014.12.106.

[15] A. Mai, S. Commuri, C. P. Dionne, J. Day, W. J. J. Ertl, and J. L. Regens, "Residual Muscle Contraction and Residuum Socket Interface Force in Men with Transtibial Osteomyoplastic Amputation," *JPO: Journal of Prosthetics and Orthotics,* vol. 25, no. 3, pp. 151-158, 2013, doi: 10.1097/JPO.0b013e31829a965c.

[16] S. C. A Mai, "Adaptive Dynamic Programming-Based Control of an Ankle Joint Prosthesis," in *Informatics in Control, Automation and Robotics*, O. G. Jean-Louis Ferrier, Kurosh Madani, Jurek Sasiadek Ed.: Springer International Publishing, 2015, ch. 5.

[17] M. L. Handford and M. Srinivasan, "Robotic lower limb prosthesis design through simultaneous computer optimizations of human and prosthesis costs," (in eng), *Sci Rep,* vol. 6, pp. 19983-19983, 2016, doi: 10.1038/srep19983.
[18] A. Nair, R. S. Hanspal, M. S. Zahedi, M. Saif, and K. Fisher, "Analyses of prosthetic episodes in lower limb amputees," *Prosthetics and Orthotics International,* vol. 32, no. 1, pp. 42-49, 2008, doi: 10.1080/03093640701610615.
[19] K. A. Raichle *et al.*, "Prosthesis use in persons with lower- and upper-limb amputation," (in eng), *Journal of rehabilitation research and development,* vol. 45, no. 7, pp. 961-972, 2008, doi: 10.1682/jrrd.2007.09.0151.
[20] M. F. Allende, S. W. Levy, and G. H. Barnes, "Epidermoid cysts in amputees," (in eng), *Acta Derm Venereol,* vol. 43, pp. 56-67, 1963.
[21] S. W. Levy, "Skin problems of the leg amputee," *Prosthetics and Orthotics International,* vol. 4, no. 1, pp. 37-44, 1980, doi: 10.3109/03093648009103113.
[22] C. C. Lyon, J. Kulkarni, E. Zimerson, E. Van Ross, and M. H. Beck, "Skin disorders in amputees," *Journal of the American Academy of Dermatology,* vol. 42, no. 3, pp. 501-507, 2000/03/01/ 2000, doi: https://doi.org/10.1016/S0190-9622(00)90227-5.
[23] K. Ziegler-Graham, E. J. MacKenzie, P. L. Ephraim, T. G. Travison, and R. Brookmeyer, "Estimating the prevalence of limb loss in the United States: 2005 to 2050," (in eng), *Arch Phys Med Rehabil,* vol. 89, no. 3, pp. 422-9, Mar 2008, doi: 10.1016/j.apmr.2007.11.005.
[24] C. S. Molina and J. Faulk, "Lower extremity amputation," *StatPearls [Internet],* 2020.
[25] O. B. Healthcare. "International C-Leg Studies." https://media.ottobock.com/_web-site/prosthetics/lower-limb/c-leg/files/international_c-leg_studies.pdf (accessed.
[26] P. W. Moxey *et al.*, "Lower extremity amputations--a review of global variability in incidence," (in eng), *Diabet Med,* vol. 28, no. 10, pp. 1144-53, Oct 2011, doi: 10.1111/j.1464-5491.2011.03279.x.
[27] M. J. Bosse *et al.*, "An analysis of outcomes of reconstruction or amputation after leg-threatening injuries," (in eng), *N Engl J Med,* vol. 347, no. 24, pp. 1924-31, Dec 12 2002, doi: 10.1056/NEJMoa012604.
[28] B. M. Isaacson, S. R. Weeks, P. F. Pasquina, J. B. Webster, J. P. Beck, and R. D. Bloebaum, "The road to recovery and rehabilitation for injured service members with limb loss: a focus on Iraq and Afghanistan," (in eng), *US Army Med Dep J,* pp. 31-6, Jul-Sep 2010.
[29] A. Cristian, *Lower limb amputation: A guide to living a quality life*. Demos Medical Publishing, 2005.
[30] R. Amali, S. Noroozi, J. Vinney, P. Sewell, and S. Andrews, "Predicting Interfacial Loads between the Prosthetic Socket and the Residual Limb for Below-Knee Amputees–A Case Study," *Strain,* vol. 42, no. 1, pp. 3-10, 2006.
[31] A. F. Mak, G. H. Liu, and S. Lee, "Biomechanical assessment of below-knee residual limb tissue," *Journal of rehabilitation research and development,* vol. 31, no. 3, pp. 188-198, 1994.
[32] M. W. Legro *et al.*, "Issues of importance reported by persons with lower limb amputations and prostheses," *Journal of rehabilitation research and development,* vol. 36, no. 3, pp. 155-163, 1999.
[33] B. Christensen, B. Ellegaard, U. Bretler, and E. Østrup, "The effect of prosthetic rehabilitation in lower limb amputees," *Prosthetics and Orthotics International,* vol. 19, no. 1, pp. 46-52, 1995.
[34] S. M. Jaegers, J. H. Arendzen, and H. J. de Jongh, "Prosthetic gait of unilateral transfemoral amputees: a kinematic study," *Archives of physical medicine and rehabilitation,* vol. 76, no. 8, pp. 736-743, 1995.
[35] A. Gitter, J. Czerniecki, and K. Weaver, "A reassessment of center-of-mass dynamics as a determinate of the metabolic inefficiency of above-knee amputee ambulation," *American journal of physical medicine & rehabilitation,* vol. 74, no. 5, pp. 332-338, 1995.
[36] "MUSCLES OF THE LEG: Anterior view," ed.

[37] G. V. B. Cochran, *A primer of orthopaedic biomechanics*. Churchill Livingstone, 1982.
[38] Y. Sagawa Jr, K. Turcot, S. Armand, A. Thevenon, N. Vuillerme, and E. Watelain, "Biomechanics and physiological parameters during gait in lower-limb amputees: a systematic review," *Gait & posture,* vol. 33, no. 4, pp. 511-526, 2011.
[39] M. H. Schwartz, J. P. Trost, and R. A. Wervey, "Measurement and management of errors in quantitative gait data," *Gait & posture,* vol. 20, no. 2, pp. 196-203, 2004.
[40] B. C. Clark, T. M. Manini, N. R. Ordway, and L. L. Ploutz-Snyder, "Leg muscle activity during walking with assistive devices at varying levels of weight bearing11No commercial party having a direct financial interest in the results of the research supporting this article has or will confer a benefit on the authors or on any organization with which the authors are associated," *Archives of Physical Medicine and Rehabilitation,* vol. 85, no. 9, pp. 1555-1560, 2004/09/01/ 2004, doi: https://doi.org/10.1016/j.apmr.2003.09.011.
[41] V. Kalapatapu, J. F. Eidt, and R. S. Berman, "Techniques for lower extremity amputation," *Internet]. Waltham (MA): UpToDate,* 2017.
[42] T. Bae, K. Choi, and M. Mun, "Level walking and stair climbing gait in above-knee amputees," *Journal of medical engineering & technology,* vol. 33, no. 2, pp. 130-135, 2009.
[43] E. D. Ledoux, "Inertial Sensing for Gait Event Detection and Transfemoral Prosthesis Control Strategy," *IEEE Transactions on Biomedical Engineering,* vol. 65, no. 12, pp. 2704-2712, 2018, doi: 10.1109/TBME.2018.2813999.
[44] E. Isakov, O. Keren, and N. Benjuya, "Trans-tibial amputee gait: Time-distance parameters and EMG activity," *Prosthetics and orthotics international,* vol. 24, no. 3, pp. 216-220, 2000.
[45] C. M. Powers, S. Rao, and J. Perry, "Knee kinetics in trans-tibial amputee gait," *Gait & posture,* vol. 8, no. 1, pp. 1-7, 1998.
[46] N. Vanicek, S. Strike, L. McNaughton, and R. Polman, "Gait patterns in transtibial amputee fallers vs. non-fallers: Biomechanical differences during level walking," *Gait & Posture,* vol. 29, no. 3, pp. 415-420, 2009.
[47] L. Schutte, U. Narayanan, J. Stout, P. Selber, J. Gage, and M. H. Schwartz, "An index for quantifying deviations from normal gait," *Gait & posture,* vol. 11, no. 1, pp. 25-31, 2000.
[48] T. A. Wren, K. P. Do, R. Hara, F. J. Dorey, R. M. Kay, and N. Y. Otsuka, "Gillette Gait Index as a gait analysis summary measure: comparison with qualitative visual assessments of overall gait," *Journal of Pediatric Orthopaedics,* vol. 27, no. 7, pp. 765-768, 2007.
[49] V. L. Chester, M. Tingley, and E. N. Biden, "An extended index to quantify normality of gait in children," *Gait & posture,* vol. 25, no. 4, pp. 549-554, 2007.
[50] L. Kark, D. Vickers, A. McIntosh, and A. Simmons, "Use of gait summary measures with lower limb amputees," *Gait & Posture,* vol. 35, no. 2, pp. 238-243, 2012.
[51] M. H. Schwartz and A. Rozumalski, "The Gait Deviation Index: a new comprehensive index of gait pathology," *Gait & posture,* vol. 28, no. 3, pp. 351-357, 2008.
[52] B. C. Wehe, "An overview of transfemoral socket designs," 1993.
[53] T. Manfredi, "Types of Leg Prosthetics," 2020. [Online]. Available: https://www.healthguidance.org/entry/15868/1/Types-of-Leg-Prosthetics.html.
[54] "Above Knee Leg Prosthetics." INFINITE TECHNOLOGIES ORTHOTICS AND PROSTHETICS. https://www.infinitetech.org/above-knee-leg-prosthetics/ (accessed 2021).
[55] D. Popovic, R. Tomovic, D. Tepavac, and L. Schwirtlich, "Control aspects of active above-knee prosthesis," *International journal of man-machine studies,* vol. 35, no. 6, pp. 751-767, 1991.
[56] B. W. Heller, P. H. Veltink, N. J. Rijkhoff, W. L. Rutten, and B. J. Andrews, "Reconstructing muscle activation during normal walking: a comparison of symbolic and connectionist machine learning techniques," *Biological cybernetics,* vol. 69, no. 4, pp. 327-335, 1993.

[57] S. Jonic, T. Jankovic, V. Gajic, and D. Popvic, "Three machine learning techniques for automatic determination of rules to control locomotion," *IEEE transactions on biomedical engineering,* vol. 46, no. 3, pp. 300-310, 1999.

[58] G. G. Scandaroli, G. A. Borges, A. F. da Rocha, and F. A. de Oliveira Nascimento, "Adaptive knee joint control for an active amputee prosthesis," in *2008 IEEE Latin American Robotic Symposium*, 2008: IEEE, pp. 164-169.

[59] B. E. Lawson, H. A. Varol, and M. Goldfarb, "Ground adaptive standing controller for a powered transfemoral prosthesis," in *2011 IEEE International Conference on Rehabilitation Robotics*, 29 June-1 July 2011 2011, pp. 1-6, doi: 10.1109/ICORR.2011.5975475.

[60] A. H. Shultz, B. E. Lawson, and M. Goldfarb, "Running With a Powered Knee and Ankle Prosthesis," *IEEE Transactions on Neural Systems and Rehabilitation Engineering,* vol. 23, no. 3, pp. 403-412, 2015, doi: 10.1109/TNSRE.2014.2336597.

[61] M. R. S. Tirtashi, K. Mazlumi, and A. Rohani, "TCPS controller design using Fuzzy Logic Controller for power system stability enhancement," in *2010 IEEE International Conference on Power and Energy*, 29 Nov.-1 Dec. 2010 2010, pp. 195-199, doi: 10.1109/PECON.2010.5697581.

[62] V. Azimi, T. Shu, H. Zhao, R. Gehlhar, D. Simon, and A. D. Ames, "Model-Based Adaptive Control of Transfemoral Prostheses: Theory, Simulation, and Experiments," *IEEE Transactions on Systems, Man, and Cybernetics: Systems,* vol. 51, no. 2, pp. 1174-1191, 2021, doi: 10.1109/TSMC.2019.2896193.

[63] T. Chau, "A review of analytical techniques for gait data. Part 2: neural network and wavelet methods," *Gait & posture,* vol. 13, no. 2, pp. 102-120, 2001.

[64] J. A. Hertz, *Introduction to the theory of neural computation*. CRC Press, 2018.

[65] N. E. Cotter, "The Stone-Weierstrass theorem and its application to neural networks," *IEEE Transactions on Neural Networks,* vol. 1, no. 4, pp. 290-295, 1990, doi: 10.1109/72.80265.

[66] T. Leephakpreeda, "Novel determination of differential-equation solutions: universal approximation method," *Journal of Computational and Applied Mathematics,* vol. 146, no. 2, pp. 443-457, 2002/09/15/ 2002, doi: https://doi.org/10.1016/S0377-0427(02)00397-7.

[67] R. Lafuente, J. M. Belda, J. Sánchez-Lacuesta, C. Soler, and J. Prat, "Design and test of neural networks and statistical classifiers in computer-aided movement analysis: a case study on gait analysis," (in eng), *Clin Biomech (Bristol, Avon),* vol. 13, no. 3, pp. 216-229, Apr 1998, doi: 10.1016/s0268-0033(97)00082-x.

[68] S. Au, M. Berniker, and H. Herr, "Powered ankle-foot prosthesis to assist level-ground and stair-descent gaits," (in eng), *Neural Netw,* vol. 21, no. 4, pp. 654-66, May 2008, doi: 10.1016/j.neunet.2008.03.006.

[69] A. Mai and S. Commuri, "Gait identification for an intelligent prosthetic foot," in *2011 IEEE International Symposium on Intelligent Control*, 2011: IEEE, pp. 1341-1346.

[70] C. Chow and D. Jacobson, "Studies of human locomotion via optimal programming," *Mathematical Biosciences,* vol. 10, no. 3-4, pp. 239-306, 1971.

[71] B. J. Fregly, J. A. Reinbolt, K. L. Rooney, K. H. Mitchell, and T. L. Chmielewski, "Design of patient-specific gait modifications for knee osteoarthritis rehabilitation," *IEEE Transactions on Biomedical Engineering,* vol. 54, no. 9, pp. 1687-1695, 2007.

[72] A. Seth and M. G. Pandy, "A neuromusculoskeletal tracking method for estimating individual muscle forces in human movement," *Journal of biomechanics,* vol. 40, no. 2, pp. 356-366, 2007.

[73] G. G. Rigatos, "Model-based and model-free control of flexible-link robots: A comparison between representative methods," *Applied Mathematical Modelling,* vol. 33, no. 10, pp. 3906-3925, 2009.

[74] H. Kanoh, S. Tzafestas, H. G. Lee, and J. Kalat, "Modelling and control of flexible robot arms," in *1986 25th IEEE Conference on Decision and Control*, 1986: IEEE, pp. 1866-1870.

[75] D. A. Winter, *Biomechanics and Motor Control of Human Movement*. Wiley, 2009.

[76] W. Back and H. M. Clayton, *Equine Locomotion - E-Book*. Elsevier Health Sciences, 2013.
[77] L. Torburn, J. Perry, E. Ayyappa, and S. L. Shanfield, "Below-knee amputee gait with dynamic elastic response prosthetic feet: a pilot study," *J Rehabil Res Dev,* vol. 27, no. 4, pp. 369-84, 1990.
[78] S. W. Hill, A. E. Patla, M. G. Ishac, A. L. Adkin, T. J. Supan, and D. G. Barth, "Kinematic patterns of participants with a below-knee prosthesis stepping over obstacles of various heights during locomotion," *Gait & Posture,* vol. 6, no. 3, pp. 186-192, 1997/12/01/ 1997, doi: https://doi.org/10.1016/S0966-6362(97)01120-X.
[79] R. D. Snyder, C. M. Powers, C. Fountain, and J. Perry, "The effect of five prosthetic feet on the gait and loading of the sound limb in dysvascular below-knee amputees," *Journal of rehabilitation research and development,* vol. 32, pp. 309-315, 1995.
[80] S. A. Gard, "Use of Quantitative Gait Analysis for the Evaluation of Prosthetic Walking Performance," *JPO: Journal of Prosthetics and Orthotics,* vol. 18, no. 6, pp. P93-P104, 2006. [Online]. Available: https://journals.lww.com/jpojournal/Fulltext/2006/01001/Use_of_Quantitative_Gait_Analysis_for_the.11.aspx.
[81] P. A. Macfarlane, D. H. Nielsen, D. G. Shurr, and K. Meier, "Perception of Walking Difficulty by Below-Knee Amputees Using a Conventional Foot Versus the Flex-Foot," *JPO: Journal of Prosthetics and Orthotics,* vol. 3, no. 3, pp. 114-119, 1991. [Online]. Available: https://journals.lww.com/jpojournal/Fulltext/1991/06000/Perception_of_Walking_Difficulty_by_Below_Knee.7.aspx.
[82] D. Torricelli *et al.*, "Human-like compliant locomotion: state of the art of robotic implementations," *Bioinspiration & biomimetics,* vol. 11, no. 5, p. 051002, 2016.
[83] L. Torburn, C. M. Powers, R. Guiterrez, and J. Perry, "Energy expenditure during ambulation in dysvascular and traumatic below-knee amputees: a comparison of five prosthetic feet," *Journal of rehabilitation research and development,* vol. 32, pp. 111-111, 1995.
[84] M. Peasgood, J. McPhee, and E. Kubica, "Stabilization and Energy Optimization of a Dynamic Walking Gait Simulation," in *ASME 2005 International Design Engineering Technical Conferences and Computers and Information in Engineering Conference*, 2005, vol. Volume 6: 5th International Conference on Multibody Systems, Nonlinear Dynamics, and Control, Parts A, B, and C, pp. 339-349, doi: 10.1115/detc2005-84509. [Online]. Available: https://doi.org/10.1115/DETC2005-84509
[85] L. K. Hansen and P. Salamon, "Neural network ensembles," *IEEE Transactions on Pattern Analysis and Machine Intelligence,* vol. 12, no. 10, pp. 993-1001, 1990, doi: 10.1109/34.58871.
[86] J. A. DeLisa, U. S. V. H. A. Scientific, and T. P. Section, *Gait Analysis in the Science of Rehabilitation*. Department of Veterans Affairs, Veterans Health Administration, Rehabilitation Research and Development Service, Scientific and Technical Publications Section, 1998.
[87] S. M and M. G, "In defence of gait analysis. Observation and measurement in gait assessment," *The Journal of Bone and Joint Surgery. British volume,* vol. 67-B, no. 2, pp. 237-241, 1985, doi: 10.1302/0301-620x.67b2.3980533.
[88] A. Mai and S. Commuri, "Adaptive Dynamic Programming-Based Control of an Ankle Joint Prosthesis," in *Informatics in Control, Automation and Robotics*: Springer, 2015, pp. 91-105.
[89] J. R. Cram, "The History of Surface Electromyography," *Applied Psychophysiology and Biofeedback,* vol. 28, no. 2, pp. 81-91, 2003/06/01 2003, doi: 10.1023/A:1023802407132.
[90] C. L. Nikias and M. Raghuveer, "Bispectrum estimation: A digital signal processing framework," *Proceedings of the IEEE,* vol. 75, pp. 869-891, 1987.
[91] R. F. Kleissen, J. H. Buurke, J. Harlaar, and G. Zilvold, "Electromyography in the biomechanical analysis of human movement and its clinical application," (in eng), *Gait Posture,* vol. 8, no. 2, pp. 143-158, Oct 1 1998, doi: 10.1016/s0966-6362(98)00025-3.

[92] S. Shahid, "Higher order statistics techniques applied to EMG signal analysis and characterization," University of Limerick, 2004.
[93] A. Godfrey, R. Conway, D. Meagher, and O. L. G, "Direct measurement of human movement by accelerometry," (in eng), *Med Eng Phys,* vol. 30, no. 10, pp. 1364-86, Dec 2008, doi: 10.1016/j.medengphy.2008.09.005.
[94] "Orthocare Stropwatch." https://orthocareinnovations.com/stepwatch/ (accessed.
[95] K.-T. Han and P.-C. Wang, "Empirical Examinations of Effects of Three-Level Green Exercise on Engagement with Nature and Physical Activity," *International Journal of Environmental Research and Public Health,* vol. 15, p. 375, 02/22 2018, doi: 10.3390/ijerph15020375.
[96] X. Jia, M. Zhang, and W. C. Lee, "Load transfer mechanics between trans-tibial prosthetic socket and residual limb—dynamic effects," *Journal of biomechanics,* vol. 37, no. 9, pp. 1371-1377, 2004.
[97] FLEXIFORCE. FLEXIFORCE™ SENSORS USER MANUAL [Online] Available: https://camatsystem.com/wp-content/uploads/2019/01/FlexiForce-Sensors-RevK.pdf
[98] J. Perry and J. R. Davids, "Gait analysis: normal and pathological function," *Journal of Pediatric Orthopaedics,* vol. 12, no. 6, p. 815, 1992.
[99] J. D. Miller, M. S. Beazer, and M. E. Hahn, "Myoelectric walking mode classification for transtibial amputees," *IEEE Transactions on Biomedical engineering,* vol. 60, no. 10, pp. 2745-2750, 2013.
[100] M. B. Hansen, S. E. Nielsen, and K. Berg, "Re-examination and further development of a precise and rapid dye method for measuring cell growth/cell kill," *Journal of Immunological Methods,* vol. 119, no. 2, pp. 203-210, 1989/05/12/ 1989, doi: https://doi.org/10.1016/0022-1759(89)90397-9.
[101] H. Bateni and S. J. Olney, "Kinematic and kinetic variations of below-knee amputee gait," *JPO: Journal of Prosthetics and Orthotics,* vol. 14, no. 1, pp. 2-10, 2002.
[102] T. E. Store. "Disposable Surface Electrodes (Single-Patient-Use)." https://electrodestore.com/collections/surface-electrodes-disposable (accessed.
[103] L. Paternò, M. Ibrahimi, E. Gruppioni, A. Menciassi, and L. Ricotti, "Sockets for limb prostheses: a review of existing technologies and open challenges," *IEEE Transactions on Biomedical Engineering,* vol. 65, no. 9, pp. 1996-2010, 2018.
[104] Physiopedia. "Lower Limb Prosthetic Sockets and Suspension Systems." https://www.physiopedia.com/Lower_Limb_Prosthetic_Sockets_and_Suspension_Systems (accessed.
[105] V. L. Winslow, *Classic Human Anatomy in Motion: The Artist's Guide to the Dynamics of Figure Drawing*. Potter/Ten Speed/Harmony/Rodale, 2015.
[106] F. Gottschalk, "Transfemoral amputation: biomechanics and surgery," *Clinical Orthopaedics and Related Research®,* vol. 361, pp. 15-22, 1999.
[107] G. M. Hobusch, K. Döring, R. Brånemark, and R. Windhager, "Advanced techniques in amputation surgery and prosthetic technology in the lower extremity," (in eng), *EFORT Open Rev,* vol. 5, no. 10, pp. 724-741, Oct 2020, doi: 10.1302/2058-5241.5.190070.
[108] C. Dionne, "Residual Limb Measures During Biomechanical Work-Related Activities in Adult Oklahomans with Unilateral-Trans-Tibial Amputation due to a Traumatic Event," *IRB Number,* vol. 15713, 2011.
[109] C. Dionne, "Work Task Performance in Amputees with Trans-Tibial Amputation Due to a Traumatic Event (TTAT)," *IRB Number,* vol. 15948, 2011.